AN INITIAL STUDY OF BINARY AND TERNARY Ti-BASED ALLOYS MANUFACTURED USING LASER ENGINEERED NET SHAPING (LENS^{TM})

Alyn M. Gray, B.S.

Thesis Prepared for the Degree of

MASTER OF SCIENCE

UNIVERSITY OF NORTH TEXAS

December 2015

APPROVED:

Dr. Marcus Young, Major Professor

Dr. Peter C. Collins, Minor Professor

Dr. Rajarshi Banerjee, Committee Member

Dr. Narendra Dahotre, Committee Member

Gray, Alyn M. *An Initial Study of Binary and Ternary Ti-Based Alloys Manufactured Using Laser Engineered Net Shaping (LENS^{TM})*. Master of Science (Materials Science and Engineering), December 2015, 101 pp., 24 tables, 50 figures, references, 41 tiles.

In this study an initial assessment of the composition – microstructure – property relationships in binary and ternary Ti – based systems are made possible using LENS^{TM} technology. Laser Engineering Net Shaping (LENS^{TM}), a rapid prototyping, directed laser deposition methodology of additive manufacturing (AM) was used to create bulk homogenous specimens that are compositionally graded. Compositionally graded specimens were made possible by incorporating elemental blends of powder during the LENS^{TM} process.

While there have been numerous studies assessing the influence of common elements (e.g., V, Mo, Al, and Cr) on the resulting microstructure in titanium alloys, other elements have been neglected. A systematic study of the Ti – Fe – Al ternary system based upon varying compositions of the eutectoid former, Fe with Al to stabilize the α and β phases respectively has also been neglected. This research effort focuses on exploiting the LENS^{TM} process by rapidly assessing the composition – microstructure – property relationships in a combinatorial approach for the Ti – W, Ti – Fe, and Ti – Fe – Al systems.

Compositionally graded specimens of Ti – xW ($0<x<40$wt.%(14.79at.%)), Ti – xFe ($0<x<35$wt.%(36.37at.%)), and Ti – xFe – yAl ($0<x<40$wt.%(36.37at.%)), y=5,10, 15wt.%) have been heat treated to also assess the influence of thermal history on microstructural features such as phase composition and volume fraction.

Lastly, a Ti – xMo ($0<x<40$wt.%(24.96at.%)) compositionally graded specimen was deposited to re-assess the Mo-equivalency nature of W, as well as assess the role of phase

separation in microstructural evolution at temperatures above and below the invariant point (~695°C) of the Ti – W binary system.

ACKNOWLEDGEMENTS

I would first and foremost like to thank my advisers, Dr. Marcus Young and Dr. Peter Collins, for providing me with the opportunity to work under their supervision. This body of work would not have been possible without their guidance in understanding the fundamentals of the LENS™ process and extensive knowledge of Ti alloys.

I would also like to thank the Department of Materials Science and Engineering faculty and staff as well as my fellow graduate students at the University of North Texas. Specifically, Dr. Peyman Samimi for his patience in training me on the Optomec LENS™ 750 system and teaching me how to troubleshoot common issues encountered during the deposition process. I am also grateful to Jessica Rimza who has been a great friend over my graduate career. Lastly, Dr. Richard F. Reidy for his open door policy and friendship.

I would also like to express my appreciation to Dr. Rajarshi Banerjee for his invaluable help and generosity in providing access to his laboratory and the LENS™ Optomec 750 system.

I would like to acknowledge my mentors, Dr. Ramesh Minisandram and Dr. Robin Forbes-Jones. The freedom provided to me to explore multiple projects during my time as an R&D Intern at ATI Specialty Materials inspired me to want to become a metallurgist.

Lastly, and most importantly, I would like to thank my best friend Tim Bonner. Your words of encouragement and guidance over the last 3 years have been invaluable. I am constantly reminded to stay focused and to see the bigger picture. I would not be the person I am today if it weren't for our conversations and your friendship.

TABLE OF CONTENTS

LIST OF TABLES

LIST OF FIGURES

LIST OF EQUATIONS

CHAPTER 1

INTRODUCTION AND PROBLEM STATEMENT

1 Motivation

There is a general consensus regarding the significance of processing, thermal history, and the influence of composition on the resulting microstructure and mechanical properties of metallic materials. This study will assess two missing details:

- The influence of composition on the resulting microstructure and properties of a specimen subjected to a uniform thermal history
- The influence of thermal history on the resulting microstructure and properties of a compositionally graded specimen

Studies have shown that near β and metastable β-Ti alloys possess generally high ratio strength, good fatigue, and toughness properties. Reported literature [19 ï 20] attributes these properties to the Al (*see Equation 1.1.*) and Mo (*see Equation 1.2.*) equivalency. For this reason, it is important to reassess the W component of the Mo equivalency equation as well as observe the influence of thermal history on the resulting microstructure and properties of a Ti ï xW (0<x<40wt.%(14.79at.%)) compositionally graded alloy manufactured using the LENS^{TM} process.

Equation 1.1 [12] $[Al]_{eq}$: [Al] + 0.33[Sn] + 0.17[Zr] + 10[O + C + 2N]

Equation 2.1 [12] $[Mo]_{eq}$: [Mo] + 0.67[V] + 0.44[W] + 0.28[Nb] + 0.22[Ta] + 2.9[Fe] + 1.6[Cr] + 1.25[Ni] + 1.7[Mn] + 1.7[Co]

Similar to V, Mo is one of the most important and commonly used β stabilizers in Ti ï based alloys [30]. The previously mentioned Mo equivalent (*Equation 1.2.*) details a comparison of Mo with other β stabilizing elements (e.g. Fe, W, Ta, Cr) influence in stabilizing the β phase of Ti. As Equation 1.2. displays, Fe nearly is 3 times stronger at stabilizing the β phase in comparison to Mo. Interests in reinvestigation the W component of the Mo equivalency equation arises from the inconsistencies with respect to the reported phase diagram of the Ti ï W binary system. Therefore, the motivation behind the reinvestigation the Ti ï W binary system using LENS^{TM} technology is to bypass the historical challenges that have hindered a greater understanding of this system (e.g. solute segregation, slow diffusion rates, high density W ï based inclusions). This approach in characterized by very high solidification rates approaching rapid solidification (10^2Ks^{-1} ï 10^3Ks^{-1}). This is realized by conduction of heat through the substrate (Ti ï 6Al ï 4V for this study), the temperature of the substrate as successive layers are built, and the energy of the laser.

With respect to both the Ti ï Fe and Ti ï Fe ï Al systems, Figure 1.1.B and Figure 1.2. respectively, sufficient knowledge of the Ti ï rich corner of these diagrams is rather limited. Much attention by Raghavan, Gosh, and Siebold [13] has focused on high temperature isothermal sections that explore the existence of attractive ternary phases and their homogeneity ranges with respect to the Fe and Al rich regions of the Gibbs triangle. These efforts have resulted in a liquidus surface projection, partial and full isothermal sections that range from 800 ï 1300°C. Further, literature is lacking regarding studies of isothermal sections below the mentioned isothermal sections and even more so with respect to microstructure and properties of the ternary system. With the exception of a partial 550ÁC isothermal section (Ti ï

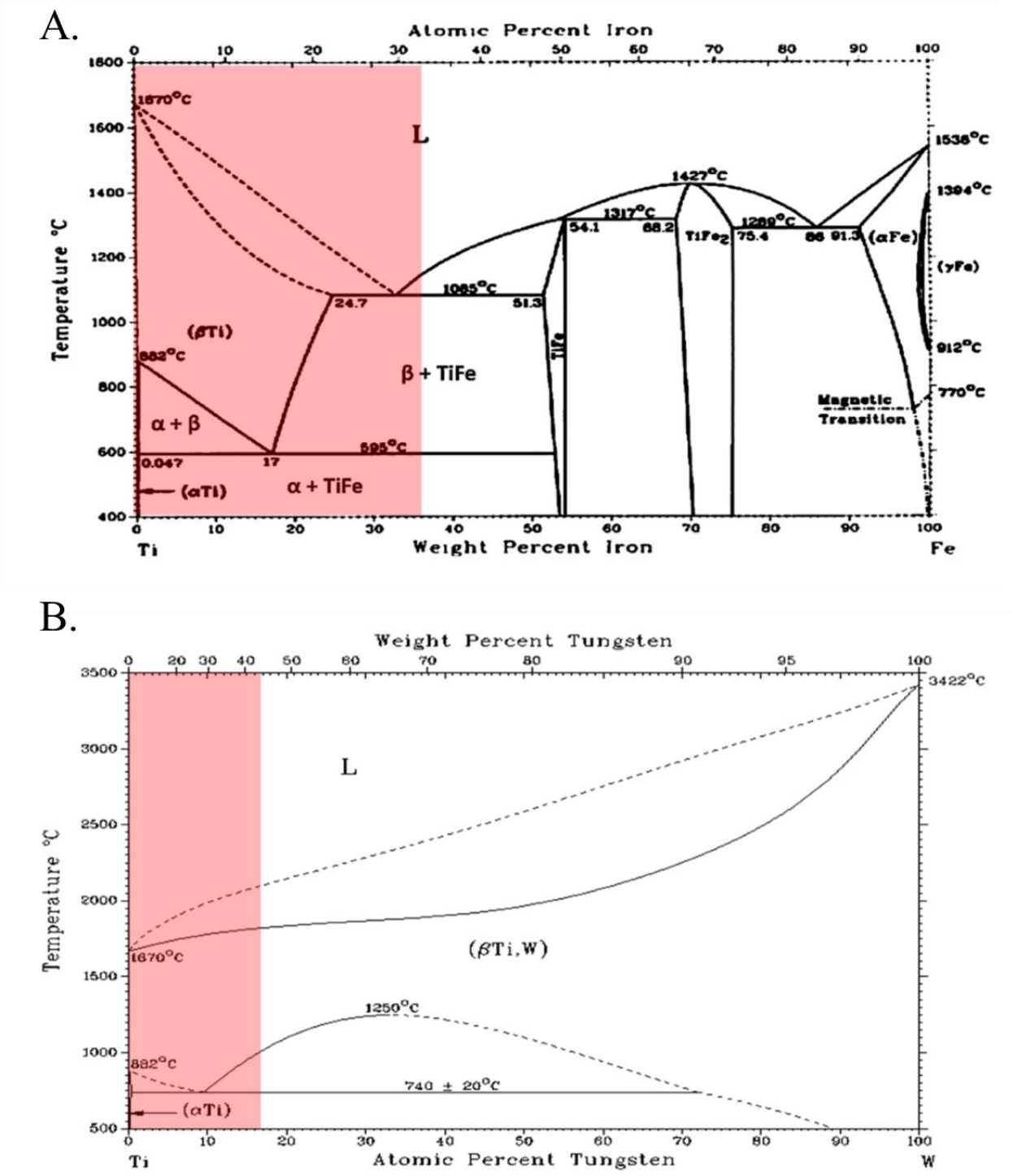

Figure 1.1. (A) Ti ï xFe binary phase diagram with highlighted composition range of interest. (B) Ti xW binary phase diagram with highlighted composition range of interest.

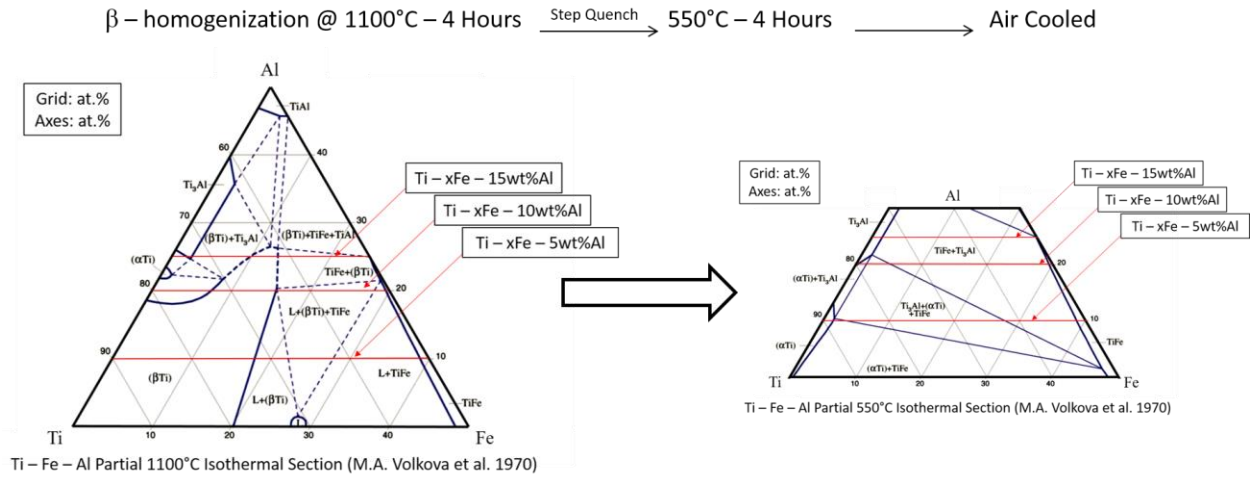

Figure 1.2. Diagram of heat-treatment operation performed to explore the theoretically postulated phase boundaries of the 1100°C partial isothermal section and the 550°C partial isothermal section for the directly aged temperature of the Ti – *x*Fe – *y*Al LENS^{TM} deposited specimens.

rich,100at.%Ti – 50at.%Fe – 50at.%Al) provided by Volkova et. al *(see Figure 1.2.)*, recent efforts in exploring the phases compositions and volume fraction as a function of thermal history is lacking. Therefore, an exploration of these unexplored phase fields will be assessed in a manner similar to what is displayed Figure 1.2.

An assessment of the influence of thermal history on resulting microstructure of a compositionally graded specimen will be performed by a using a two powder feedstock Optomec LENS^{TM} 750 at the University of North Texas. Obtaining a clear understanding of the composition – microstructure – property relationships in these simple systems will allow for a greater understanding of the influences of each element when exploring complex multicomponent systems for alloy development.

CHAPTER 2

BACKGROUND AND LITERATURE REVIEW

2 Background

2.1 Metal Additive Manufacturing

Traditional metal manufacturing follows a subtractive approach. This process requires dedicated tools for fashioning intricate and customizable components. This methodology of part fabrication is costly and wasteful yet has remained the standard in the metal manufacturing industry. Specifically, the cost of fabricating a part from billet or plate material is rather wasteful and usually requires additional tooling.

Metal additive manufacturing (AM) has emerged as a promising alternative to conventional metal manufacturing techniques [18], [28], [29], [31]. With the potential to revolutionize the metal manufacturing industry, AM has also attracted a lot of attention in the scientific community due to the freedom of design capabilities. Additive manufacturing is a general term that encompasses a collection of layer – by – layer building strategies that provide complex components from a design file (i.e. CAD). General advantages of AM consist of relatively inexpensive fabrication of complex and customizable components, parts are also produced directly from design files, the cornerstone of additive technology, reducing the time between conception and product realization, and the cost associated with operation of metallic powders is relatively low. This is highly attractive in the fabrication of metal components for aerospace applications. Specifically, in the case of titanium alloys which make up a significant percent of components in jet turbine engines and is an expensive class of alloys relative to nickel - based superalloys and specialty steels.

Metal AM systems generally consist of 3 different types of methodologies:

1. Powder-bed methodologies consist for four commonly used techniques:
    - Selective laser sintering (SLS)
    - Selective laser melting (SLM)
    - Direct metal laser sintering (DMLS)
    - Electron beam melting (EBM)

    All four powder-bed techniques share the same process of spreading a layer of powder over the previously melted or fused layer. A layer of powder (0.1mm thickness) is typically spread by a blade or roller. The energy source then fuses the layer of powder along the cross section of the build piece or along the parameters of the design file. After the cycle is complete, a layer of powder is spread over the previously fused layer and the process repeats until the specified component is achieved.
2. A wire-fed methodology like electron beam additive manufacturing (EBAM) incorporates an electron beam and wire feedstock inside a vacuum environment to produce near net shape components. This process is relatively faster in realization of the finished product while maintaining high level of efficiency. Another advantage afforded to wire-fed EBAM is that the process occurs under vacuum reducing the imperfections caused by oxidation. But requires post processing in the form of surface finishing and
3. Powder-fed rapid prototyping methodologies include laser engineering net shaping (LENS^{TM}) and electron beam additive manufacturing (EBAM). This system as the name implies, operates by feeding powder into a stream that converges on the power source. A feedstock system typically consists of 2 – 4 hoppers for composition control, and the powders are streamed from these hoppers into the deposition head of the system by an inert

gas in the case of laser engineering net shaping (LENS^{TM}). These systems also include an X-Y table that raster relative to the deposition head that moves vertically creating successive layers of the sliced design file. This layer-by-layer process is continued until part completion. An advantage to powder-fed systems is the ability to create compositionally net shaped specimens by adjusting the mass flow rate of elemental blends introduced to the power source. This flexibility in design has attracted much attention in the field of alloy development.

Commercially available alloys suitable for additive manufacturing using metal powders include stainless steels, aluminum, Inconel, cobalt-chrome, and titanium (Ti – 6Al – 4V and Ti – 6Al – 4V ELI). Additionally, they're over 25 metallic powders available to for metal powder systems. It is important to note that a porosity that does occur in the additively manufactured components and a HIP (Hot Isostatic Pressing) process is required to eliminate porosity.

2.2 LENS^{TM} Technology

As previously mentioned, AM technologies, digital design driven production techniques, have become increasingly attractive because of the benefits listed in Table 2.1. when compared to traditional metal manufacturing techniques (e.g. subtractive). One such system is the Laser Engineering Net Shaping (LENS^{TM}) system. Laser Engineering Net Shaping (LENS^{TM}) was developed at Sandia National Laboratories and has since been commercialized and disturbed by Optomec.

Table 2.1 List of benefits afforded to additive manufacturing (AM).

Feature	Benefit
Digital Data Driven	Faster Time To Market
Reduced Process Steps	Reduced Operation Cost and Time
Additive Methodology	Lower Material Waste
Properties	Improved Product Performance
Novel Geometries	Mass Customization

The Optomec LENS^{TM} system consists of a four copper nozzle assembly which metal powder is injected into a melt pool produced by a high power laser source. Specifically, a powder feedstock controls the mass flow of powders that are introduced to an argon gas that carries elemental and/or elemental blends of powder through the deposition head that expels these powders onto the focus of the laser beam. The laser source (Nd:YAG or Fiber Optic CO_2) simultaneously liquefies the metal powders and locally creates a melt pool on the substrate fixed to a X-Y motion control stage. The liquefied powder is then introduced to the local melt pool and is rapidly solidified as the X-Y stage raster along the geometry of the design file parameters for each designated layer. After each layer, the deposition head is moved along the Z – direction creating successive layers of the component until completion.

2.3 Physical Metallurgy of Titanium Alloys

2.3.1 Classification of Titanium Alloys

Elemental Ti exists in more than one crystallographic structure. The stable room temperature phase of Ti consists of the hexagonal closed – packed (*hcp*) crystal structure. Upon heating above 882°C, pure Ti becomes denser and transforms martensitically (*massive*) to the body centered – cubic (*bcc*) structure. These two structural variants of Ti are commonly known as the *hcp* - α and *bcc* - β phase (*see Table 2.2. for lattice parameters and crystal structure information*).

Solute additions to elemental Ti act to control the temperature at which this phase transformation occurs. Specifically, Al, O, and Ga (special metals) stabilize the α phase and increase the temperature at which the β phase becomes stable. Conversely,

Table 2.2. Crystal structure and lattice parameters of the allotropic forms of Ti.

Ti					
Phase	**Crystal Structure**				**Lattice Parameters (nm)**
	P	SN	PS	SG	
a - Ti	Mg	A3	hP2	P63/mmc	$a = 0.295$ $c = 0.468$
b - Ti	W	A2	cI2	Im-3m	$a = 0.330$

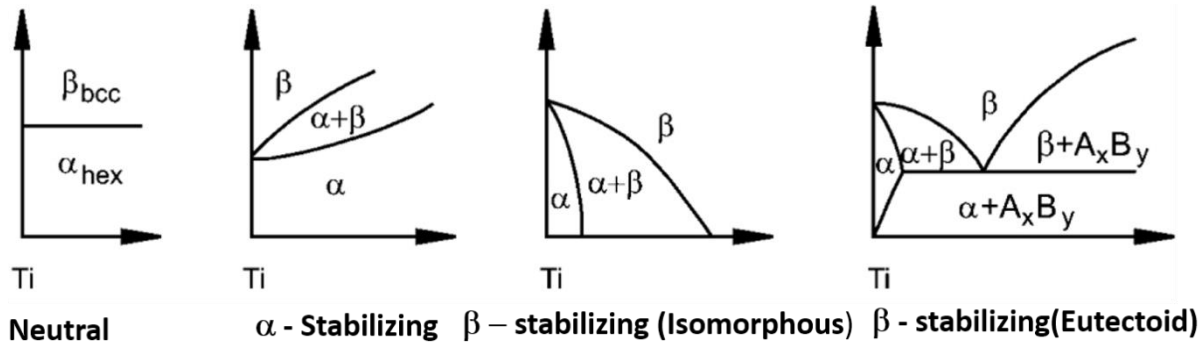

Figure 2.1. Effect of alloying elements on phase composition.

transition metals (Mo, V, Fe, W, and Nb) denoted as "β stabilizers", decrease the temperature at which the β phase is stable. A subcategory of β stabilizers shown in Figure 2.1. exists; β – isomorphous and β – eutectoid formers. β - isomorphous formers consists of solute additions to elemental Ti like V, Zr, Mo, and Hf. These elements are soluble in the β phase. The β - eutectoid group forms eutectoid systems with transformation temperatures far lower than the α → β transformation temperature of elemental Ti. The temperature at which Ti transforms from

hexagonal closed packed to body-centered cubic is commonly known as the β - transus. The β - transus represents the lowest equilibrium temperature at which 100% of the β phase is stable. With this understanding, engineered Ti based alloys can be classified into the following categories:

- α
- α + β
- β

2.3.1.1 α alloys

Technical α alloys typically consist of the a as the dominate phase with trace amounts of β. The small amounts of β phase present to α + β and β alloys are due to the trace amount of Fe found in the processing of titanium sponge. Generally, commercially pure Ti, α, and near α (alloys with relatively low amounts of β stabilizers and large quantities of α stabilizers) alloys exhibit high corrosion resistant qualities and demonstrate improved weldability when compared to other alloys of the Ti system. Additionally, these alloys possess good creep resistance relative to α + β and β alloys. α alloys are limited with respect to strengthening through heat treatments because the microstructure of these alloys stays mostly α or all α.

2.3.1.2 α + β alloys

α + β alloys are engineered when elements that favor the stabilization of both the α and β phase are alloyed with elemental Ti. The chemistry of these alloys are heavier in b stabilizing elements which extends the overall composition of the alloy away from the α phase solvus. This results in microstructures that consist of the β as the dominant phase. This is possible because the β-transus is lowered and it is easier to obtain fully β microstructures before subsequently cooling after solution treating. The advantage attributed to α + β alloys is the ability for these alloys to be

strengthened by transforming the microstructure to complete β by heating through the β transus, then subsequently aging at a temperature below the transus to produce additional changes in the transformed β phase in the form of martensites, acicular α or retained β phase.

2.3.2 β alloys

Metastable β alloys are characterized by the ability to completely retain the metastable β phase upon air cooling and water quenching (thick specimens) to room temperature. Alloys of this classification are relatively richer in β stabilizers than α + β and near β alloys. It is important to note that β alloys are metastable and can form the α phase at slightly elevated temperatures as a means of reaching equilibrium. The metastability of β alloys are exploited to produce principal advantage such as great forgeability, high hardenability, and good formability when solution-treated. It is for the long range tendency of this classification of Ti alloys to transform to an α + β form as the equilibrium state, that most recommended aging practices include direct aging to temperatures of 450 – 650°C after solution treatment forming finely dispersed α particles in retained β.

2.4 Review of Binary Ti – X Systems and the Ti – Fe – Al Ternary System

This section of the thesis is dedicated to a review of the literature regarding the binary Ti – X systems of interest in this study as well as the Ti – *x*Fe – *y*Al ternary system. Specifically, attention is focused on both the proposed equilibrium phase diagrams for each system over the last decade and the currently accepted phase diagrams. With respect to the Ti – *x*Fe – *y*Al ternary system, a review of the accepted and studied isothermal sections, and effect alloying a third element to the binary intermetallic compounds of associated with this system has been reviewed.

Ti, Fe, Mo, and Al are commonly used elements in various Ti alloys. Their characteristics, along with the characteristics of W are provided in Table 2.3.

Table 2.3. Characteristics of commonly found elements in Ti alloys.

Property	**Element**				
	Al	**Ti**	**Fe**	**Mo**	**W**
Atomic number (Z)	13	22	26	42	74
Atomic weight	26.98	47.9	55.845	95.95	183.84
Density (g/cm^3)	2.7	4.506	7.874	10.28	19.25
Electronic ground state configuration	$[Ne]\ 3s^2 3p^1$	$[Ar]\ 3d^2 4s^2$	$[Ar]\ 3d^6 4s^2$	$[Kr]\ 4d^5 5s^1$	$[Xe]\ 4f^{14} 5d^4 6s^2$
Crystal Structure	fcc	bcc → hex	fcc → bcc	bcc	bcc
Allotropic Transformation (°C)	-	882	912	-	-
Melting Temperature (°C)	660.32	1668	1538	2623	3422
Boiling Temperature (°C)	2470	3287	2862	4639	5930
Enthalpy of Fusion (Δ_{Hf}) kJ/mol	10.71	14.15	13.81	37.48	35.3
Electronegativity	1.61	1.5	1.83	2.16	2.36
Metal Radius (nm)	0.143	0.147	0.126	0.139	0.139

2.4.1 Review of the Ti – Mo Binary System

Mo, an isomorphous β stabilizer, is one of the most significant and commonly used β stabilizers. Other than V, Mo has the largest influence on stabilizing the β phase and therefore is a common alloying element in all categories of Ti based alloys. The early investigations of the Ti – Mo system involved the composition of ~10wt.%Fe. In this study, various heat treatment operations were performed to study the microstructural response as a function of aging. It was concluded that upon aging at low temperatures, the ω phase formed, while precipitation of the α phase at β grain boundaries resulting in an alternating formation of α and β platelets was observed

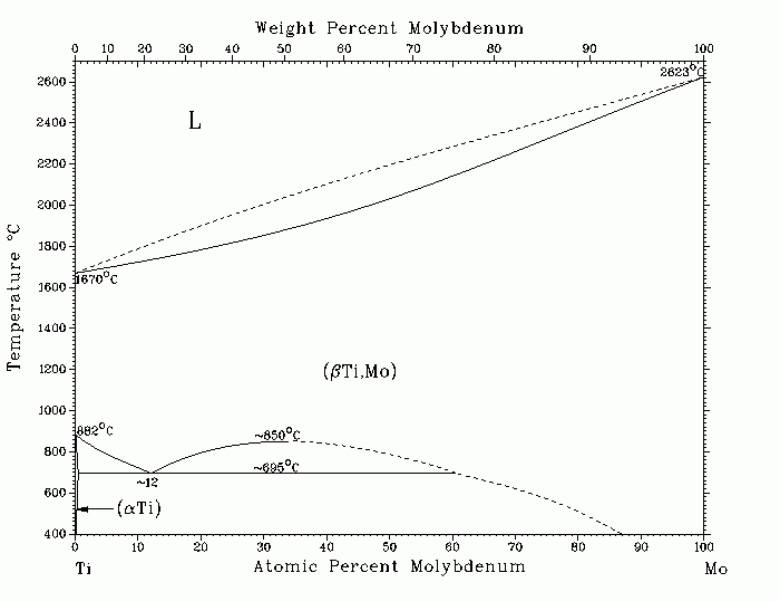

Figure 2.2. Binary Phase Diagram for Ti – Mo Binary system [1987Murry]

from aging at higher temperatures by 1968Blackburn. Additional literature investigating the Ti – Mo system by Furhara et al. focused on aging Ti – *x*Mo specimens of 10, 20, and 30wt.% at varying temperatures. The results of this investigation showed that the volume fraction of αTi reduces as a function of Mo content. S. Terauchi et. al (1977 – 1978) first proposed a phase diagram showing a monotectoid like reaction in the Ti – Mo binary system. G. Rubin and A. Finel then proposed the existence of ordering reactions in the beta phase prior to phase separation. Finally, Furuhara et. al. proposed that alpha precipitation begins at beta grain boundaries with the initiation of side plates that grow into the interior of the grain from the grain boundary for alloys in this system consisting of 10, 20, and 30wt.%Mo. Additional literature investigating the Ti –Mo system by Furhara et. al showed that the volume fraction of αTi reduces as a function of Mo content.

2.4.2 Review of the Ti – W Binary System

The currently accepted equilibrium phase diagram presented in Figure 2.3. is from 1987Murray assessment of the Ti – W binary system. Literature from 1987Murray provides a phase diagram that has a sluggish monotectoid reaction at 740°C shown below:

$$\beta \rightarrow \alpha + \beta_1$$

It is also shown in the phase diagram presented in Figure 2.2. that Ti and W exhibits mutual solid solubility in the β phase field at temperatures between the solidus and the critical temperature (1250°C) of the β miscibility gap. This system is also characterized by a miscibility gap in the β phase where β decomposes by the following reaction shown below:

$$\beta \rightarrow \beta_1 + \beta_2$$

Decomposition of the β phase into $\beta_1 + \beta_2$ consists of solute lean β_1 and solute rich β_2. The results of 1987Murray assessment also observed both closed pack hexagonal α' and orthorhombic α'' martensitic structures at W compositions of $0<x>9$wt.%W and $9<x>14$wt.%W respectively. The current phase diagram differs significantly from the previous assessments by Elliot, Hansen, and Shunk. These evaluations relied heavily on the initial diagram proposed by 1952May. In his initial assessment of the system, his results proposed that the β miscibility gap persisted up to a peritectic reaction at 1800°C:

$$L + W \rightarrow \beta\text{-Ti}$$

But this postulation was later refuted by the metallographic and X – ray analysis provided by 1968Rud. The results of 1968Rud assessment of the system showed that there existed a complete range of solid solutions (β-Ti, W) above the currently accepted critical point (1250°C) of the bcc miscibility gap.

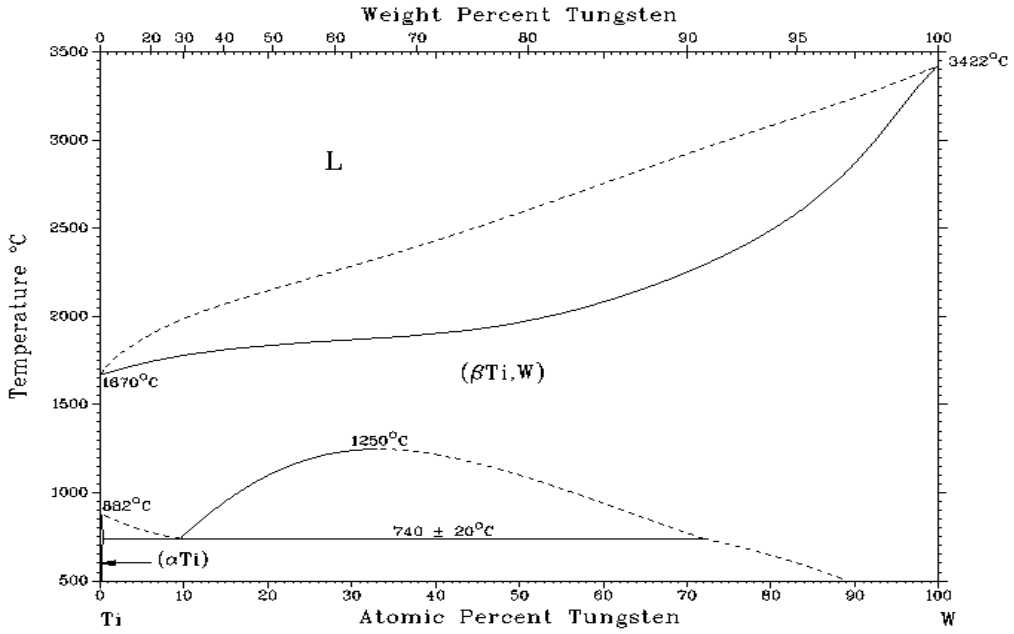

Figure 2.3. Binary Phase Diagram for Ti – W Binary system 1987Murry

2.4.3 Review of the Ti – Fe Binary System

The Ti rich corner of the Ti – Fe binary system (*see the binary phase diagram in Figure 2.4*) is characterized by the eutectoid decomposition of β-Ti for ~17wt%(14.94at.%)Fe at 595°C, given below:

$$\beta \rightarrow \alpha + TiFe$$

The maximum solid solubility of Fe in β-Ti is reported to be less than 0.5wt.%(0.43at.%)Fe. The *bcc* β-Ti phase can be fully retained in alloys containing a minimum of 4wt.%(3.45at.%)Fe upon quenching from the β phase field. The maximum solid solubility of Fe in βTi is 24.7wt.%(21.95at.%)Fe at the eutectic temperature of 1080°C. Along with the α–Ti and β–Ti solid solutions, the Ti – Fe binary phase diagram depicts two stoichiometric intermetallic compounds. The first intermetallic compound, TiFe, adopts a B2 cubic structure of the prototype

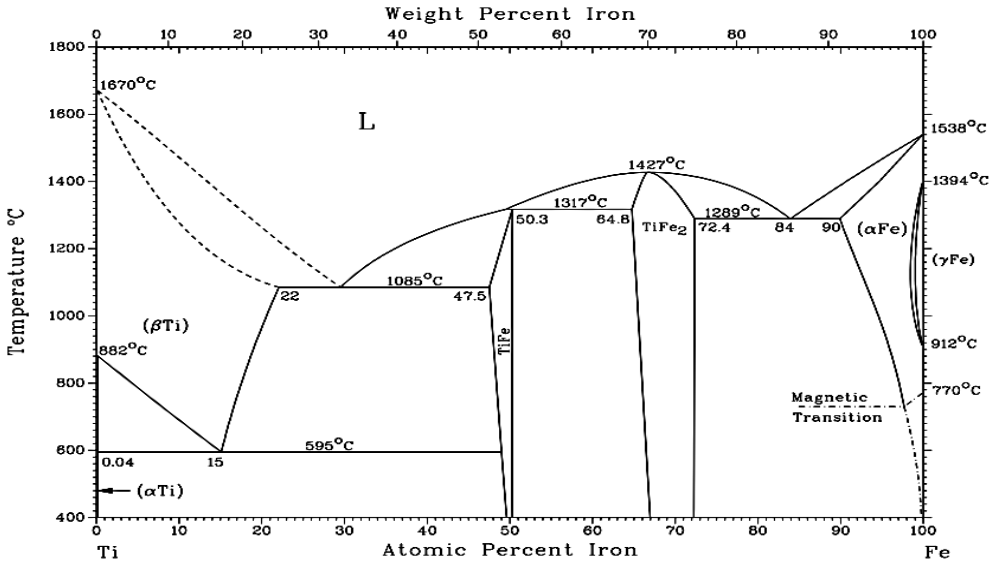

Figure 2.4. Binary Phase Diagram for Ti – Fe Binary

CsCl. Using compression testing, Schlieter et al. determined the Young's modulus of TiFe could range from 110 to 177 GPa. This was also confirmed by R.J. Contieri et al. who measured the modulus using nanohardness. Interestingly, the TiFe intermetallic compound is often studied due to its ability to store hydrogen. TiFe can absorb reversibly up to 1.9wt% hydrogen and is a prominent representative of a class of AB – type alloys known for electrochemical charging and discharging. Previous assessments of the Ti – Fe binary system by Schlieter et at. and Das et al. were aimed at controlling the morphology and size of eutectic colonies (β–Ti with Fe in solid solution + (B2)TiFe) to improve ductility in eutectic alloys exhibiting highly refined microstructural features. Schlieter et al. results showed that with varying solidification conditions, it was possible to modify the size and morphology of the eutectic structure. Additions of Sn to Ti – 27wt.%(24.08at.%)Fe alloys produce microstructures with ultra-fine eutectic distribution of supersaturated β-Ti + (B2)TiFe.

The solubility of Ti in αFe is 8.7wt.%(10at.%)Ti at 900°C when considering the Fe rich corner of the Ti – Fe binary system. The second intermetallic compound and most thermodynamically stable is the cph Laves - phase $TiFe_2$ (C14). Crystal structure data for the binary system provided in Table 2.4. shows that TiFe2 exhibits a homogeneity range from 67.94 - 75.37wt.%Fe. $TiFe_2$ exhibits magnetic properties that are strongly dependent upon the composition of the intermetallic. Specifically, $TiFe_2$ is antiferromagnetic at compositions rich in Ti while exhibiting ferromagnetic transition when the composition of $TiFe_2$ is richer in Fe content.

Table 2.4. Crystallographic data of solid phases in the Ti – Fe Binary System.

Phase	**Composition (wt.% Fe)**	**Pearson Symbol**	**Space Group**	**Prototype**
αTi	0 - 0.05	*hP2*	$P6_3/mmc$	Mg
βTi	0 - 24.75	*cI2*	*Im*-3*m*	W
TiFe	51.85 - 54.04	*cP2*	*Pm*-3*m*	CsCl
$TiFe_2$	67.94 - 75.37	*hP12*	$P6_3/mmc$	$MgZn_2$
αFe	91.30 - 100	*cI2*	*Im*-3*m*	W
γFe	99.49 - 100	*cF4*	*Fm*-3*m*	Cu

2.5 Review of the Ti – Fe – Al Ternary System

The Ti – Fe – Al ternary system, much like that of the Ti – Nb – Al and other Ti – X – Al (X = β stabilizing transition metal) systems have become the focus of much attention for development of Ti based alloys that may extend the service limit at elevated temperatures. Experimental efforts by Volkova [1969,1970, and 1971], 1981Seibold, 1995Palm, and 1973Markiv were focused on studying the phase equilibria of this system with the intent of designing materials that improve the ductile intermetallics of the Ti – Al binary system. Unfortunately, the phase equilibria of this system is insufficiently unknown, but a detailed compilation of literature surrounding the results of the various efforts in understanding this system

was performed by 2008Gosh and 1987Raghavan and will be referenced for this literature review. The assessment of this system by Palm, Lacaze, and Volkova were specifically referenced in the overall study of the composition-microstructure-property relationships in the Ti – Fe – Al ternary system.

2.5.1 Effects of alloying a third element to the binary phases of Ti – Fe – Al

2.5.1.1 Ti – Fe

One characteristic of the Ti – Fe – Al ternary system is the large amount of Al that is dissolved in the intermetallic compounds associated with the Ti – Fe binary system. The Ti – Fe binary system consists of two intermediate phases, TiFe (B2 cubic) and $TiFe_2$ (C14, hexagonal). Palm [1995] found in his study of the 1000°C isothermal section of the Ti – Fe – Al system that Al could replace a substantial amount of Fe atoms in (B2)TiFe at 1000°C and provided an equation that describes how the *a* lattice constant of TiFe is altered with increasing Al content.

Equation 2.1. $a = 0.2970 + 0.000507\ (50 - X_{Fe})$ nm

Similar to the (*B2*)TiFe intermetallic compound, Palm also studied the solubility limit of Al in the *C14*Laves – phase $TiFe_2$ and discovered that the maximum solubility of Al is 47.5at.% at 1000°C. He also provided an equation that shows how the *a* lattice constant of $TiFe_2$ increases linearly with increasing alloying of Al. This linearity is limited only to the *a* lattice constant as the *c* lattice constant increases non-linearly.

Equation 2.2. $a = 0.4770 + 0.000506\ (70 - X_{Fe})$ nm

Equation 2.3. $c = 0.7783 + 0.001406\ (70 - X_{Fe}) - [6.78532 \times 10^{-6}\ (70 - X_{Fe})^2]$ nm

Lastly, Palm provided a solubility limit of 22at.%Al in the β phase allotrope of Ti when also alloyed with 15at.%Fe at 1000°C.

2.5.1.2 Ti – Al

Conversely, the solubility of Fe in the intermetallics of the Ti – Al system (shown in Table 2.3.) is severely limited. Specifically, at 1000°C 1.2, 2.5, 0.8, and 1.5at.%Fe can be dissolved in $TiAl_3$, $TiAl_2$, Ti_2Al_5, and Ti_3Al respectively.

2.5.1.3 Fe – Al

The effect additions of Ti to the solid phases of the Fe – Al binary system is similar to Al with respect to the large solubility of Al in the intermetallics of the binary Ti – Fe system and the expansion of their lattice parameters.

2.5.2 Ternary Phases

Of the three ternary phases provided in Table 2.5, only two have been confirmed; primitive tetragonal Al_2FeTi (τ_2,) and cubic Al_8FeTi_3 (τ_3, $L1_2$ structure, $AuCu_3$ type). The third ternary phase, AlFe2Ti (τ_1, cubic) is considered doubtful. When considering 1987Raghavan discussion of the ternary phases that exist in this system, his results varies little from those of 1981Seibold. In this discussion, Raghavan considers the existence of the cubic (τ_1) phase $AlFe_2Ti$ to be doubtful. This is also similar across literature by 1995M. Palm that disputes the existence of the τ_1 ternary phase. 1981Seibold postulated that the formation of the τ_1 phase in his study of the solidification reactions associated with the Ti – Fe – Al system could be related to the heating effects when considering the order-disorder reactions in αFe. Experimental evidence is lacking with regard to 1981Seibold postulation, thus 2002Raghavan disregarded the peritectic formation that would have theoretically supported the existence of the τ_1 ternary phase.

Table 2.5. Crystallographic data of solid phases in the Ti – Fe – Al System.

Phase	**Pearson Symbol**	**Space Group**	**Prototype**
Al	*cF4*	*Fm-3m*	Cu
α - Fe	*cI2*	*Im-3m*	W
γ - Fe	*cF4*	*Fm-3m*	Cu
β - Ti	*cI2*	*Im-3m*	W
α - Ti	*hP2*	*P6$_3$/mmc*	Mg
$TiAl_3$	*tI8*	*I4/mmm*	$TiAl_3$
Ti_2Al_5	*tP28*	*P4/mmm*	Ti_2Al_5
$TiAl_2$	*tI24*	*I41/amd*	$HfGa_2$
TiAl	*tP4*	*P4/mmm*	AuCu
Ti_3Al	*hP8*	*P6$_3$/mmc*	Ni_3Sn
α_1 - Fe_3Al	*cF16*	*Fm-3m*	BiF_3
α_2 - FeAl	*cP2*	*Pm-3m*	CsCl
ε - Fe_2Al_3	*cI16?*		
$FeAl_2$	*aP18*	*P1*	$FeAl_2$
η - Fe_2Al_5	*oC24*	*Cmcm*	Fe_2Al_5
Fe_4Al_{13}	*mC102*	*C2/m*	Fe_4Al_{13}
$TiFe_2$	*hP12*	*P6$_3$/mmc*	$MgZn_2$
TiFe	*cP2*	*Pm-3m*	CsCl
*τ_1 - $TiFe_2Al$	*cF16*	*Fm-3m*	Cu_2AlMn
*τ_2	*cF**	*F-43m*	
*τ_2'	*cF116*	*Fm-3m*	Th_6Mn_{23}
*τ_3 - $Ti_8Fe_3Al_{22}$	*cP4*	*Pm-3m*	$AuCu_3$

2.5.3 Isothermal Sections

Significant efforts in understanding the equilibria associated with the Ti – Fe – Al system have been made with the production of proposed full and partial isothermal sections provided at 1300°C, 1200°C – partial isothermal section of Ti rich corner, 1200°C – partial isothermal section of Al rich corner, 1150°C partial isothermal section, 1100°C – partial isothermal section, 1000C full isothermal section, 900 full isothermal section, 800°C isothermal section, and 550°C partial isothermal section. Of particular interest are the accepted 1000°C and 800°C isothermal sections provided my [1995Palm] and the 550°C isothermal section provided my Volkova. The 800°C isothermal section provided by Palm was experimentally explored using 99.99%Al, 99.97%Fe, and 99.77%Ti to create 59 ternary alloys using the levitation melting method. Aging of these alloys were performed at 1000 and 800°C for 100 and 500 hours respectively, then subsequently quenched in a brine solution.

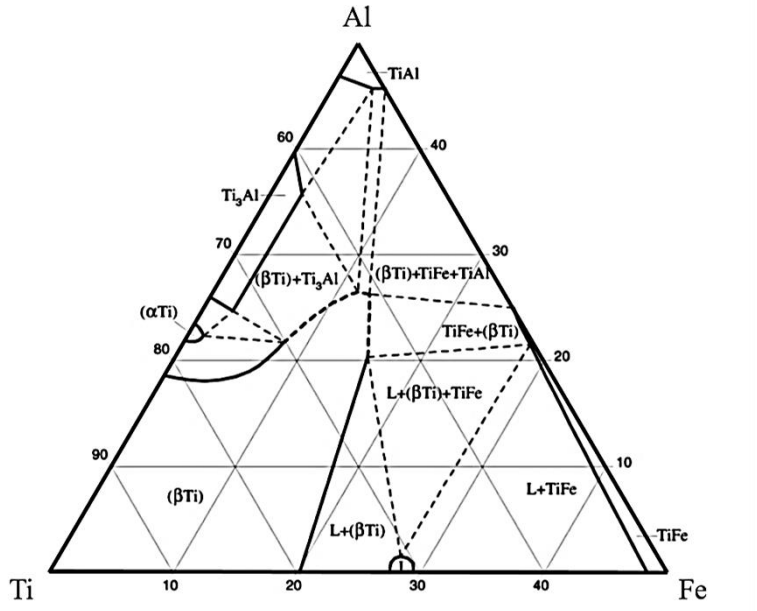

Figure 2.5. Partial Isothermal Section at 1100°C of the Ti – Fe – Al system (M.A. Volkova – 1970).

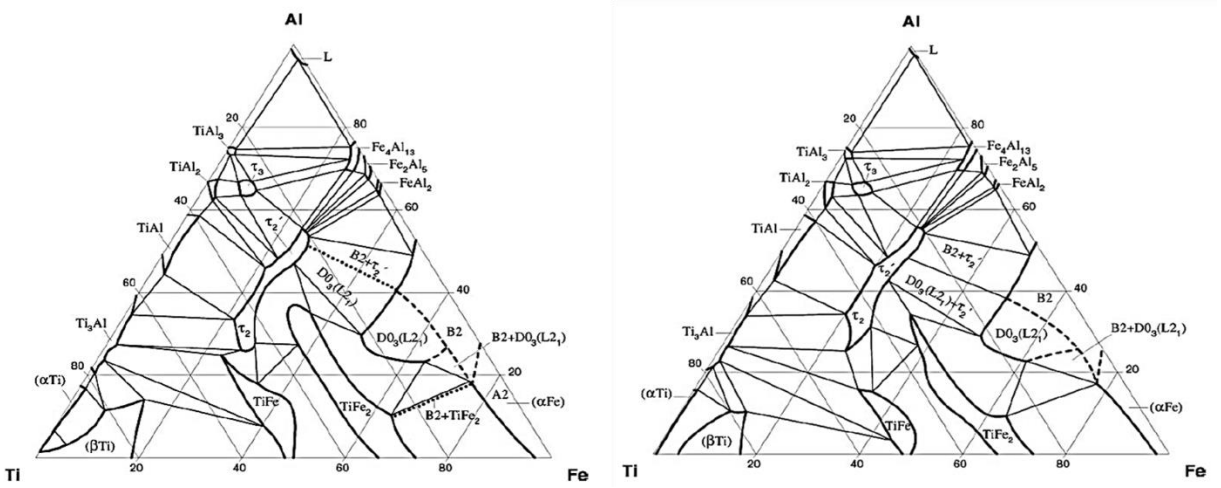

Figure 2.6. Ti – Fe – Al 900°C (left) and 800°C (right) Isothermal Section by 1999Gorzel and 1995Palm, respectively.

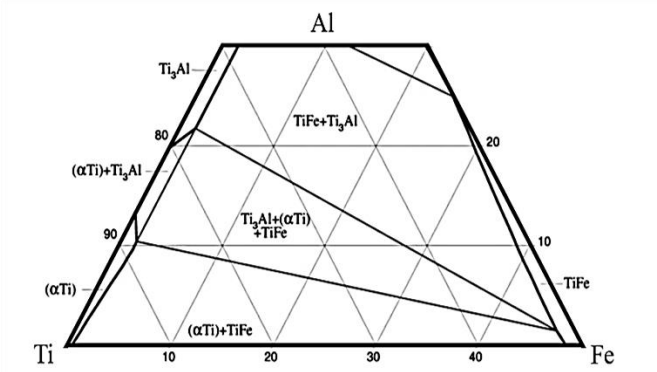

Figure 2.7. Partial Isothermal Section at 550°C of the Ti – Fe – Al system (M.A. Volkova – 1970).

2.5.4 Liquidus Projection

Of the 13 primary areas of crystallization, a number of well-established invariant reactions occur near the Al – rich corner characterizes the liquidus projection of the Ti – Fe – Al ternary system. The isotherms provided in the liquidus projection of the Ti – Fe – Al ternary system shown

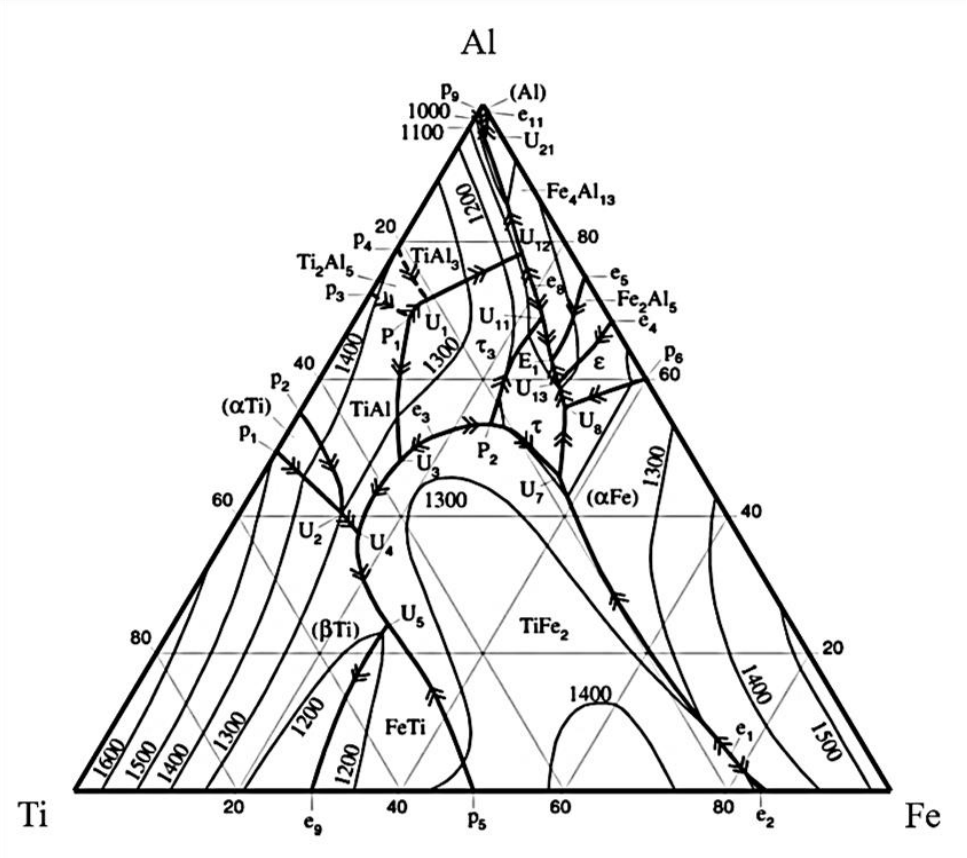

Figure 2.8. Ti – Fe – Al Liquidus Surface Projection (R. Ducher – 2003)

in Figure 2.8. were adopted from the initial study of the solidification reactions by 1981Seibold with later. adaptations to his projection by 1995Palm and Raghavan with regard to the existence of the ternary phase, τ_1. Seibold proposed that the τ_1 ternary phase formed by a ternary peritectic reaction, but was later disputed and disregarded in the updated of the liquidus surface projection by 1995Palm. Additional modifications to the initial liquidus projection were made with respect to the homogeneity range of the τ_2 phase and the occurrence of τ_2 at high temperature and Ti content. Specifically, results from Palm 1995 study of the solidification reactions of the Ti – Fe – Al system showed that the stability of τ_2 widens with a reduction in temperature. His results also showed that the τ_2 phase covers a wider composition than previously reported by 1981Seibold at 800°C. The homogeneity range of 21.0 – 50.0at.%Al for τ_2 at 800°C as well as the occurrence of

τ_2 to separate into two composition islands with varying Ti composition (21 – 31.5at%Ti and 37.5 – 44.0at.%Ti) at 1000°C suggested the addition of a ternary peritectic reaction for Ti rich content. The last modification of the liquidus project was made to accommodate the ordering reaction of disordered β–Ti(A2) to ordered β–Ti(B2) with sufficient Al content in the Ti rich corner of the Gibbs triangle. The ordering formation of βTi(B2) implies a continuous solid solution with the intermetallic compound (B2)TiFe creating a three phase equilibrium between β–Ti + (B2)TiFe + L that extends to the composition at which the eutectic reaction occurs for the binary Ti – Fe system.

CHAPTER 3

EXPERIMENTAL METHODS

3 Experimental Methods

The major experimentations consisted of Material Processing via the LENS^{TM} process, Vickers microhardness indentation testing, and characterization (including SEM and XRD).

This chapter will detail the parameters established for the LENS^{TM} process including the powder size and shape, as well as a detailed list of heat-treatment operations performed. The last section of this chapter will focus on the characterization techniques administered with process parameters for obtaining XRD spectra and experimental setup for acquiring results from Vickers microhardness indentation tests.

3.1 Materials Processing

3.1.1 Laser Engineered Net – Shaping (LENS^{TM})

3.1.1.1 Instrumentation and Processing Parameters

High purity elemental powders provided in Table 3.1. were used to synthesize compositionally graded, Ti – x**X** (**X** = Fe, W, Mo) and Ti – xFe – yAl specimens. Compositionally graded Ti – x**X** and Ti – xFe – yAl specimens were possible using a two-hopper feedstock Optomec LENS^{TM} 750 at the University of North Texas. The LENS^{TM} process for creating laser deposited, three-dimensional specimens, starts by generating a computer – aided design (CAD) file with the desired geometrical dimensions of a 1.25in x 0.40in cylindrical solid.

Table 3.1. Powders used.

Powder	Source	Purity (%)	Size	Shape
Ti	Alfa Aesar	99.9	-150	Spherical
Mo	Alfa Aesar	99.99	< 150	-
Mo	AEE*	99.9	-100	-
W	Alfa Aesar	99.9	-100	Faceted
Fe	Alfa Aesar	99+	-200	-
Al	AEE	99.8	140	-

This design file serves as a tool path where the file is then sliced into layers with a spacing (T_{LS}) of .254mm. On each of these individual layers, the motion control stage will raster parallel lines with a hatch spacing (T_{HS}) of .381mm within the 0.40 diameter layer with respect to the fixed laser head. Elemental blends of powders for each of the compositionally graded alloys specified in Table 3.1. were mechanically mixed using a Penta KB Drive for 24 hours at 453rpm prior to loading in two powder feeders. Specifically, hopper one (H1) consists of elemental Ti while hopper two (H2) contains the targeted composition range for alloy Ti – *x***X** (**X** = Fe, Mo, W) or Ti – *x*Fe – *y*Al. Targeted composition ranges for each Ti – *x***X** binary and Ti – xFe – yAl ternary specimens for this study are presented in Table 3.2. Argon was used to carry both alloyed and elemental blends of Ti powder from their perspective hoppers into the controlled argon atmosphere (glove box). A motor that varies the mass flow of powder from 1 – 10 g/min controls the flow rate of the powders introduced to the laser within the glove box. Both elemental blend and elemental Ti powders are then flowed through the deposition head where the blended powders exit through 4 copper nozzles that converge on the pathway of the laser.

Table 3.2. Targeted composition range.

System	Composition (wt.%)(at.%)
Ti - Mo	Ti - 0<*x*<40wt.% (24.96at.%)Mo
Ti - W	Ti - 30wt.% (10.04at.%)W
Ti - W	Ti - 35wt.% (12.30at.%)W
Ti - W	Ti - 40wt.% (14.79at.%)W
Ti - W	Ti - 0<*x*<40wt.% (14.79at.%)W
Ti - Fe	Ti - 0<*x*<35wt.% (36.37at.%)Fe
Ti - Fe - Al	Ti - *x*Fe - 5wt.%Al (0<*x*<35wt.%)
Ti - Fe - Al	Ti - *x*Fe - 10wt.%Al (0<*x*<35wt.%)
Ti - Fe - Al	Ti - *x*Fe - 15wt.%Al (0<*x*<35wt.%)

A Nd: YAG laser (350 – 650 W) was used to simultaneously intercept the converging blended powders and create a melt pool on a 4.25in x 4.25in x 0.30in Ti – 6Al – 4V substrate for this study. As the blended powders converge on the Nd: YAG laser, with sufficient laser power (P_L), the powders are melted and traverse the pathway of the laser via an argon carrier stream down into the localized melt pool. In a layer-by-layer and line-by-line manner, the computer motion control stage moves the fixed positioned Ti – 6Al – 4V substrate at a specified vector speed/ velocity (V_1). The vector speed of the stage as well as the executed transitions in mass flow rate from each hopper as a function of layers deposited is designated in a preprogrammed Medical Manager DML System Script (DMC) file. This allows for the localized melt pool to fill with the melted blended powder and solidify in a routine comparable to rapid solidification.

Through the LENS^{TM} process, compositionally graded specimens are created by controlling the mass flow rate of elemental blends of powder in each hopper. The optimal mass flow rate for elemental titanium in hopper one (H1) for all binary Ti – *x***X** specimens was held at 3 g/min while the optimal mass flow rate for hopper two (H2) varies across both Ti – *x***X** and Ti – xFe – *y*Al specimens. The variance in mass flow rate for the powders listed in Table 3.1 is due to the

combined flowability of the mixed powders as well as the composition of alloying additions to elemental Ti powder in hopper two (H2). It is important to note the influence of powder processing on the resulting shape of the powders used in this study. All Ti powder from Alfa Aesar were spherical in shape, where all other manufactured powders were created using the hydride – dehydride (HDH) process, which results in a faceted structure as displayed in Figure 3.1. With the established optimal flow rates for each system listed in Table 3.3**.**, the compositional gradient is established by decreasing the optimal flowrate of elemental titanium in H1 by 6.66% and increasing the flow rate of H2 from 0 by 6.66% of H2's optimal flowrate after every 15 layers (one layer = .254mm).

Table 3.3. Deposition Parameters used in this thesis

Alloy	**Powder Flow:**	**Laser Power (Watts):**	**Layer Thickness (mm):**	**Hatch Width (mm):**	**Travel Speed (mm/s):**	**Exposure (MJ/mm^3)**
Ti - xMo	3 – 5	360	.254	.381	8.46	4.39×10^{-4}
Ti - xMo*	3 – 6	459	.254	.381	4.23	10×10^{-4}
Ti - 30wt%W	3 – 4	459	.254	.381	8.46	5.60×10^{-4}
Ti - 35wt%W	3 – 4	459	.254	.381	8.46	5.60×10^{-4}
Ti - 40wt%W	3 – 4	459	.254	.381	8.46	5.60×10^{-4}
Ti - xW	3 – 4	459	.254	.381	8.46	5.60×10^{-4}
Ti - xW*	3 – 4	459	.254	.381	4.23	10×10^{-4}
Ti - xFe	3 – 7	350	.254	.381	8.46	4.27×10^{-4}
Ti - xFe - 5wt%Al	3 – 7	350	.254	.381	8.46	4.27×10^{-4}
Ti - xFe - 10wt%Al	3 – 7	350	.254	.381	8.46	4.27×10^{-4}
Ti - xFe - 15wt%Al	3 – 7	350	.254	.381	8.46	4.27×10^{-4}

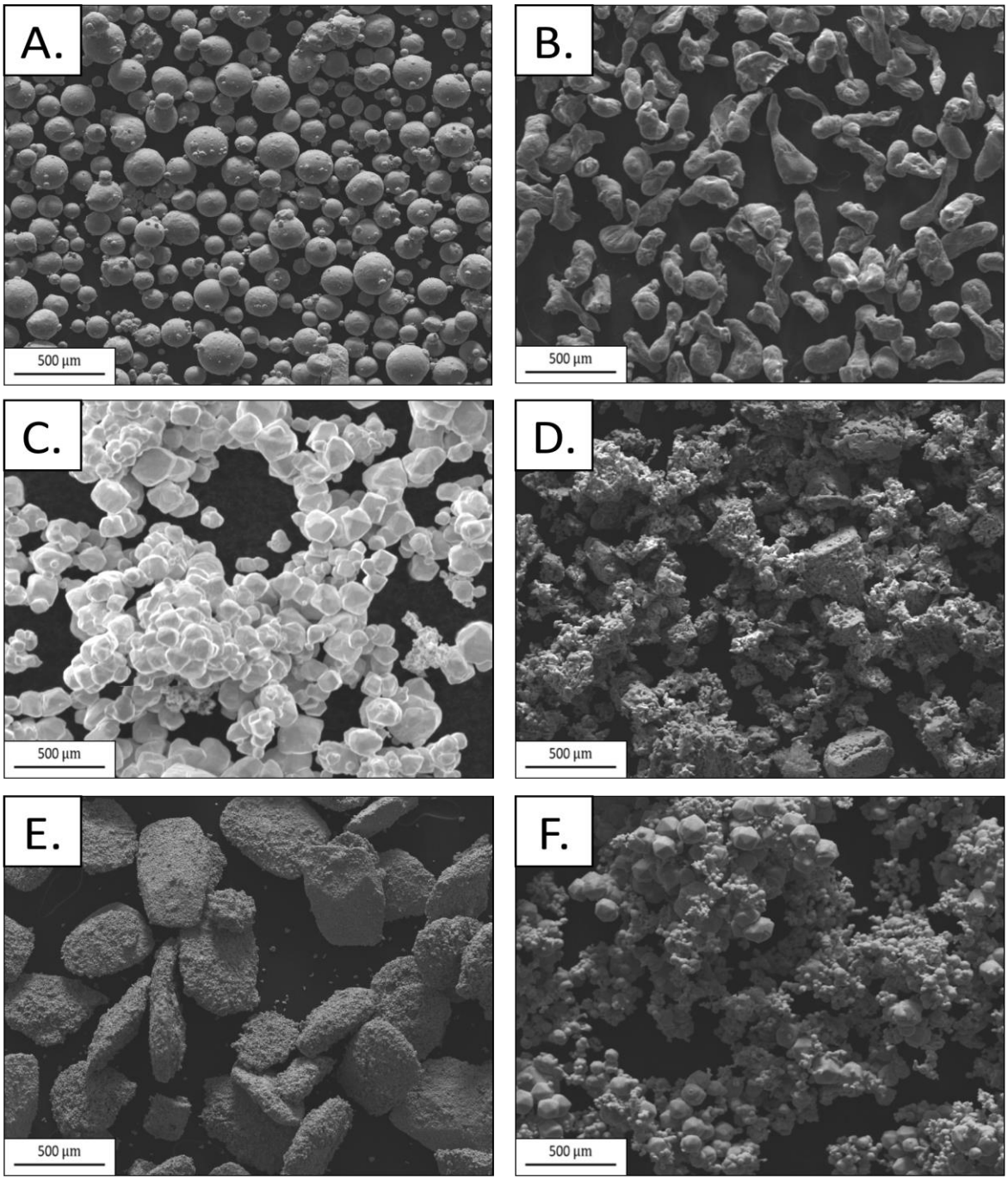

Figure 3.1. SEM Secondary electron micrographs of the powders used in this study. A. Titanium, B. Aluminum, C. Tungsten, D. Iron, E. Molybdenum - AEE , F.

3.2 Heat Treatments

3.2.1 Sample Preparation

Following the sectioning of LENS^{TM} deposited gradients from the Ti – 6Al – 4V substrate, all compositionally graded specimens, as presented in Figure 3.2, were cross-sectioned into fourths and prepared using conventional metallographic techniques.

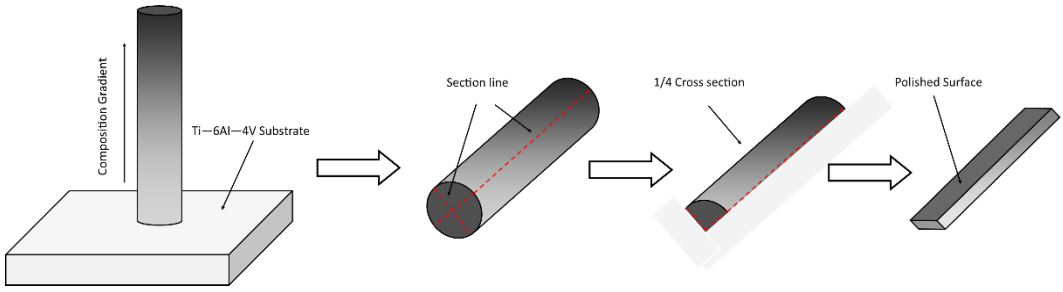

Figure 3.2. Sectioning of LENS^{TM} deposited specimens.

Specifically, a MultiPrep^{TM} system from Allied High Tech was used to grind specimens using a multi step process from 60, 120, 240, 400, 600, and 800-grit SiC abrasive papers. Following the 800-grit step, the surface of each specimen was etched in Kroll's reagent for 10 seconds. After the etchant step in Kroll's reagent, each specimen is final polished on a diamond embedded cloth using 0.04 □m colloidal silica suspension for 35 minutes at 350 rpm. Samples were cleaned using a Branson ultrasonic cleaner in the following series; acetone, water, water + surfactant, water, ethanol, then methanol. The surface of each sample is then rinsed with methanol and immediately dried using compressed air.

3.2.2 Heat-treatment Operations

All prepared samples were encapsulated in fused silica ampules. Each ampule was back filled with argon, evacuated, then back filled with argon and sealed with titanium sponge as an oxygen getter for any residual oxygen in the enclosed atmosphere. All encapsulated specimens were

Table 3.4 Heat – treatment operations performed.

Specimen	β – Homogenization	Step Quench
Ti - 0<*x*<40wt.% (24.96at.%)Mo	975°C for 4 Hours WQ	-------
Ti - 0<*x*<40wt.% (24.96at.%)Mo	975°C for 4 Hours	550°C for 4 Hours AC
Ti - 0<*x*<40wt.% (24.96at.%)Mo	975°C for 4 Hours	650°C for 4 Hours AC
Ti - 0<*x*<40wt.% (24.96at.%)Mo	975°C for 4 Hours	750°C for 4 Hours AC
Ti - 0<*x*<40wt.% (24.96at.%)Mo*	975°C for 4 Hours WQ	-------
Ti - 0<*x*<40wt.% (24.96at.%)Mo*	975°C for 4 Hours	550°C for 4 Hours AC
Ti - 0<*x*<40wt.% (24.96at.%)Mo*	975°C for 4 Hours	650°C for 4 Hours AC
Ti - 0<*x*<40wt.% (24.96at.%)Mo*	975°C for 4 Hours	750°C for 4 Hours AC
Ti - 30wt.% (10.04at.%)W	1000°C 100 Hours	550°C for 50 Hours AC
Ti - 30wt.% (10.04at.%)W	1100°C 125 Hours	650°C for 50 Hours AC
Ti - 30wt.% (10.04at.%)W	1100°C 125 Hours	800°C for 50 Hours AC
Ti - 35wt.% (12.30at.%)W	1000°C 100 Hours	550°C for 50 Hours AC
Ti - 35wt.% (12.30at.%)W	1100°C 125 Hours	650°C for 50 Hours AC
Ti - 35wt.% (12.30at.%)W	1100°C 125 Hours	800°C for 50 Hours AC
Ti - 40wt.% (14.79at.%)W	975°C for 100 Hours WQ	-------
Ti - 40wt.% (14.79at.%)W	1100°C for 50 Hours WQ	-------
Ti - 40wt.% (14.79at.%)W	1100°C for 100 Hours WQ	-------
Ti - 0<*x*<40wt.% (14.79at.%)W*	1100°C for 125 Hours WQ	-------
Ti - 0<*x*<40wt.% (14.79at.%)W*	1100°C for 125 Hours	550°C for 50 Hours AC
Ti - 0<*x*<40wt.% (14.79at.%)W*	1100°C for 125 Hours	650°C for 50 Hours AC
Ti - 0<*x*<40wt.% (14.79at.%)W*	1100°C for 125 Hours	800°C for 50 Hours AC
Ti - 0<*x*<40wt.% (14.79at.%)W*	1100°C for 125 Hours	800°C for 50 Hours WQ
Ti - 0<*x*<35wt.% (36.37at.%)Fe	975°C for 4 Hours WQ	-------
Ti - 0<*x*<35wt.% (36.37at.%)Fe	975°C for 4 Hours	550°C for 4 Hours AC
Ti - 0<*x*<35wt.% (36.37at.%)Fe	975°C for 4 Hours	650°C for 4 Hours AC
Ti - 0<*x*<35wt.% (36.37at.%)Fe	975°C for 4 Hours	750°C for 4 Hours AC
Ti - *x*Fe - 5wt.%Al (0<*x*<35wt.%)	975°C for 4 Hours WQ	-------
Ti - *x*Fe - 5wt.%Al (0<*x*<35wt.%)	1100°C for 4 Hours WQ	-------
Ti - xFe - 5wt.%Al (0 < x < 35wt.%)	1100°C for 4 Hours	550°C for 4 Hours AC
Ti - xFe - 5wt.%Al (0 < x < 35wt.%)	1100°C for 4 Hours	650°C for 4 Hours AC
Ti - xFe - 5wt.%Al (0 < x < 35wt.%)	1100°C for 4 Hours	800°C for 4 Hours AC
Ti - xFe - 10wt.%Al (0 < x < 35wt.%)	1100°C for 4 Hours	550°C for 4 Hours AC
Ti - xFe - 10wt.%Al (0 < x < 35wt.%)	1100°C for 4 Hours	650°C for 4 Hours AC
Ti - xFe - 10wt.%Al (0 < x < 35wt.%)	1100°C for 4 Hours	800°C for 4 Hours AC
Ti - xFe - 15wt.%Al (0 < x < 35wt.%)	1100°C for 4 Hours	550°C for 4 Hours AC
Ti - xFe - 15wt.%Al (0 < x < 35wt.%)	1100°C for 4 Hours	650°C for 4 Hours AC
Ti - xFe - 15wt.%Al (0 < x < 35wt.%)	1100°C for 4 Hours	800°C for 4 Hours AC

subject to a solution heat treatment above the β transus and water quenched to obtain a sol ution treatment time and temperature sufficient enough to fully homogenize the gradient. Once a β – solution time and temperature was established, each specimen was homogenized above the β – transus and subsequently step-quenched to temperatures above or below the invariant point for each of the binary systems. 800, 650, and 550°C isothermal sections were selected as direct aging temperatures for the ternary Ti – *x*Fe – *y*Al specimens following a β – solution step at 1100°C for 4 hours. All step-quenched samples were air cooled upon completion of each heat-treatment. A complete list of all heat-treatment operations performed for this study is presented in Table 3.4 For this study, a Thermcraft tube furnace was used to homogenize each sample above the β – transus and immediately transferred to the adjacent furnace with the desired step quenching temperature.

3.3 Characterization Methods

3.3.1 Scanning Electron Microscopy (SEM

A FEI Quanta 200 environmental scanning electron microscope was used to assess the change in microstructure as a function of composition across the surface of the cross-sectioned specimens. Equipped was an EDAX Sapphire Si (Li) detecting unit, 30mm^2 detector crystal and Genesis software, energy dispersive spectroscopy (EDS) was employed for elemental quantification of the local changes in composition and microstructural features across isothermal sections. EDS was also used to relate composition to the local Vickers Indentation tests across each specimen.

3.3.2 Energy Dispersive Spectroscopy (EDS)

All elemental quantification was carried out using an accelerating voltage of 15kV to prevent the interaction volume of features deeper within the sample. Additionally, the accuracy and sensitivity of this technique limits the overall analytical accuracy to 2% because of factors

such as errors that may occur during the correction of the raw data. Additional factors include errors that may occur due to standard used to calibrate the system as well as large background noise that limits the detection of smaller peaks. For these reasons, elemental quantification of microstructural features in the form of spot scans, lines scan, or full frame scans were performed for longer count times, specifically until 20,000 counts of each element.

3.3.3 X – Ray Diffraction (XRD)

A Rigaku Ultima 3 diffractometer equipped with a CuK_a source was used for phase identification and measurement of lattice parameters. The emitted x – ray wavelength was 1.5418Å while the current and operating voltage was 44mA and 40 kV. X – Ray diffraction experiments were performed with a 2θ range from 20 to 90°. The sample step size and scanning speed parameters for all experiments were 0.10 and 0.80 deg/min respectively. Specimen thickness was ~2.50 mm. The selection slit, divergence height limiting slit and receiving slit box used for this study was 5, 2mm, and 5° respectively. Post processing of the raw. data file was interpreted using JADE 10 software.

3.3.4 Hardness Testing

3.3.4.1 Vickers Microhardness

A Simadzu HMV – S microhardness indenter was used to perform indentation tests across the cross section of the compositional gradients. This method of characterization was used to correlate the mechanical properties of each specimen as a function of composition and microstructure. All testing was performed using a four-sided pyramid tip and each test consisted of a load of 9.807 N for 10 seconds. Specifically, tests were performed in three rows along the length of the LENS^{TM} deposit .5mm apart to prevent the overlapping of plastic deformation fields.

CHAPTER 4

INITIAL STUDIES OF BINARY AND TERNARY TITANIUM SYSTEM

4 Introduction

Compositionally graded alloys selected in this chapter are Ti – *x*Mo (0<*x*<40wt.%), Ti – *x*W (0<*x*<40), Ti – *x*Fe (0<*x*<35), and Ti – *x*Fe – *y*Al ((0<*x*<35wt.%), *y* = 5, 10, and 15wt.%). The Ti – *x*Fe system was selected to first study the composition – microstructure – property relationships in a simple binary system as an initial investigation of the more complex Ti – Fe – Al ternary system. An assessment of how varying additions of Al content influences the microstructure - property relationship in the binary Ti – Fe system would allow for a better understanding of multi-component systems based upon additions of Ti, Fe, and Al. The Ti – Fe – Al ternary system was selected because Al provides low density while strengthening the α phase and Fe additions as a solid solution strengthener ductilizes the β phase. Additionally, alloying Al would extend the α/β interactions within the solute lean regions of the compositionally graded specimen. Furthermore, assessing the relationships in the Ti – Fe – Al ternary system would isolate the effects of alloying additions such as Fe and Al on the microstructure and resulting properties. Lastly, the Ti – Fe – Al ternary system possesses high symmetry ternary phases that are attractive for high temperature applications.

4.1 Motivation

The Ti – *x*W LENS^{TM} deposited specimen has been characterized with the goal of using the LENS^{TM} process to demonstrate this methodology of additive manufacturing as a feasible approach to studying a system that has historically been difficult to realize using traditionally metal manufacturing practices. This study also includes the influence of additive manufacturing

processing, specifically Laser Engineering Net shaping (LENS^{TM}), on the resulting as – deposited product of a compositionally graded Ti – *x*W (0<*x*<40wt.%) specimen. Additionally, Indentation tests with performed to assess the Vickers microhardness as a general correlation of mechanical properties as the varying composition (wt.%W) influences the resulting microstructure. Lastly, this system was chosen to compare with the Ti – Mo system with respect to reassessing the ability of W to stabilize the b phase in the Mo equivalency equation.

The Ti – Fe binary system has been characterized at 3 isothermal sections to assess the microstructural evolution of the intermetallic compound (B2)TiFe as an initial step in ultimately gaining a better understanding of the composition – microstructure relationships of a compositionally graded Ti – *x*Fe – *y*Al alloy that contains up to 35wt.%Fe. The principle characterization of the Ti – *x*Fe – *y*Al is to assess the precipitation of the ordered compounds Ti_3Al, (B2)TiFe, and (B2)β-Ti.

4.2 Ti – Mo and Ti - W

4.2.1 Introduction

Efforts in alloy development over the last decade involving Ti alloyed with the two Group 6a elements, Mo and W, has emphasized exploiting the potential of alloys that exhibit good high temperature strength and improved ductility at lower temperatures. The favorable attributes of Mo and W include high moduli of elasticity and high melting temperatures. Unfortunately, like most *bcc* elements, W and Mo exhibit a ductile-brittle transition at ~0.15T_m which limits their effectiveness in service. Additionally, these are two elements that are prone to solute segregation when alloyed using traditional methods. Both W and Mo have rather high densities as shown in Table 2.1.; 19.25 and 10.28 g/cm^3 respectively. But this is ignored due to the previously mentioned attributes and their high temperature strength to density ratio. This chapter is dedicated to

imploring the LENS^{TM} process as a means to bypass the historical challenges (i.e. solute segregation, long homogenization times) in alloying W with Ti as well as exploring higher concentration of W as it relates to the binary phase diagram; a system that has been largely neglected over the years. This chapter will include an assessment of the composition – microstructure – relationships in Ti – *x*W alloys as well as a reassessment of the molybdenum equivalency.

4.2.2 Experimental Methods for the Ti – Mo and Ti – W Systems

Compositionally graded specimens were created using an Optomec LENS™ 750 at the University of North Texas. Equipped with a dual powder feeder system, each hopper, designated PF#1 and PF#2, are utilized to create a gradient alloy ranging from a preselected initial and terminal compositions provided in Table 4.1. For these studies, PF#1 (i.e., powder feeder #1) contains titanium powder while PF#2 (i.e., powder feeder #2) contains a blend of elemental powders with a target composition specified in Table 4.1. The powders sourced for this study are detailed in Table 4.2 A LENS™ deposit is created by introducing a blended powder with "x" composition in PF#2 and elemental titanium in PF#1 into the melt pool produced using an Nd:YAG laser operating at a wavelength of 1.064 μm. By independently controlling the mass flow rates of the two powder feeders, it is possibly to vary the relative amount of powder fed into the melt pool from each powder feeder. The depositions are made onto a Ti – 6Al – 4V substrate. Following deposition, the gradient sample is then cut from the substrate, sectioned into quarters, ground and polished using conventional metallographic polishing techniques, and lastly encapsulated in quartz glass ampules. Each sample is backed filled with 1/3 atmosphere argon and encapsulated with titanium sponge to act as an oxygen getter during the heat treatments. These encapsulated samples

Table 4.1 Alloy systems and their targeted composition range

Alloy System	Composition (wt.%)
Ti – xW	0 < x < 40
Ti – xMo	0 < x < 40
Ti – xFe	0 < x < 30

Table 4.2 Powders used for this study.

Powder	Source	Purity (%)	Mesh Size
Ti	Alfa Aesar	99.99	-150
Mo	AEE	99.9	-100
Mo*	Alfa Aesar	99.9	<150
W	Alfa Aesar	99.9	-100

Table 4.3. Heat – treatment operations performed for the Ti – W and Ti – Mo systems.

Specimen	β – Homogenization	Step Quench
Ti - 0 < x < 40wt.% (24.96at.%)Mo	975°C for 4 Hours WQ	-------
Ti - 0 < x < 40wt.% (24.96at.%)Mo	975°C for 4 Hours	550°C for 4 Hours AC
Ti - 0 < x < 40wt.% (24.96at.%)Mo	975°C for 4 Hours	650°C for 4 Hours AC
Ti - 0 < x < 40wt.% (24.96at.%)Mo	975°C for 4 Hours	750°C for 4 Hours AC
Ti - 0 < x < 40wt.% (24.96at.%)Mo*	975°C for 4 Hours WQ	-------
Ti - 0 < x < 40wt.% (24.96at.%)Mo*	975°C for 4 Hours	550°C for 4 Hours AC
Ti - 0 < x < 40wt.% (24.96at.%)Mo*	975°C for 4 Hours	650°C for 4 Hours AC
Ti - 0 < x < 40wt.% (24.96at.%)Mo*	975°C for 4 Hours	750°C for 4 Hours AC
Ti - 30wt.% (10.04at.%)W	1000°C 100 Hours	550°C for 50 Hours AC
Ti - 30wt.% (10.04at.%)W	1100°C 150 Hours	650°C for 50 Hours AC
Ti - 30wt.% (10.04at.%)W	1100°C 150 Hours	800°C for 50 Hours AC
Ti - 35wt.% (12.30at.%)W	1000°C 100 Hours	550°C for 50 Hours AC
Ti - 35wt.% (12.30at.%)W	1100°C 150 Hours	650°C for 50 Hours AC
Ti - 35wt.% (12.30at.%)W	1100°C 150 Hours	800°C for 50 Hours AC
Ti - 40wt.% (14.79at.%)W	975°C for 100 Hours WQ	-------
Ti - 40wt.% (14.79at.%)W	1100°C for 50 Hours WQ	-------
Ti - 40wt.% (14.79at.%)W	1100°C for 100 Hours WQ	-------
Ti - 0 < x < 40wt.% (14.79at.%)W*	1100°C for 150 Hours WQ	-------
Ti - 0 < x < 40wt.% (14.79at.%)W*	1100°C for 150 Hours	550°C for 50 Hours AC
Ti - 0 < x < 40wt.% (14.79at.%)W*	1100°C for 150 Hours	650°C for 50 Hours AC
Ti - 0 < x < 40wt.% (14.79at.%)W*	1100°C for 150 Hours	800°C for 50 Hours AC
Ti - 0 < x < 40wt.% (14.79at.%)W*	1100°C for 150 Hours	800°C for 50 Hours WQ

were then β – solutionized and subsequently step quenched to the heat treatment operations shown in Table 4.3. followed by air-cooling to room temperature.

The second deposition of the compositionally graded specimens for the Ti – Mo and Ti – W systems were deposited with an exposure of 10 x 10^{-4}. This exposure corresponds to the alteration of parameters prior to the LENS^{TM} process. The first parameter that was changed was the vector speed, $V_{s.}$ The initial vector speed for the first set of deposited specimens was 8.46mm/s, this setting was changed to 4.23mm/s. The vector speed was lowered to allow more time for the melt pool to melt the Mo particles as they are introduced to the melt pool as well as study the influence of vector speed on the dendritic formation in the as deposited Ti – *x*W specimens. This would also aid in the remelting of any partially reacted Mo and W particles when each successive layer is deposited. The second parameter that was altered with regard to depositions for the Ti – *x*Mo alloys was the laser power. The maximum laser power admitted for the Optomec LENS^{TM} 750 at the University of North Texas is 46 amps (488 W). The source of powder incorporated in the deposition of these compositionally graded specimens was from Alfa Aesar *(see Table 4.2 for particle size)*. Prior to blending of the Mo powder with elemental Ti powder to the targeted composition, the Mo powder was sieved and dried to increase the flowability of the powder particles.

Samples were characterized using a Rigaku Ultima III high resolution X – ray diffractometer for XRD phase analysis as well as a FEI Nova NanoSEM 230 equipped with energy dispersive spectroscopy (EDS) for elemental analysis in order to confirm the crystal structures, their lattice parameters and composition, and the distribution of the phases throughout the microstructure. Vickers Microhardness tests were performed using a Shimadzu HMV microhardness tester using a 9.807 N load for 10 seconds. Local compositions of the

microstructure relative to specific indentations were assessed using energy dispersive spectroscopy (EDS).

4.2.3 Ti – *x*Mo

4.2.3.1 Results and Discussion

The initial study of the compositionally graded alloys for the Ti – Mo binary system using a vector speed of 8.46mm/s and powder sourced from Atlantic Equipment Engineers (non-uniform powder size) resulted in inhomogeneous microstructures. Further, partially reacted Mo particles ~150 microns in size are randomly distributed throughout the microstructure of all Ti – Mo LENS^{TM} deposited specimens. In areas closer to these partially reacted particles, the microstructure exhibits very little α phase Ti indicating some degree of local melting, but insufficient time for complete melting. In addition to partially reacted Mo particles, all specimens displayed a "fish scaled" effect. The "fish scale" effect observed in these LENS™ deposited specimens (*shown in Figure 4.1.*) display a redistribution of solute content around the contours of the bands due to successive layering during the LENS™ process. The "scales" represent the overlapping melt pools that have rapidly solidified as the motion control stage raster through the specified design parameters. As each layer is deposited in creating a LENS™ gradient specimen, a portion of each previous layer is re-melted. This, in combination with the complex thermal conditions and solidification phenomenon, can produce this effect for most additively manufactured specimens.

Similar to current literature concerning the study of the Ti – Mo binary system, as the weight percentage of Mo increases (0 to 35 percent), the volume fraction of α–Ti decreases. The

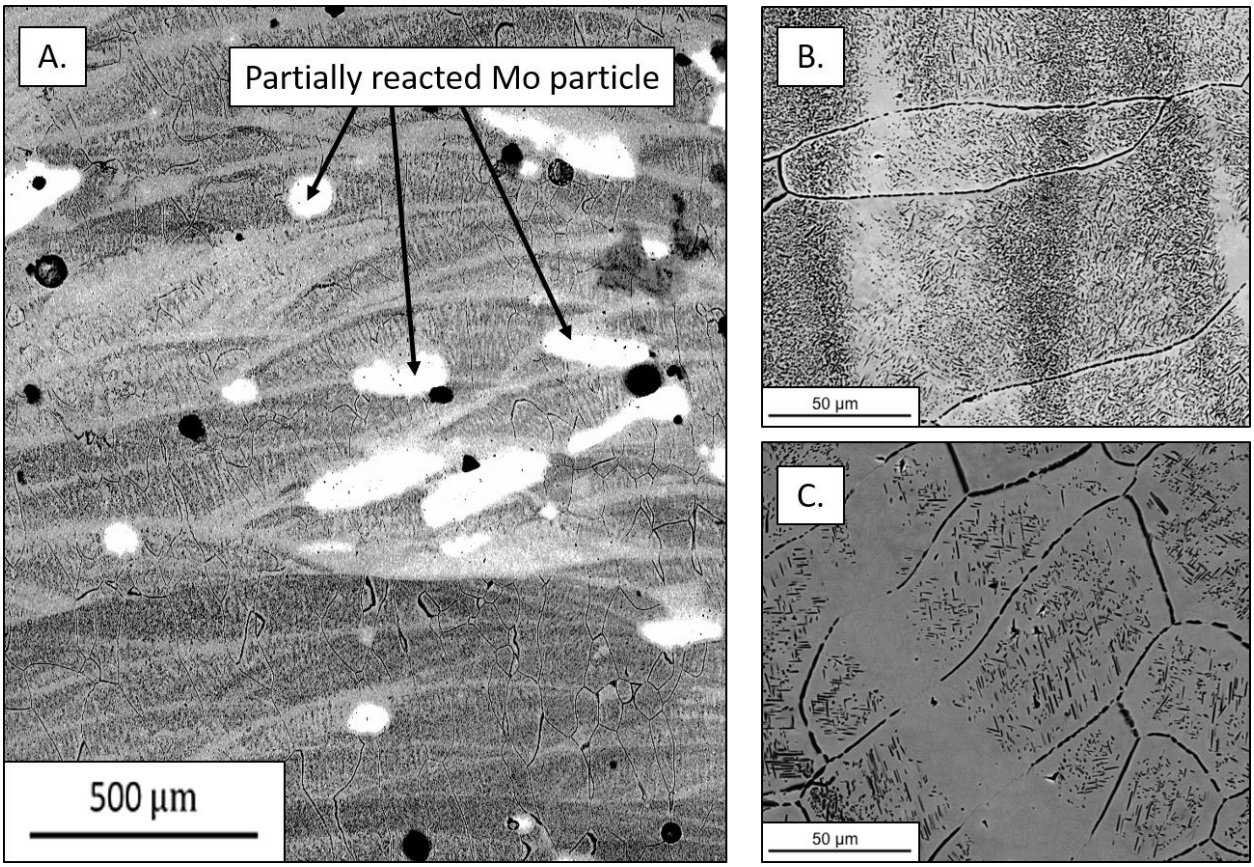

Figure 4.1 Representative backscatter electron micrographs of the LENS^{TM} deposited Ti – *x*Mo (0<*x*<40wt.%) compositionally graded specimen exhibiting a "fish scale" effect in A. as well as higher magnification micrographs of the resulting microstructure in region within these overlapping bands B and C.

micrographs shown in Figure 4.2 illustrates this influence of Mo content on the volume fraction of the α phase. Low compositions of Mo in the 550°C step quenched specimen exhibited a coarse continuous layer nucleated at the grain boundaries. A bimodal distribution of the α phase is observed in these microstructures. Initially there appears to be a depletion region delineating primary α–Ti nucleated at the grain boundaries, but after closer examination, a fine scale precipitation of secondary α–Ti is observed. The 650°C directly aged specimen exhibited influences from the "fish scale" effect within the microstructure shown in figures 4.1.B. and 4.1.C. for Ti – 21.57wt.%Mo and Ti – 30.27wt.%Mo, respectively. Because of the redistribution of solute

content within the layering of the "scales" or overlapping bands, one can see there are distinct areas where there are finer α indicating the average local composition in these regions are higher in Mo content while the appearance of relatively larger α laths in scale correspond to local areas that are lean in Mo content.

Adjustments to the LENS™ deposition parameters for the Ti – xMo alloys were made to address the issue of *partially* reacted Mo particles present in the as deposited alloy. The presence of *such partially* unmelted molybdenum particles significantly alters the local microstructure. Lowering the traverse speed and using 45 amps (459 Laser Power) to melt the Ti – xMo powder blend was used to build a Ti – xMo gradient up to x = 40wt%Mo.

Representative micrographs taken at 50X magnification are shown in Figure 4.3 of the as – deposited Ti – xMo LENS™ sample. In contrast to previously deposited Ti – xMo samples, adjusting the traverse speed and increasing the laser power to 459 from 360 results in a microstructure void of *partially* reacted Mo particles. It is important to note the differences in microstructure. The "fish scale" effect has significantly diminished and the microstructure is significantly more uniform throughout the deposit. There is no redistribution of solute from the overlapping of bands. Figure 4.3 does highlight one area of the LENS™ deposit where a small number of *partially* reacted particles exist. The highlighted region in Figure 4.3 represents a region of the deposit where the program was paused due to the warming of the laser. It is at this point where insufficient fusing of two layers occur. As a result of insufficient fusing, *mostly* melted particles are present because each successive layer insures the melting of particles that weren't melted in the previous layer and binds parallel deposited layers together.

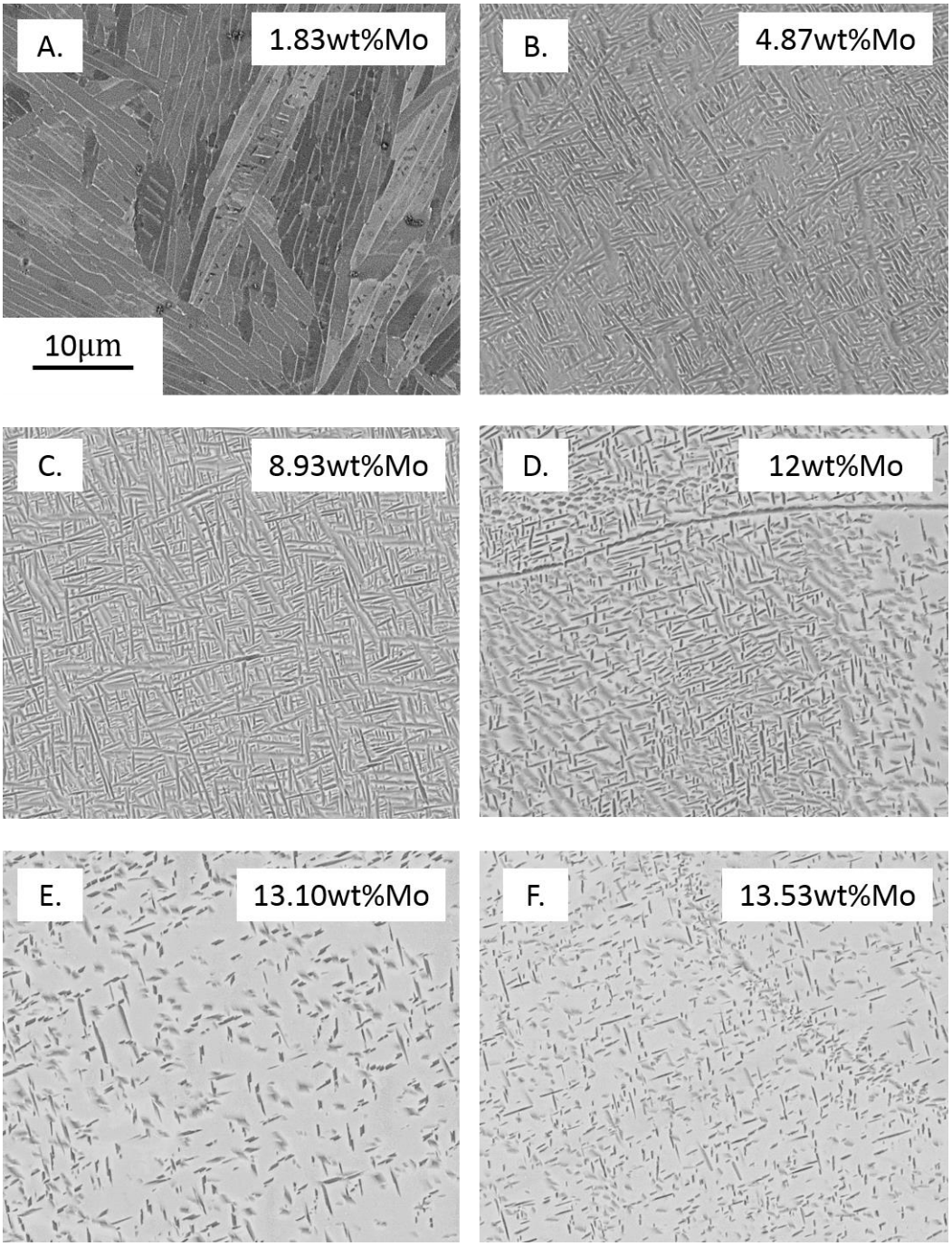

Figure 4.2. (A) – (F) Backscatter SEM micrographs taken at 5000x of the as deposited Ti – xMo LENS™ gradient displaying (A) (.92at.%) a microstructure with very coarse alpha precipitation and low volume fraction of β phase at low Mo content. (B) – (D) display a basketweave like structure that decreasing width as Mo content increases. (E) - (F) Higher Mo content increases the volume fraction of β and decreases both the morphology and thickness of grain boundary α

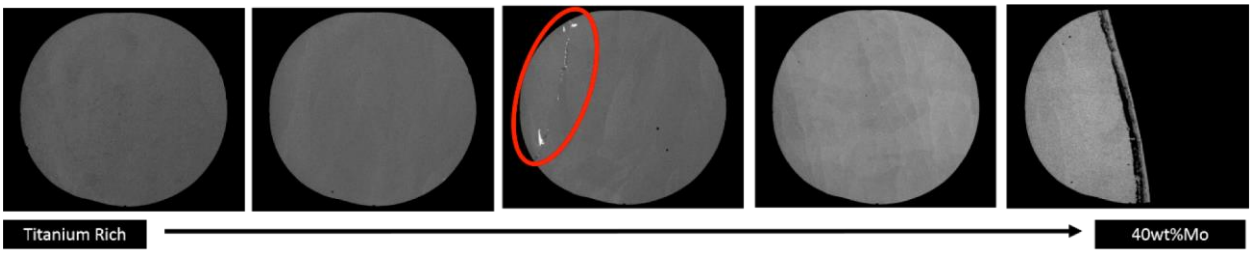

Figure 4.3. Second deposition of Ti – *x*Mo (0 < x > 40wt%Mo) gradient using a vector speed of 10 inch/min results in a microstructure clean of partially melted Mo particles. No evidence of "fish scale" effect. Highlighted region of the as – deposited microstructure represents a region of the deposit where there was insufficient fusing between layers due to a loss of laser power.

Figure 4.2 displays the microstructure of an as – deposited sample that has undergone a heat treatment. Major differences from Ti – xMo heat-treated from that of the as deposited microstructure is that of the scale of the α phase precipitated in the β matrix. The micrographs taken in Figure 4.2. were recorded at 5000X magnification. Consistent with literature and previously heat treated Ti – xMo, the volume fraction of α laths decrease with increasing Mo content. In the case of the as deposited LENS™ sample, the presence of α laths become difficult to differentiate from the β matrix after 19wt%Mo. This observation is a direct result of the slow processing time of the LENS™ process when the vector speed is reduced to 4.23mm/s. The process is in operation for roughly 2 hours and this results in the as – deposited microstructure suggests the lower portion of the compositionally graded specimen (solute lean) has microstructurally responded to the temperature gradient that exists as successive layers are deposited.

4.2.4 Ti - xW

4.2.4.1 Introduction Ti – W

The effects of rapid solidification and aging of Ti alloyed with W, a monotectoid former, is assessed in this chapter of the study. The alloy compositions of the specimens manufactured using the LENS™ process are Ti – 30wt.%W, Ti – 35wt.%W, Ti – 40wt.%W, and a Ti – 0<x<

40wt.%W compositionally graded specimen. The heat-treatment operations as listed in Table X consisted of three isothermal holding times; one temperature located above the invariant point (800°C) and two sub-eutectoid temperatures of 650°C and 550°C. The aging response to homogenizing these alloys in the β phase field was assessed at 975°C and 1100°C for 50 and 150 hours.

4.2.4.2 Ti – W Discussion and Results

4.2.4.2.1 As – Deposited Ti – xW

Parameters were established that allowed for the complete β-solutionization of the Ti – W system for compositions up to 40wt%. Further, by carefully selecting the laser input power (i.e., by using the highest laser power) when depositing a Ti – *x*W alloy, there were very few unreacted W particles distributed throughout the sample. Particles that were present were determined to be less than 5 microns in size, which is far smaller than the starting powder size of the elemental W powder sourced from Alfa Aesar.

The initial observation of all alloys ranging from ~30 to ~40wt.% was the appearance of dendrites throughout the microstructure in the as-deposited specimens. Some representative microstructures are shown in Figure 4.4. (A) – (C). The appearance of a dendritic microstructure, a common occurrence and historically difficult obstacle to overcome when homogenizing W – based alloys, for compositions ranging between 30 - 40wt.%W initially demonstrated that the solidification rate of the LENS™ process might not be fast enough to suppress the formation of dendrites for these compositions.

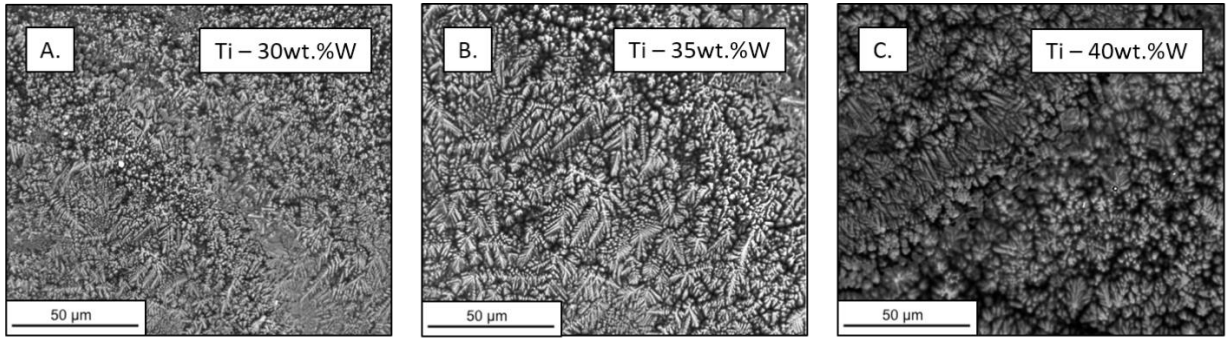

Figure 4.4 A, B, and C are representative microstructures of the as deposited microstructures of fixed Ti – 30, 35, and 40wt.%W. These alloys were deposited to assess the influence of vector speed on the resulting microstructure. As presented, all specimens exhibited a dendritic morphology indicating a vector speed of 8.46mm/s isn't a sufficient parameter in depositing alloys of this system

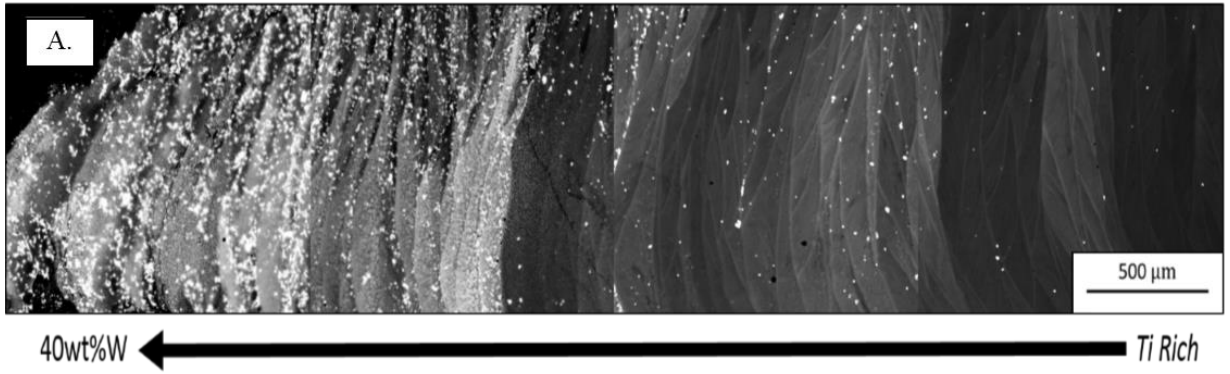

Figure 4.5 Representative collage of microstructures for a compositionally graded Ti – xW (0<x<40wt.%) specimen that is void of dendritic structures. The vector speed chosen for this specimen was 4.23mm/s.

Similar to the parameters used to deposit a "*clean*" Ti – xMo LENS™ gradient up to 40wt%Mo, a Ti – xW compositionally graded specimen up to 40wt.%W was deposited using a vector speed of 4.23mm/s while using the highest laser power of 48 amps. Previous Ti – xW LENS™ deposited alloys displayed a dendritic structure due to solute segregation during solidification. This microstructure is a consequence of inadequate time to melt and locally homogenize the blended Ti – xW powder due to using a relatively fast vector speed (8.46mm/s).

Figure 4.5.. represents the as – deposited microstructure as a result of lowering the vector speed to 4.23mm/s while using the same hydride-dehydride powder (faceted shape) and 48 amp laser power. It is important to note the microstructure of the as deposited specimen. As the gradient increases in W content, the appearance of W rich particles with a composition of 89.32wt.%W increases. There is also a noticeable absence of dendritic formation throughout the deposit. This "*clean"* microstructure is due to the local homogenization of the laser slowly raster throughout the designed geometry of the build while building successive layers at a slower vector speed, V_l.

4.2.4.2.2 β – solution at 1100˚C for 150 Hours

Representative micrographs are shown in Figure 4.6. of a Ti – xW (0<x<40wt.%) LENS™ deposition water quenched from the β phase field at 1100˚C for 150 hours. The microstructure for low concentrations of W appears to consist of an intimate mixture of platelets leading to the acicular morphology of martensite. Figure 4.7. displays the suppression of martensite at the bulk composition of 25wt.%W. The suppression of martensite in the water quenched Ti – xW specimen aged at 1100°C for 150 hours was observed at the local composition of Ti – 25wt.%W. The transformation front of martensite exhibits a "cup" and "cone" like relationship where the transformation front consisting of martensite sits around the "cone" of the fully retained β phase when observing the backscatter electron micrograph in Figure 4.7. Using this generalization,

selected area quantification of the composition of the "cup" shaped transformation of α″ was recorded as well as the composition for the region of the micrograph just outside of the suppressed transformation front. Selected area scan of the region containing α" recorded a local composition of Ti – 23.09wt.%W. Site specific scanning of the region just beyond the suppressed transformation front of martensite recorded a local composition of Ti – 25wt.%W. The Mo_{eq} equation shown below:

Equation 4.1 $$[\mathbf{Mo}]_{eq} = [\mathbf{Mo}] + 0.67\,[\mathbf{V}] + 0.44\,[\mathbf{W}] + 0.28\,[\mathbf{Nb}] + 0.22\,[\mathbf{Ta}] + 2.9\,[\mathbf{Fe}] + 1.6\,[\mathbf{Cr}] + 1.25\,[\mathbf{Ni}] + 1.7\,[\mathbf{Mn}] + 1.7\,[\mathbf{Co}]$$

From this calculation, Table 4.4. displays the composition of the transition metals necessary to stabilize the β phase. This result is slightly higher that what has been reported for the W component of the Mo_{eq} equation.

Table 4.4. Concentration of TM needed to retain β phase at RT

Group No.	Element	Critical Concentration (wt.%)/(at.%)
V	V	14.9/14.13
	Nb	35.71/22.25
	Ta	45.45/30.04
VI	Cr	6.25/5.78
	Mo	10/5.25
	W	22.72/7.11
VII	Mn	5.88/5.16
VIII(a)	Fe	3.44/2.96
VIII(b)	Co	5.88/4.83
VIII(c)	Ni	8/6.62

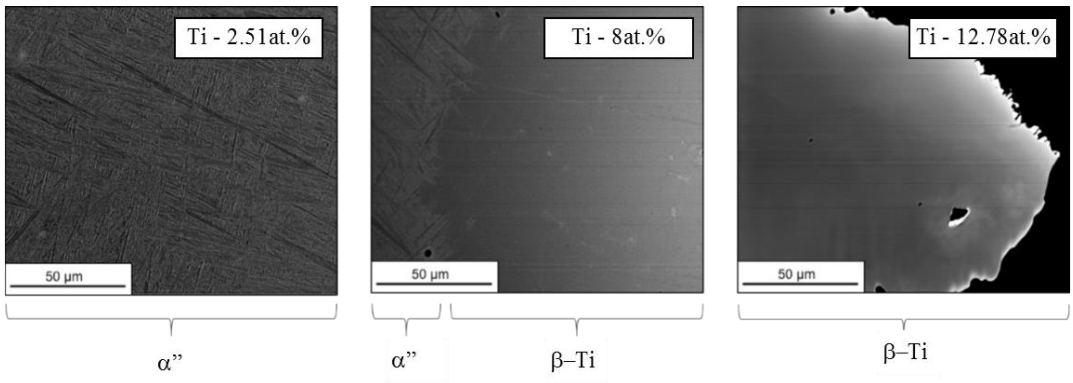

Figure 4.6 Representative micrographs of the LENS^{TM} deposited Ti – xW (0<x<40wt.%) compositionally graded specimen quenched from the β phase at 1100°C for 150 hours.

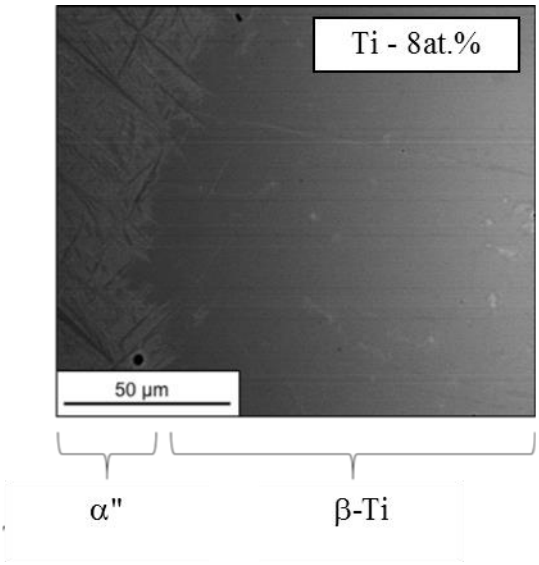

Figure 4.7 Recorded elemental quantification of selected area scans corresponding to the composition within the α’ transformation front and the retained β phase.

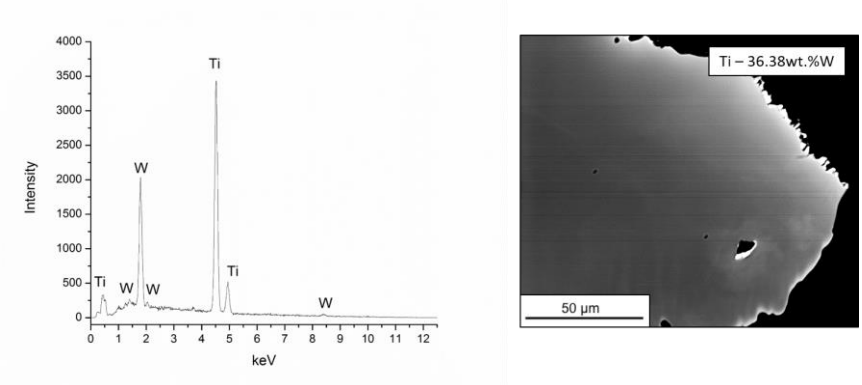

Figure 4.8. Energy dispersive spectroscopy spectra corresponding to the maximum composition of W homogenized (Ti – 36.28wt.%(12.91at.%)W) at 1100°C for 150 hours.

A common occurrence of the LENS^{TM} process and powder fed additive manufacturing is the inconsistency in achieving the targeted composition. As mentioned earlier, the targeted maximum composition for the Ti –xW composition gradient was 40wt.%. As shown by the EDS spectra in Figure 4.8, the maximum composition that was achieved and successfully homogenized at 1100°C for 150 hours was 36.38wt.%(12.91at.%)W.

4.2.4.2.3 Ti – xW Two step isothermal histories (direct aging)

Efforts to obtain microstructures of varying W compositions for directly aging below the invariant point to 550˚C for 50 hours after from the β phase field at 1100°C for 150 hours revealed microstructures that resemble an α + β microstructure achieved from α" decomposition, but the scale of these microstructures are highly refined at both low and high concentrations of W *(see Figure 4.9.)* to determine with certainty. There also doesn't appear to be any noticeable variance in the microstructure as a function of W content until 40.04wt.%W, where the fine scale needle-like structures disappear.

Direct aging in the α + β phase field just below the invariant point at 650°C for 50 hours produced microstructures consisting of coarse prior β grains with colonies of α-lamella separated by a low volume fraction of retained β phase from the 1100°C β solution for 150 hours. Low concentrations of W (6.54wt.%W) exhibited low volume fraction of retained β phase interpenetrating the α-lamellae of varying thicknesses. The volume fraction of retained β appears to increase with W content, but at a modest degree. A transition from the colonies of alternating retained β and α-lamellae to a basketweave structure is observed for W concentrations at greater than ~9.57wt.%W, while a noticeable increase in the volume fraction of β phase is observed. Microstructural variance is minimal after ~19.34wt.%W.

Direct aging at 800˚C for 50 hours provides an illustration of the influence increasing W content has on the resulting microstructure. Micrographs in Figure 4.11. (A) – (E) were taken at 500X magnification and display coarse prior β grains as a result of the high temperature and time of both the β solution (1100°C 150 hours) and the direct age (800°C for 50 hours), both which reside above the invariant point (740°C ± 20). The prior β grains of the 800°C direct aged specimen consists of colonies of α-lamellae with a refined thickness similar to the colonies observed in the 650°C direct aged specimen. This observation in the direct aged 650 and 800°C specimens is significantly different from what is observed in the 550°C direct aged specimen. Significant changes in microstructure aren't present until ~ 25wt%W, where the volume fraction of the β phase becomes quantifiable. Grain boundary α-Ti loses thickness and the widths of α-Ti reduce in size, but remain stable as W content increases. Microstructures of compositions greater than 30wt%W are clearly within the β-miscibility gap when referencing the accepted phase diagram presented in Figure 2.3 *(see section: Review of the Ti – W Binary System),* but the precipitation of the α phase could be a result of air-cooling the encapsulated samples after directly aging for such a long period of time. Further, there were no microstructures of only retained β(Ti,W) observed between the theoretically projected tie line of the two phase α + β (Ti,W – mutually soluble) and the tie line (Ti – rich) of the β-miscibility gap (~30wt.%W). this observation suggests a couple of things. First, the tie line separating the α + β(Ti,W) and β(Ti,W) phase fields may extend further than what has been previously reported theoretically. Secondly, these experimental observations that don't present a fully retained β phase between compositions of and Ti – 30wt.%W suggests that the invariant point for this binary system may be higher than what has been previously recorded (740°C ±20).

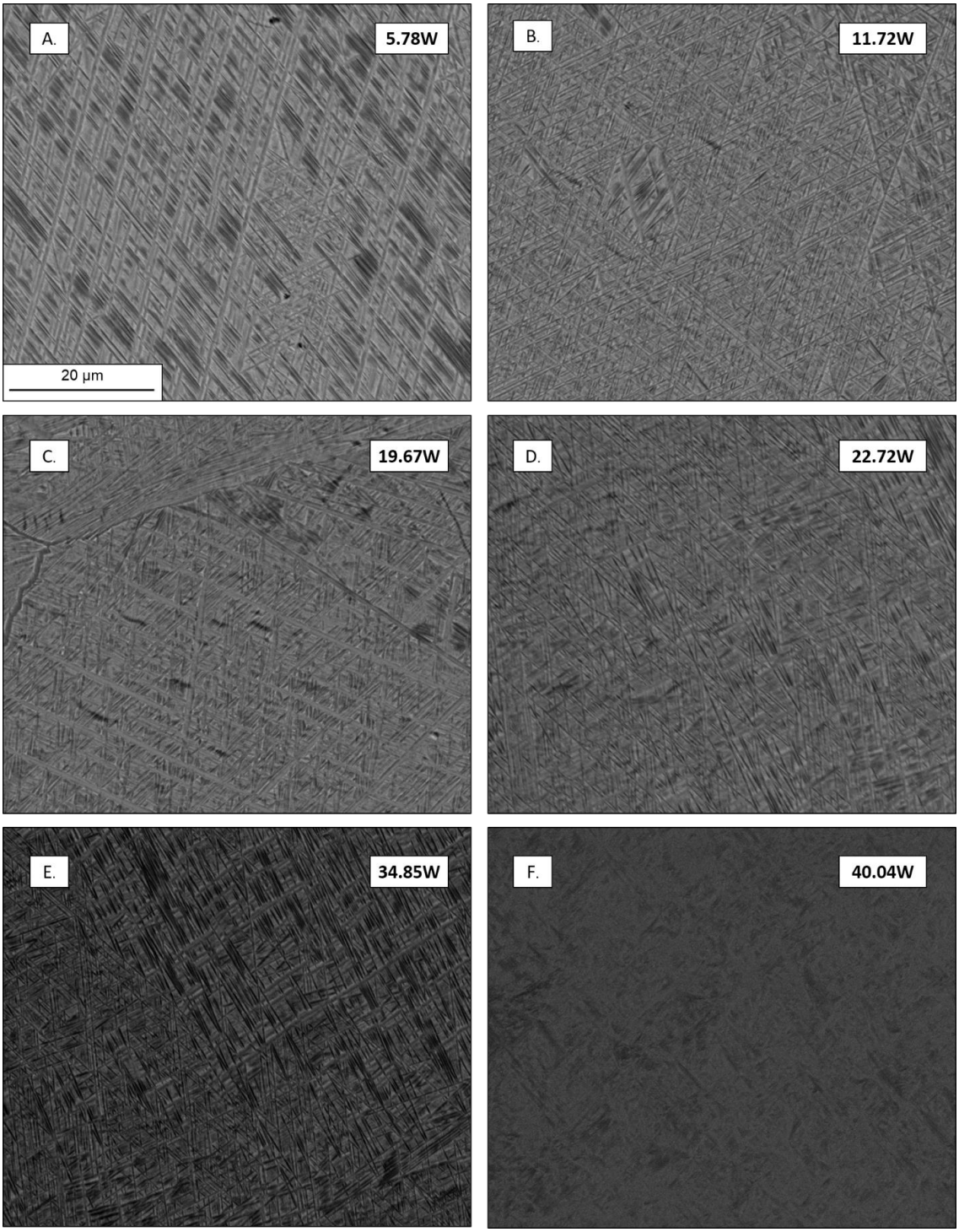

Figure 4.9. Representative backscatter electron micrographs of the LENSTM deposited Ti – xW (0<x<40wt.%) compositionally graded specimen step quenched to 550°C for 4 hours. A.5.78wt.%(1.57at.%)W, B.11.72wt.%(3.34at.%)W, C.19.67wt.%(5.99at.%)W, D. 22.72wt.%(7.11at.%)W, E. 34.85wt.%(12.23at.%)W, F. 40.04wt.%(14.81at.%)W

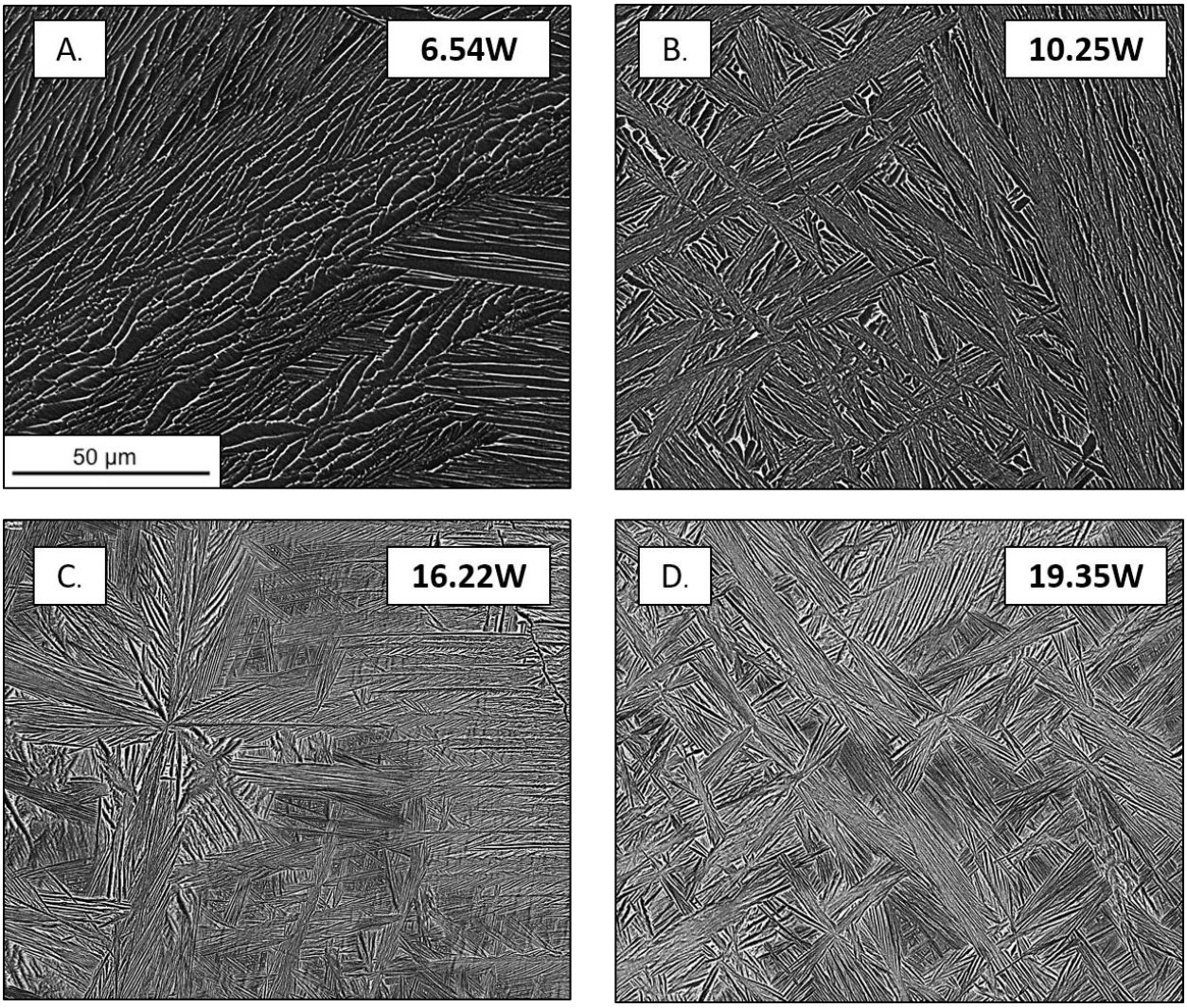

Figure 4.10. Representative backscatter electron micrographs of the LENSTM deposited Ti – xW (0<x<40wt.%) compositionally graded specimen step quenched to 650°C for 4 hours.A.6.54wt.%(1.79at.%)W, B.10.25wt.%(2.89at.%)W, C.16.22wt.%(4.80at.%)W, D.19.35wt.%(5.88at.%)

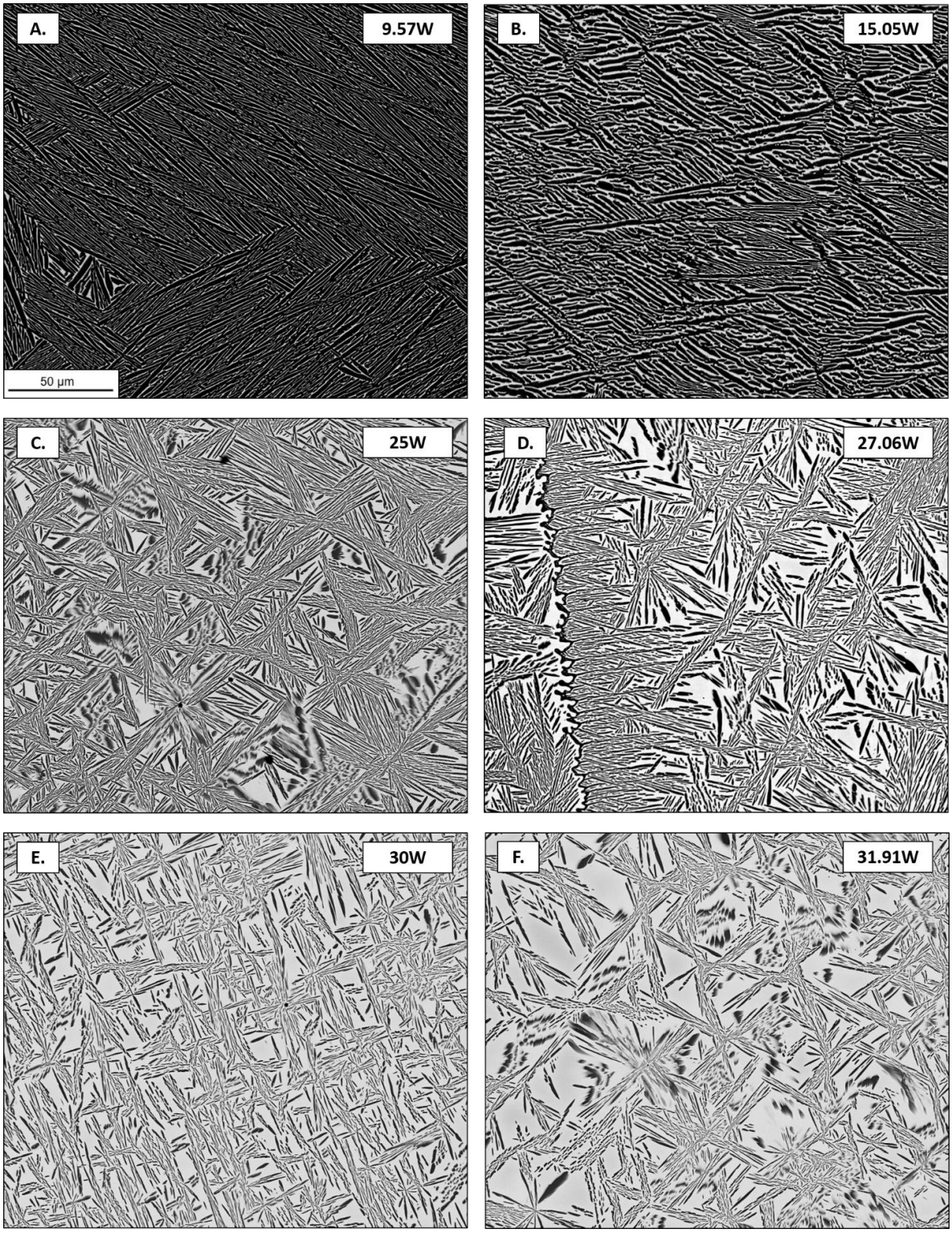

Figure 4.11. Representative backscatter electron micrographs of the LENSTM deposited Ti – xW (0<x<40wt.%) compositionally graded specimen step quenched to 800°C for 4 hours.A.9.57wt.%(2.68at.%)W, B.15.05wt.%(4.41at.%)W, C.25wt.%(7.99at.%), D. 27.06wt.%(8.81at.%)W, E.30wt.%(10.04at.%)W, F.31.91wt.%(10.88at.%)W

4.2.5 Summary of the binary Ti – Mo and Ti - W systems

Deposition parameters such as the vector speed and laser power incorporated in creating a compositional gradient using the LENS™ were adjusted and optimized to create a Ti – xMo alloy up to 40wt%Mo. These adjustments resulted in a microstructure completely void of partially reacted particles in the as – deposited microstructure. As a consequence of altering the vector speed and depositing a Ti – xMo gradient, the as deposited microstructure experienced a 2.5-hour heat treatment as the deposition built to the targeted composition of 40wt%Mo. The resulting as deposited microstructure exhibited fine scale precipitation of the α phase that is further reduced in volume fraction as Mo content increased.

Similar to the Ti – xMo system, the vector speed used to deposit a Ti – xW gradient up to 40wt%W was lowered to 4.23mm/s to insure sufficient melting of Ti and W particles. Adjusting the vector speed and using a laser power of 50 amps resulted in a dendritic free microstructure. The absence of dendrites allowed for a successful attempt in β homogenizing the Ti – xW gradient up to 36.28wt.%W for 150 hours at 1100˚C. It was determined that holding the gradient at 550˚C for 50 hours after step quenching from 1100˚C w while 650˚C and 800˚C step quenches held for 50 hours were sufficient times to effectively precipitate the α phase. Assessing the Mo_{eq}, results showed that the β phase is retained at a slightly higher concentration of 24.99wt.%W than previously recorded (22.72wt.%W)

CHAPTER 5

TITANIUM – IRON BINARY SYSTEM

5 Ti – Fe Binary System

5.1 Introduction

It is important to establish the properties of the Ti – Fe binary system, because of the fundamental properties of the Ti – Fe system are important in the development of the high order system, Ti – Fe – Al with respect to technical interests. In this chapter, a review of the Ti – Fe binary system is assessed as a constituent system of the high order Ti – Fe – Al ternary system.

5.2 Results and Discussion

5.2.1 As-Deposited Ti – xFe

In general, for low compositions of Fe, the as-deposited microstructure of the Ti – xFe gradient ($0 < x < 33$wt.%Fe) exhibited β grains with no evidence of inter or intragranular precipitation of the hcp αTi phase or the (B2)TiFe intermetallic compound. Beyond ~19.08wt.%(16.82at.%)Fe, the microstructure could be described as exhibiting a bimodal distribution of grain sizes. This is interesting, as this bimodal distribution is seen in a β – alloy that has not been subjected to deformation and recrystallization, which is the common route to obtaining this variation in grain size for β-Ti alloys. Interestingly, there is little apparent change in the hardness of the β phase in this region. However, at ~ 24.4wt.%(21.67at.%)Fe, there is a notable jump in the hardness from 537HV (~20.5wt.%(18.10at.%)Fe) to a hardness value of 607HV (~24.4wt.%(21.67at.%)Fe). There are two possible explanations for this jump in hardness. The first is related to the fact that this jump in hardness might be

Vickers Hardness vs. wt.%Fe in the as-deposited Ti - xFe LENS™ deposited gradient					
HV	(wt.%)/(at.%)	Mpa	H	V	STD
484	10.08/8.77	1635	61.89	61.94	2.13
524	16.88/14.83	1804	58.8	60.13	1.23
537	20.47/18.08	1854	58.25	59.22	0.32
571	22.64/20.06	1992	56.71	57.29	2.56
588	23.3/20.66	2052	55.95	56.31	0.35
610	25.85/23.01	---	54.62	55.61	8.9
625	26.1/23.24	---	54.49	54.43	3.2
636	30.89/27.70	---	54.38	53.62	1.2

Table 5.1. Vickers Hardness data as a function of composition in the as – deposited Ti – xFe LENS™ Deposited Gradient.

associated with a very fine scale precipitation of (B2)TiFe, which is a thermodynamically stable liquid-phase product at 24.7wt.%(21.95at.%)Fe (a composition that is effectively identical to 24.4wt.%(21.67at.%)Fe, given the uncertainty in EDS measurements). The second is related to the local grain size. While the presence of fine grains is observed as low as ~19.1wt%(16.83at.%)Fe, the fraction of fine grains increases with increasing Fe levels. The higher hardness indents are taken from these finer grain sizes (see Figure 5.1.), which may then follow a Hall-Petch relationship, known to be a dominant effect for many *bcc* materials. Above 25wt.%(22.23at.%)Fe (see Figure 5.2.), the (B2)TiFe intermetallic compound is clearly visible as precipitates which appear to be strongly correlated with the grain boundaries. It is likely that the (B2)TiFe phase precipitates from the liquid phase directly, and may be responsible for the smaller grain sizes in the lower Fe levels. As shown in Figure 5.3., the microstructure above

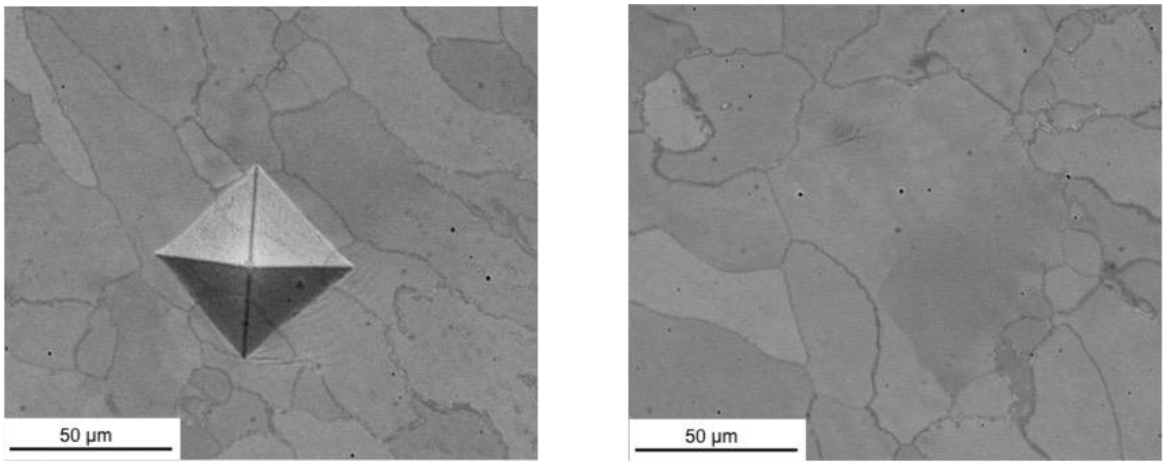

Figure 5.1. Vickers hardness indentation with representative 1000x magnification SEM micrograph of microstructure for Ti - 24.42wt%(21.67at.%)Fe**.**

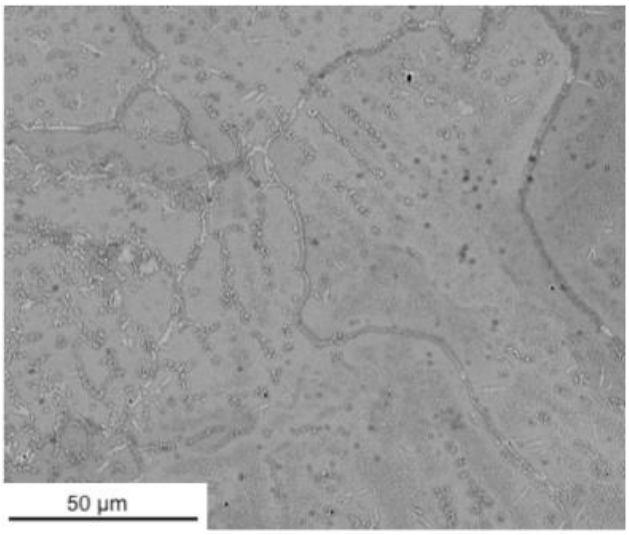

Figure 5.2. Backscatter SEM micrograph taken at 1000x magnification of the as – deposited microstructure of Ti - 25wt%(22.23at.%)Fe.

25wt.%(22.23at.%)Fe is markedly different. The (B2)TiFe that is present at the grain boundaries exhibits a composition of ~65.25wt.%(68.65at.%)Ti – 34.75wt.%(31.35at.%)Fe, as measured using energy dispersive spectroscopy (EDS). In addition, there is a second distribution of fine scale (B2)TiFe which appears within the β grains and exhibits a more "spherical" morphology. The composition of the spherical fine scale (B2)TiFe (63.92wt.%(67.39)at.%)Ti –

36.08wt.%(32.61at.%)Fe) is quite similar with that of (B2)TiFe precipitates observed at the grain boundaries. The matrix composition is 78.48wt.%(80.97at.%)Ti – 21.52wt.%(19.03at.%)Fe. The formation of these small, spherical, intragranular (B2)TiFe is expected, as the solubility of Fe in the β phase is ~7wt%(6.06at.%) less at ~600°C when compared with the maximum solubility at 1095°C. Fe is expected to come out of solid solution, precipitating out as (B2)TiFe particles within the β – grains. Not surprisingly, an increase in the wt%Fe leads to the coarsening of both intragranular "colony like" (B2)TiFe and the intermetallic compound located, at the grain boundaries. Shown in Figure 5.3., minor increase in Fe content by 1wt%(0.86at.%) can significantly coarsen the (B2)TiFe intermetallic and leads to the precipitation of coarse (B2)TiFe within the grain. This may be analogous to Oswald Ripening, whereby promoting the (B2)TiFe results in some particles growing at the expense of others, effectively eliminating the appearance of the well-aligned "colony like" (B2)TiFe precipitates. Further analysis using EDS spot scans show no difference in composition for coarse "non – colony like" (B2)TiFe located within the grain relative to grain boundary product (B2)TiFe. Additional work is required to assess the origin of the aligned spherical precipitates at the lower Fe levels.

In keeping with the results presented above, significant coarsening of the (B2)TiFe precipitates was observed for alloys whose composition exceeding ~28wt%(25at.%)Fe (see Figure 5.4.). There was a concurrent increase in the hardness levels. As can be seen, a more dendritic-like "primary" (B2)TiFe particle appears in Figure 5.5(B.), strongly suggesting that the

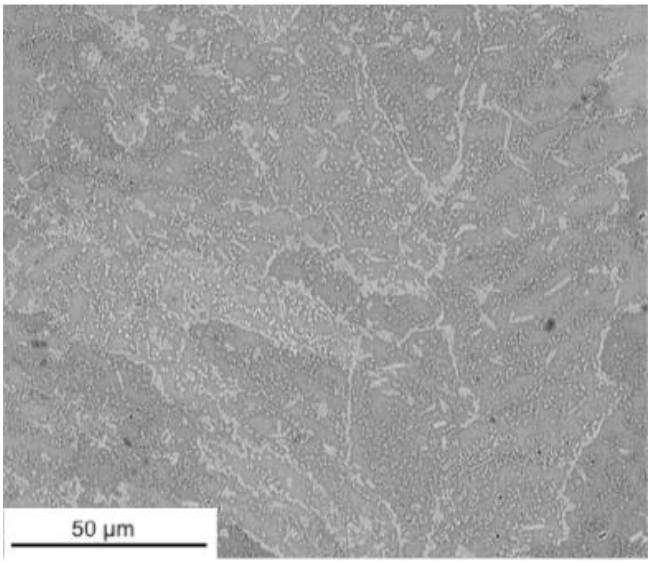

Figure 5.3. Backscatter SEM micrograph taken at 1000x magnification of the as - deposited microstructure of Ti – 26.73wt%(23.83at.%)Fe.

invariant reaction given below:

$$L \rightarrow \beta + TiFe$$

occurs at a composition below what was previously hypothesized (~33wt.%(29.69at.%)), although it is clear there is significant uncertainty in this portion of the binary phase diagram. In addition to this important observation, it is clear that colonies of (B2)TiFe still remain (consistent with the theory that they precipitate upon cooling). Further, for this non-equilibrium processing, with increasing Fe content, the composition of the spherical (B2)TiFe has changed to 59.77wt.%(63.41at.%)Ti – 40.23wt.%(36.59at.%)Fe while the overall matrix (i.e.,β-Ti) composition has increased in Ti content, 81.32wt.%(83.55at.%)Ti – 18.68wt.%(16.45at.%)Fe. This matrix composition also supports the theory that the maximum solid solubility of the □ phase is less than previously reported. At 31.13wt%(27.93at.%)Fe, the second largest microhardness value of 610HV was recorded. The local microstructure at the site of the indentation test has coarse

"primary" (B2)TiFe with fine scale colonies, but with a variety of morphologies. Specifically, "primary" (B2)TiFe is dendritic in morphology as shown in Figure 5.5. The appearance of an increase in the volume fraction of this morphology (with respect to Figure 5.4.) of (B2)TiFe at higher Fe content is consistent with what has been observed previously and what is expected, as well as what has been reported in the literature. Specifically, it has been reported that directionally solidified Ti – *x*Fe alloys exhibited high mechanical properties where a combination of fine scale eutectic (B2)TiFe and supersaturated β – Ti were coupled with a varied distribution of coarse/ primary (B2)TiFe exhibiting a dendritic morphology by Schlieter and Contieri. The composition of (B2)TiFe located at 31.13wt%(27.93at.%)Fe is consistent with coarse primary intragranular and grain boundary product (B2)TiFe (65.25wt.%(68.65at.%)Ti – 34.75wt.%(31.35at.%)Fe) found throughout the as – deposited LENS™ specimen. The other microstructural feature that is strikingly different are the "quasi-continuous" Fe-rich precipitates that are present throughout the microstructure. The origin of such features is unknown, and requires careful consideration.

5.2.2 Ti – xFe Isothermal Heat treatments

After the β-homogenization and subsequent step quenching of a fourth of the Ti – *x*Fe LENS™ gradient for 4 hours at 550°C, a series of Vickers hardness tests were conducted along the gradient. Notably, 550°C is ***below*** the reported invariant point.

For Fe compositions less than ~10wt.%(8.70at.%), the microstructure exhibited fine α laths. Not surprisingly, as the β phase is stabilized with increasing Fe content, there is a decrease in the volume fraction of the α laths up to ~23wt%(20.39at.%)Fe where (B2)TiFe appears as a

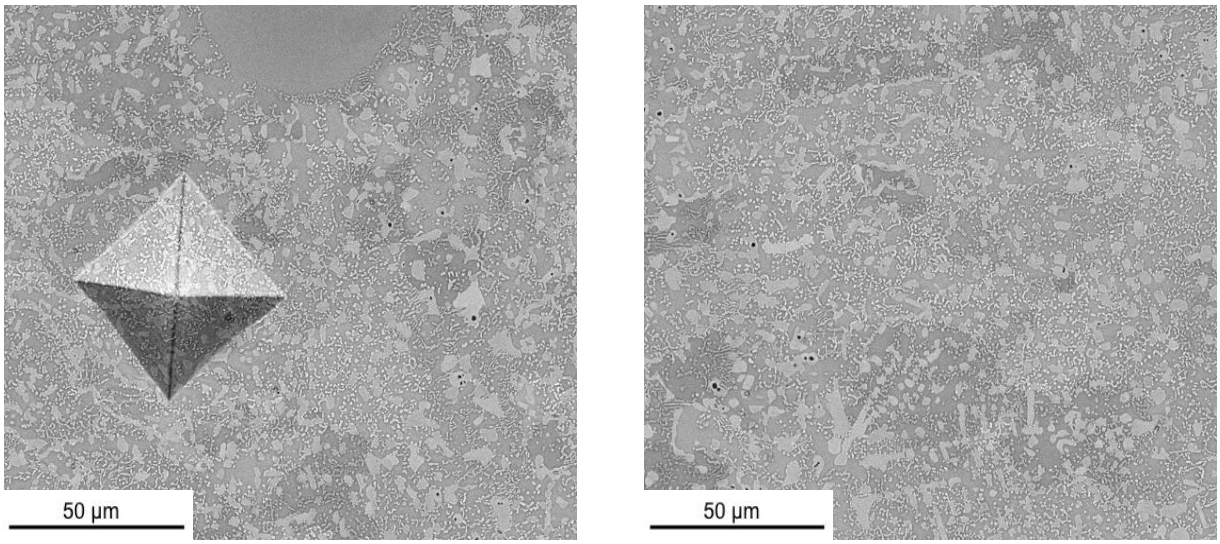

Figure 5.4. Backscatter SEM micrograph taken at 1000x magnification of the as - deposited microstructure of Ti – 31.13wt%(27.93at.%)Fe with corresponding Vickers indentation.

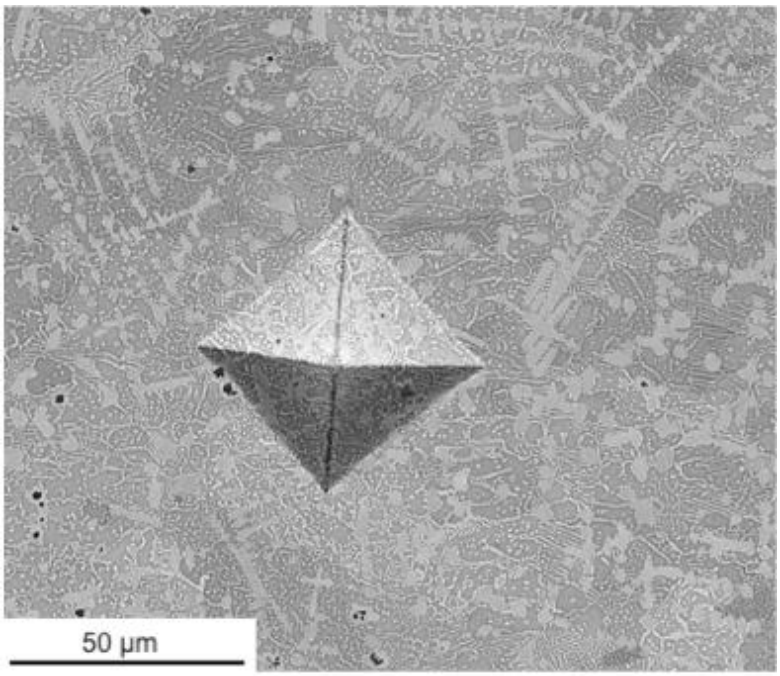

Figure 5.5. Backscatter SEM micrograph taken at 1000x magnification of the as - deposited microstructure displaying dendritic structure of TiFe intermetallic compound

Vickers Hardness vs. wt.%Fe in the directly aged 550°C Ti - xFe LENS™ deposited gradient					
HV	(wt.%)/(at.%)	Mpa	H	V	STD
435	8.06/6.99	1439	66.08	64.5	0.03
452	8.39/7.28	1505	63.4	64.69	1.04
473	11.94/10.41	1588	62.21	62.97	0.56
496	14.56/12.75	1686	61.95	60.32	2.34
535	19.3/17.02	1846	58.54	59.18	7.9
540	20.54/18.14	1865	58.51	58.65	12.43
556	24.47/21.74	1933	57.69	57.78	2.34
562	25.43/22.62	1958	57.21	57.61	0.54
581	31.08/27.88	2028	55.2	57.74	2.82
557	33.37/30.04	1937	56.53	58.87	0.05
574	34/30.64	2004	55.25	58.4	6.03

Table 5.2. Vickers Hardness data as a function of composition in the 550°C direct aged Ti – *x*Fe LENS™ Deposited Gradient.

grain boundary product. The Vickers hardness shown in Table 5.2. for the 550°C directly aged specimen is similar to the results of the as – deposited LENS™ specimen. Significant differences in morphology of (B2)TiFe found in the 550°C air cooled specimen relate to the volume fraction of (B2)TiFe. The morphology of the (B2)TiFe intermetallic compound found in the as-deposited specimen consisted of a variation of both primary (B2)TiFe as a grain boundary product that then appears intragranularly with increasing Fe content. A fine distribution of (B2)TiFe also appears spherical in morphology until reaching 28wt%(25at.%)Fe. Above this composition, there is a combination of both elongated and spherical (B2)TiFe. The (B2)TiFe found in the 4 hour step quenched specimen at 550°C displays coarse “primary” (B2)TiFe as a grain

Vickers Hardness vs. wt.%Fe in the directly aged 650°C Ti - *x*Fe LENS™ deposited gradient					
HV	(wt.%)/(at.%)	Mpa	H	V	STD
469	13.89/12.15	1572	62.95	62.78	0.03
494	15.06/13.20	1678	61.11	61.44	2.43
505	17.41/15.31	1725	60.94	60.21	3.63
506	18.54/16.33	1730	60.41	60.7	1.45
555	21.66/19.16	1928	57.19	58.37	2.87
545	22.42/19.86	1961	57.2	57.59	7.21
563	23.27/20.64	1869	58.56	58.57	13.76
589	29.79/26.67	---	51.97	53.69	2.56
664	30.72/27.54	---	56.74	56.1	8.78
554	31.17/27.97	1946	57.98	57.2	18.66

Table 5.3. Vickers Hardness data as a function of composition in the 650°C direct aged Ti – *x*Fe LENS™ Deposited Gradient.

boundary product as seen in Figure 5.5., but coarser in scale. Similar to the as - deposited specimen, upon increasing Fe content, the hardness value of the gradient specimen increases with the appearance of spherical (B2)TiFe. Spherical (B2)TiFe is finer in scale as compared to "primary" (B2)TiFe that also consists of a different composition; 59.77wt.%(63.41at.%)Ti – 40.23wt.%(36.59at.%)Fe, but still within the stoichiometry of the intermetallic compound. Although the Vickers hardness value for both specimens are similar, the microstructures that relate to the given hardness values at similar compositions can be different.

Two Ti – *x*Fe LENS™ deposited specimens were homogenized in the β phase field for 4 hours at 975˚C followed by quenching to 650 and 750°C, temperatures above the reported

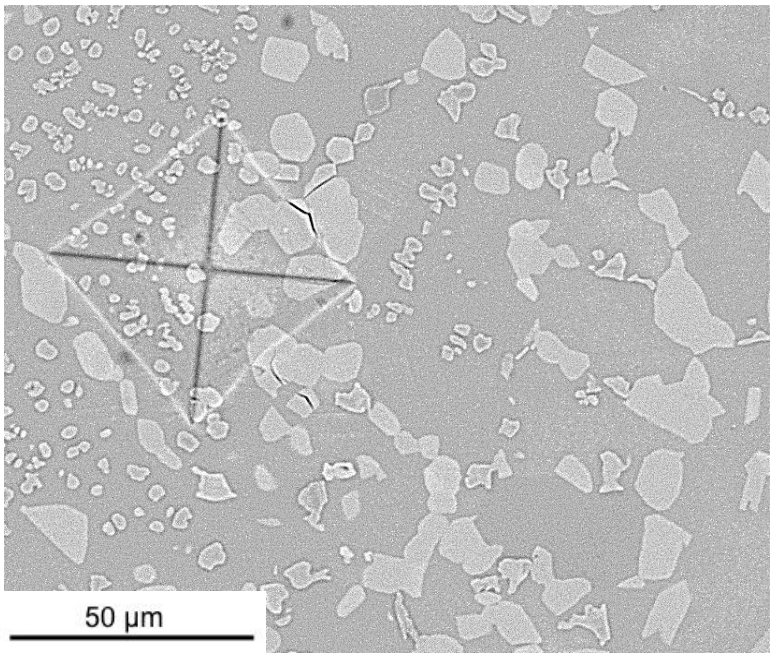

Figure 5.7. Vickers Indentation with local microstructure for 750˚C Ti – xFe at 24wt%(21.31at.%)Fe.

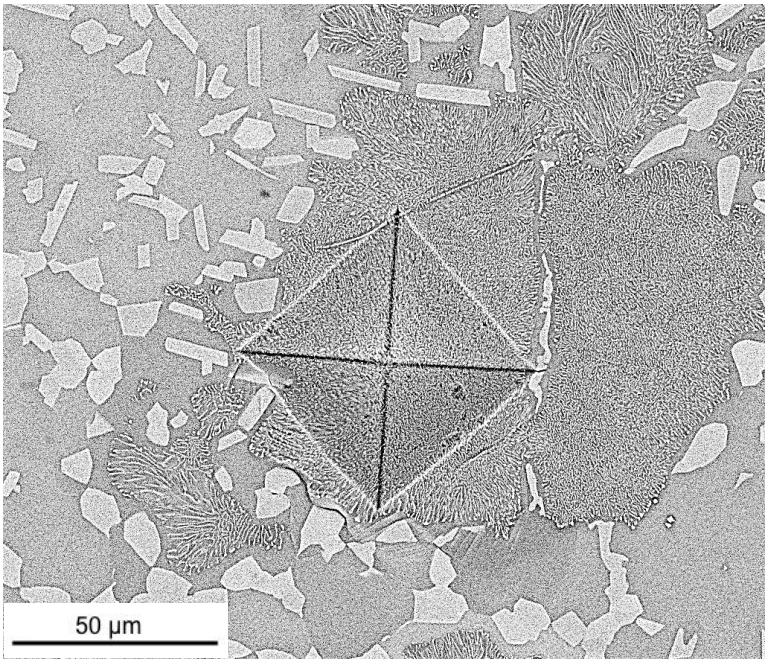

Figure 5.6. Vickers Indentation on ultra-fine eutectic microstructure for 650˚C Ti – *x*Fe at 24wt%(21.31at.%)Fe.

Vickers Hardness vs. wt.%Fe in the directly aged 750°C Ti - *x*Fe LENS™ deposited gradient					
HV	(wt.%)/(at.%)	Mpa	H	V	STD
511	12.54/10.95	2062	55	56	7.43
526	14/12.25	1812	59.54	59.19	2.45
520	19/16.74	1788	58.72	60.72	1.65
522	24.65/21.90	1796	58.77	60.47	8.76
523	25.4/22.60	1800	58.98	60.13	10.32
554	28.99/25.93	1924	56.34	59.4	24.73
556	31.91/28.66	1933	56.72	58.82	5.45
557	32.75/29.45	1937	56.96	58.38	7.53

Table 5.4. Vickers Hardness data as a function of composition in the 750°C direct aged Ti – xFe LENS™ Deposited Gradient.

invariant point. These specimens exhibited an increase in hardness value with increasing Fe content. Table 5.3 and 5.4. shows a comparison of Vickers hardness values for the two Ti – *x*Fe LENS™ deposited specimens directly aged at 650 and 750°C. The high Vickers hardness values of the Ti – *x*Fe gradient step quenched to 650˚C and held for 4 hours is attributed to the precipitation of ultra-fine eutectic microstructure consisting of supersaturated β-Ti + (B2)TiFe appearing at ~24wt%(21.31at.%)Fe. Figure 5.6. shows the local microstructure associated near the Vickers micro – indentations at 24wt.%(21.31at.%)Fe. Figure 5.7. shows the Vickers indentation with local microstructure exhibiting the same hardness value of 511HV at 24.78wt%(22.02at.%)Fe for the Ti – xFe gradient step quenched to 750˚C for 4 hours, but with a completely different

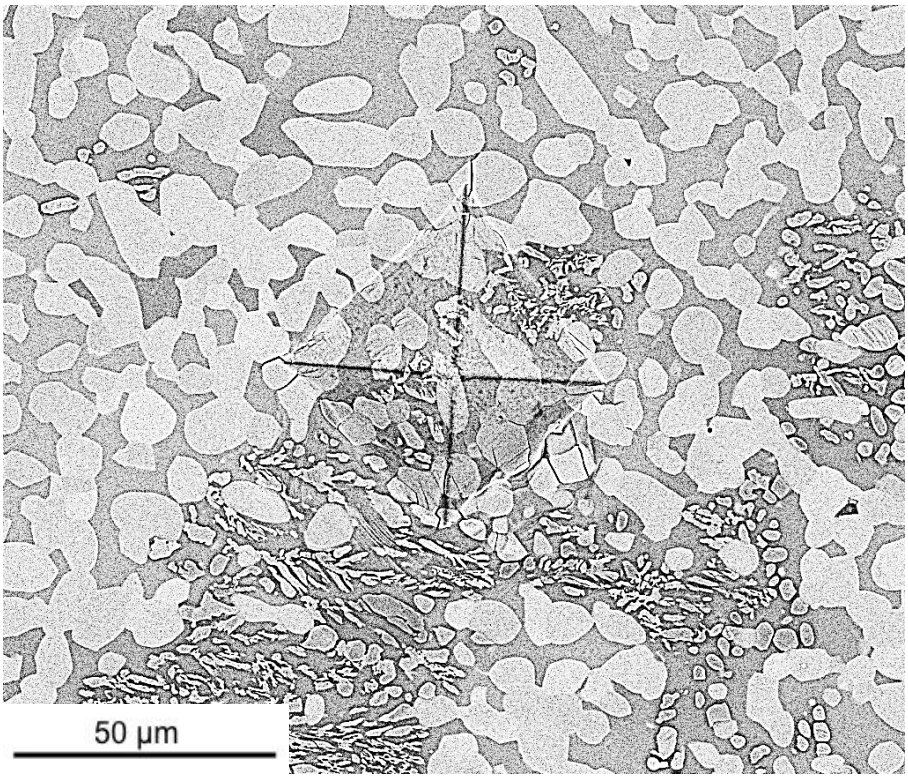

Figure 5.8. Vickers Indentation and local microstructure for Ti – 30.72wt%(27.54at.%)Fe step quenched for 4 hours at 650˚C. The micrograph represents a microstructure that has a higher hardness value than the equivalent composition for a Ti – 30.72wt%(27.54at.%)Fe step quenched at 750˚C for 4 hours after β solution at 975˚C for 4 hours.

microstructure. Clearly, 24wt%(21.31at.%) lies within the β–Ti+ (B2)TiFe two-phase field at 650°C, but lies in the single-phase β phase field at 750°Ç. Increasing Fe content in Ti – xFe gradients step quenched above the invariant point leads to the coarsening of (B2)TiFe. The coarsening of both primary (B2)TiFe and the finer distribution of spherical (B2)TiFe leads to the reduction in the mean inter-particle spacing. It is in this microstructural evolution that a correlation can be drawn that relates to the distance between the different morphologies of the intermetallic compound (B2)TiFe and the value of Vickers hardness. As "primary" (B2)TiFe in both LENS™ deposited specimens not only coarsen but also increase in volume fraction with increasing Fe content, the coarse (B2)TiFe precipitates impinge upon one another. Not only does this decrease

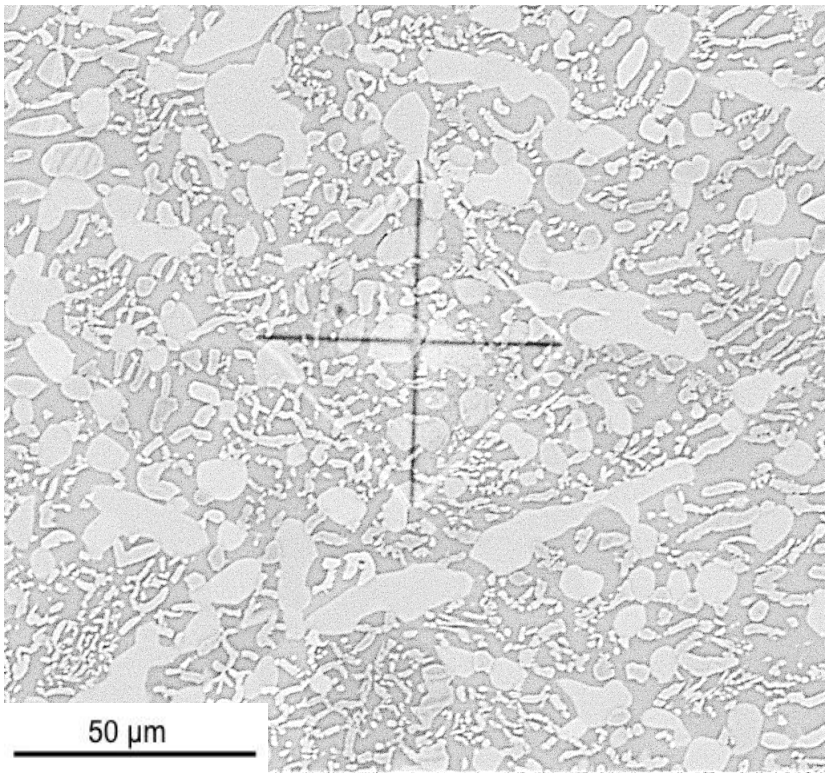

Figure 5.9. Vickers Indentation with local microstructure for 750˚C Ti – xFe at 24wt%(21.31at.%)Fe.

the allowable regions for dispersion of the finer spherical morphology of (B2)TiFe but this morphology of (B2)TiFe begins to coalesce into a fine elongated morphology in comparison to the size of primary (B2)TiFe as well.

The highest Vickers hardness value of 664HV was recorded at 30.72wt%(27.54at.%)Fe in the 4 hour 650˚C step quenched LENS™ deposit. A representative backscatter SEM micrograph in Figure 5.8. shows the local microstructure for the Vickers indentation. Comparing the local microstructures of the highest hardness value in the 650 and 750˚C step quenched specimens confirms the correlation that relates intermetallic spacing to the mechanical properties of Ti – xFe alloys, x > 28wt%(25at.%)Fe.

5.2.3 Summary of the Ti – Fe Binary System

The Ti – *x*Fe LENS™ gradient up to 33wt%(29.69at.%)Fe exhibit a duplex microstructure in the as – deposited form which lead to a consistent trend in Vickers hardness values. The precipitation of the intermetallic compound (B2)TiFe displayed a variation in morphology and size distribution for heat treatment operations both above and below the invariant point for increasing Fe content. Specifically, Ti – *x*Fe gradients heat-treated above the invariant point exhibited a strong intermetallic spacing correlation with Vickers hardness values and this is apparent in the comparison of the recorded Vickers microhardness across the as – deposited, 550, 650, and 750°C directly aged Ti – *x*Fe specimens. As the distance between primary (B2)TiFe and spherical colonies, or elongated diminished for increased Fe content, the hardness value for the given composition increased regardless of the heat treatment operation above the invariant point.

CHAPTER 6

TITANIUM – IRON – ALUMINUM

6 Ti – Fe – Al Ternary System

6.1 Introduction

The Ti – Fe – Al ternary system has been the focus of much attention over recent years because of the promise of high symmetry intermetallics with attractive high temperature properties relative to the low symmetry intermetallic compounds of the binary Ti – Al system. Prior to the current interest in alloys of the Ti – Fe – Al system, Ti alloys with Fe as one of the major alloying additions were first developed as a low cost alternative to Ti alloys such as Ti – 6Al – 4V in the 1980s. Fe, a β – eutectoid former, is the 4th most abundant element in earth's crust and was specifically incorporated into Ti alloys as a low cost alternative to expensive β stabilizers like Mo and V. One particular Ti – Fe – Al alloy developed was Ti – 5Al – 2.5Fe (Tikrutan LT 35). In this alloy, Fe is substituted for V and implored as permanent implants (i.e., sockets for hip prosthesis, bone nails, screws, etc.), as Fe possesses relatively good biocompatibility. A fine grain microstructure of α + β is achievable when Ti – 5Al – 2.5Fe is thermomechanically processed in the α + β phase field, then aged at 850°C (1560°F). This recommended heat-treatment strategy produce Vickers hardness values that range between 320 – 340HV. Typically, the Young's modulus for Ti – 5Al – 2.5Fe ranges from 105 to 120 GPa when processed using the heating strategy previously mentioned. Fe was also substituted for V in the Ti – Fe – Al alloy, Ti – 6Al – 1.7Fe – 0.1Si (TIMETAL 62S or commonly known as 62S). Transformed β microstructures of 62S consist of Widmanstätten α when rapidly cooled and a colony structure when air cooled

similarly to the microstructural heating response of Ti – 6Al – 4V. With mechanical properties that are equivalent to Ti – 6Al – 4V and a relatively lower formation cost, this alloy has become a practical substitute for expensive engineering materials used in automotive and defense applications.

Commercially available Ti alloys that contain Fe consist of compositions that restrict the formation of the intermetallic compounds associated with the binary Ti – Fe system. Further, development of these Ti alloys has been restricted to exploring different heating strategies and thermomechanically processing to discover new properties. Literature surrounding the exploration of high Fe content Ti – Fe – Al alloys is severely limited. This study is an investigation into the composition – microstructure and resulting properties of a compositionally graded Ti – *x*Fe – *y*Al ($0<x<35$wt.%, y=5,10,15) LENS^{TM} deposited specimen. Specifically, in this study the effect of direct aging to 550, 650, and 800°C after β-solution on the resulting microstructure of a compositionally graded specimen as well as the resulting microstructural influence on Vickers hardness recorded for fixed Al content in Ti – *x*Fe – *y*Al (y=0,5,10,15) is assessed.

6.2 Experimental Methods

6.2.1 Heat Treatment Operations

The heat treatment operations for the Ti – *x*Fe – *y*Al LENS^{TM} deposited specimens provided in Table 6.1 were held at the same aging times and temperatures as the specimens used in the previous study of the binary Ti – Fe system. The difference in the heat-treatment operations for the ternary alloys only occurs in the initial step of aging process (β - solution). Because of the additions of Al, the β - solution temperature in the initial homogenization of the specimens in the β phase field was increased to accommodate the elevated β - transus.

Table 6.1. Heat – treatment operations performed for the Ti – Fe – Al system

Specimen	**β – Solution**	**Step Quench**
Ti - xFe - 5wt.%Al (0 < x < 35wt.%)	975°C for 4 Hours WQ	-------
Ti - xFe - 5wt.%Al (0 < x < 35wt.%)	1100°C for 4 Hours WQ	-------
Ti - xFe - 5wt.%Al (0 < x < 35wt.%)	1100°C for 4 Hours	550°C for 4 Hours AC
Ti - xFe - 5wt.%Al (0 < x < 35wt.%)	1100°C for 4 Hours	650°C for 4 Hours AC
Ti - xFe - 5wt.%Al (0 < x < 35wt.%)	1100°C for 4 Hours	800°C for 4 Hours AC
Ti - xFe - 10wt.%Al (0 < x < 35wt.%)	1100°C for 4 Hours	550°C for 4 Hours AC
Ti - xFe - 10wt.%Al (0 < x < 35wt.%)	1100°C for 4 Hours	650°C for 4 Hours AC
Ti - xFe - 10wt.%Al (0 < x < 35wt.%)	1100°C for 4 Hours	800°C for 4 Hours AC
Ti - xFe - 15wt.%Al (0 < x < 35wt.%)	1100°C for 4 Hours	550°C for 4 Hours AC
Ti - xFe - 15wt.%Al (0 < x < 35wt.%)	1100°C for 4 Hours	650°C for 4 Hours AC
Ti - xFe - 15wt.%Al (0 < x < 35wt.%)	1100°C for 4 Hours	800°C for 4 Hours AC

6.2.2 Vickers Indentation

Vickers microhardness indentation tests were performed to assess the change in hardness of the gradient specimens as a function of Fe content in specimens with a fixed composition of 5, 10, and 15wt.%Al. In addition to measuring the microhardness hardness across the gradient specimens, each test as seen in Figure 6.1. and Figure 6.2. served as a fiduciary marker in measuring the local composition of each test using energy dispersive spectroscopy (EDS). Each test was performed in two rows with a test spacing of 0.5mm to avoid overlapping deformation fields and to provide a large number of compositional measurements across the specimen. The results of comparing the increase in Fe content as a function of test distance shows that there is a large range of the specimen that contains the desired transitions in Fe content as you move along the composition gradient.

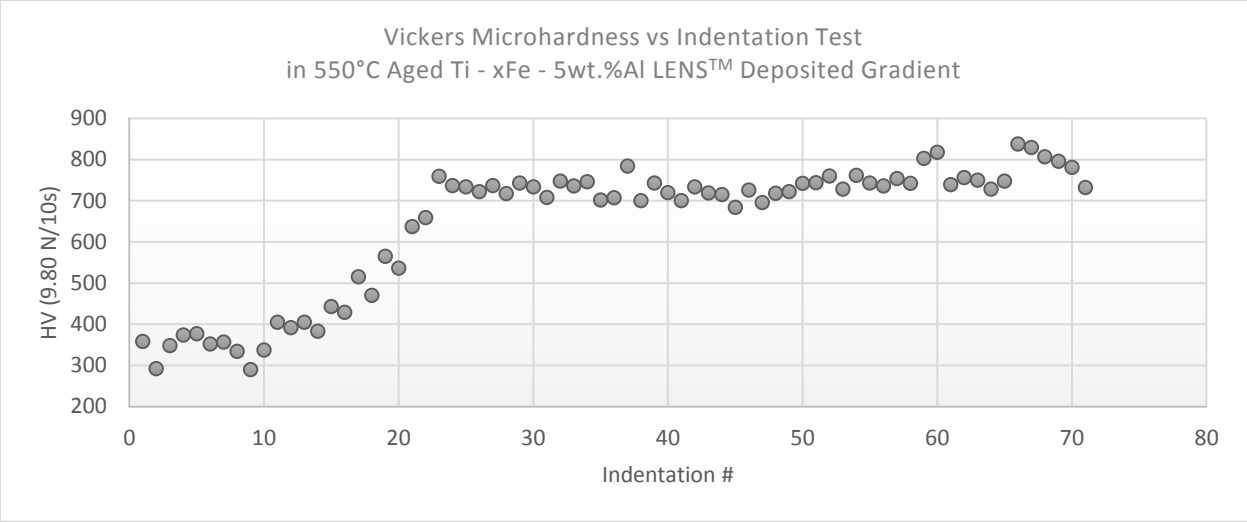

Figure 6.1. Graph displaying the HV of each indentation test performed using a Ti – xFe – 5Al specimen subject to β homogenization at 1100°C for 4 hours, step quenched to 550°C for 4 hours, then air cooled.

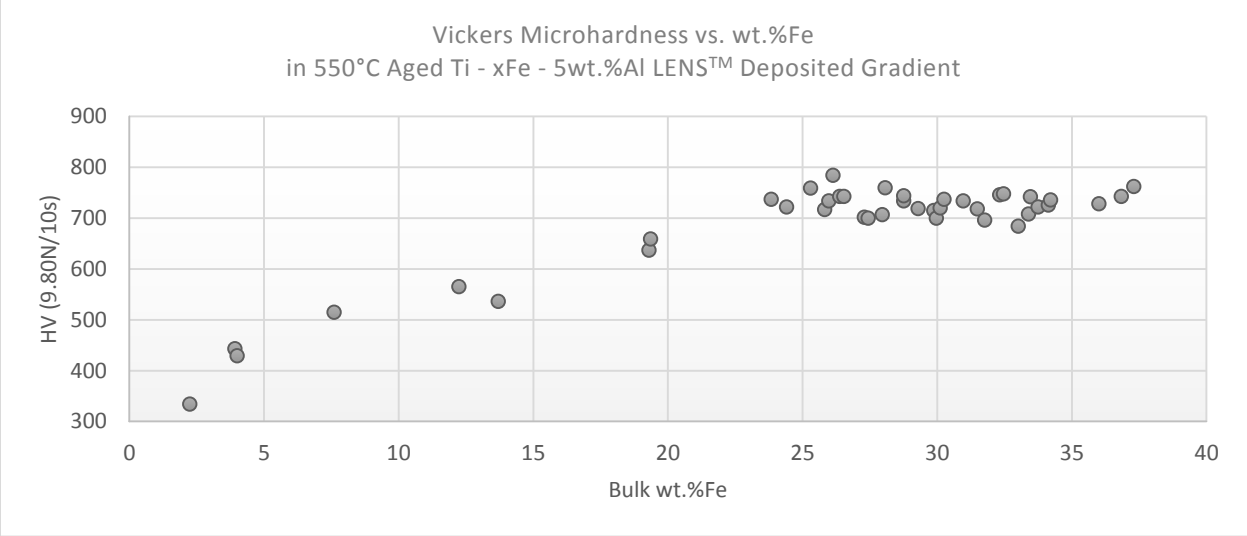

Figure 6.2. Graph displaying the HV as a function of Fe content of a Ti – xFe – 5Al specimen subject to β homogenization at 1100°C for 4 hours, step quenched to 550°C for 4 hours, then air cooled.

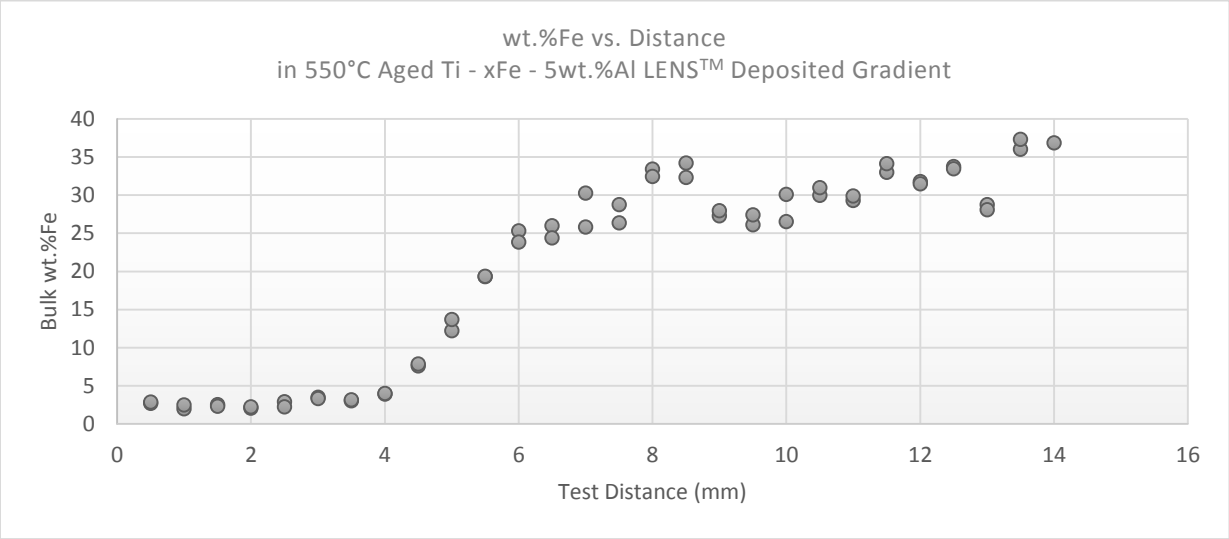

Figure 6.3. Graph displaying the composition gradient of Fe content as you move along the distance of a Ti – xFe – 5Al specimen subject to β homogenization at 1100°C for 4 hours, step quenched to 550°C for 4 hours, then air cooled.

6.3 Results and Discussion

6.3.1 Ti – *x*Fe – 5Al

6.3.1.1 Isothermal Heat treatments (direct aging)

The Ti – *x*Fe – 5Al LENS™ deposited gradient was homogenized at 1100°C for 4 hours, step quenched to 550°C for 4 hours, then air-cooled. The resulting microstructure for low solute content of Fe (average local composition <5wt.%) exhibited α with a Widmanstätten lath-like morphology (*shown in Figure 6.4.A.*). The volume fraction of α-laths is significantly reduced exhibiting a fine scale microstructure for the hypoeutectoid composition of ~7wt.%(5.83at.%)Fe. Placement on the 550°C isothermal section provided by Volkova in Figure 2.6 shows that for this local composition, the microstructure should consist of αTi + (B2)TiFe. It is expected for (B2)TiFe to nucleate as a finely dispersed precipitate because the local composition is Ti rich and the

previously studied Ti – Fe binary system displayed a strong correlation between Fe content and the coarsening of (B2)TiFe phase. This microstructure persists up to ~19.30wt.%(16.36at.%) where the grain boundaries are decorated by a fine scale structure shown in Figure 6.4.E. There is also an observed grain boundary product in Figure 6.4.E. that may be the C14 Laves phase $TiFe_2$ (more information is needed to confirm). It is observed at ~27.29wt.%(23.40at.%)Fe that the intermetallic compound (B2)TiFe nucleates as a grain boundary product. Interestingly, (B2)TiFe is only observed in regions of the grain that are decorated when not precipitated intragranularly. The characteristic dendritic morphology of (B2)TiFe is observed for Fe compositions in excess of 30wt.%(25.83at.%)Fe. Spectra obtained from XRD experiments taken from a region within the vicinity of compositions that average Ti – (12.2 – 23.83)wt.%Fe – 5wt.%Al reveal that α–Ti orders to α_2-Ti_3Al. The observed ordering transition displayed below:

$$\alpha\text{–Ti} \rightarrow \alpha + \alpha_2\text{-}Ti_3Al$$

could explain the fine scale microstructure decorating the grains boundaries in Figures 6.4.B. and C. Reported literature has shown that the α phase can decompose to $\alpha + Ti_3Al$ in alloys containing Al content >6wt.%Al. The nucleation of the ordered Ti_3Al phase for the 550°C specimen is submicron in size and requires transmission electron microscopy (TEM) for better analysis. The dendritic morphology of (B2)TiFe suggests that the B2 phase forms first from the liquid, followed by Ti_3Al for local compositions that rest in the three phase field Ti_3Al + βTi + (B2)TiFe (*see reaction scheme below*).

$$L \rightarrow \beta\text{–Ti} + \text{(B2)TiFe}$$

$$\beta\text{-Ti} + \text{(B2)TiFe} \rightarrow \beta\text{–Ti} + \text{(B2)TiFe} + Ti_3Al$$

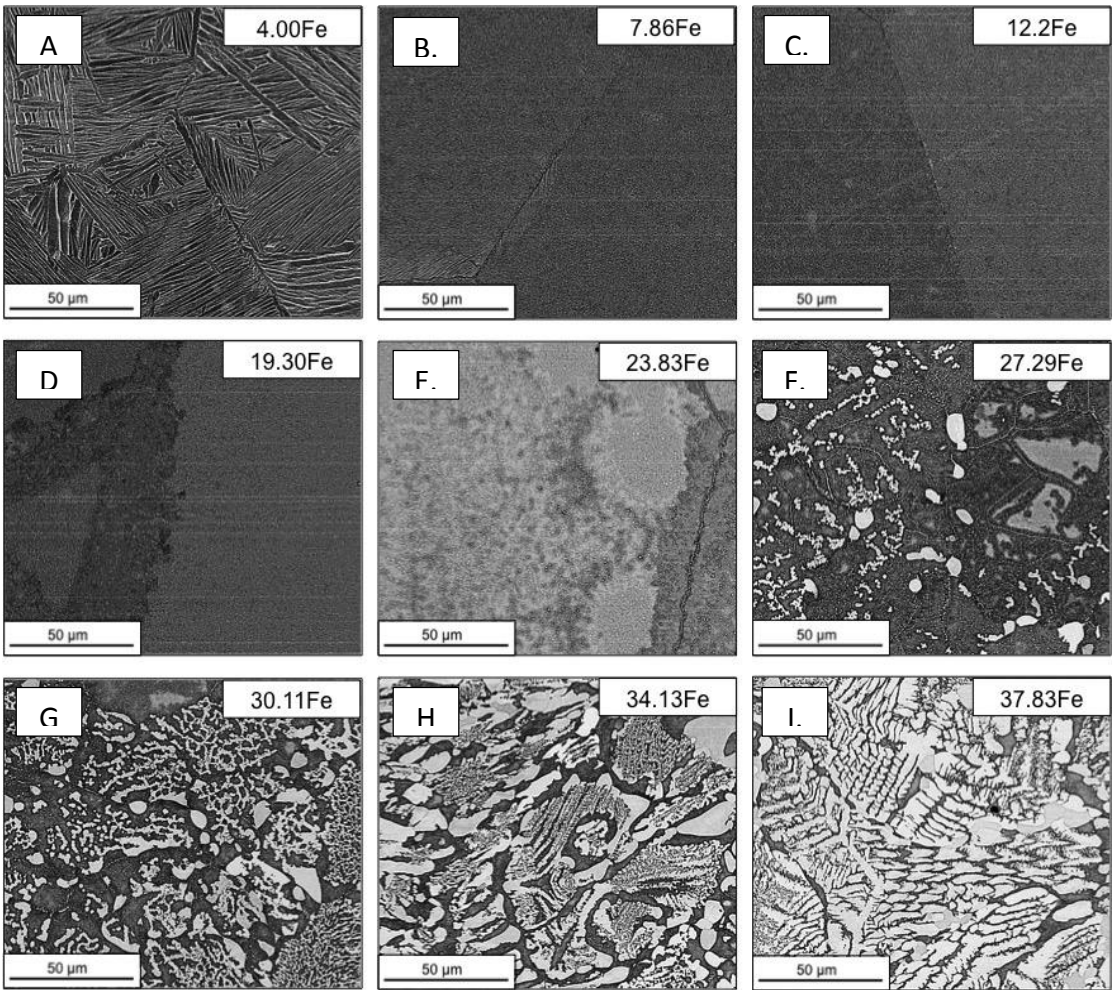

Figure 6.4. Scanning electron micrographs (1000X Magnification) of a Ti – xFe – 5Al aged at 550°C for 4 hours. A. corresponding microstructure of $Ti_{88.09} – Fe_{3.32} – Al_{8.59}$ alloy exhibiting Widmanstätten a lathes, B. fine scale microstructure for hypoeutectoid composition of $Ti_{84.81} – Fe_{6.56} – Al_{8.64,}$ C. continued fine scale microstructure at $Ti_{81.07} – Fe_{10.24} – Al_{8.69}$, D. grain boundary decoration observed at $Ti_{74.86} – Fe_{16.36} – Al_{8.77}$, E. Grain boundary product observed at $Ti_{70.84} – Fe_{20.33} – Al_{8.83}$, F. Grain boundary precipitation of (B2)TiFe at $Ti_{67.72} – Fe_{23.40} – Al_{8.87}$, G. dual morphology of (B2)TiFe (dendritic and globular) at $Ti_{65.17} – Fe_{25.92} – Al_{8.91}$, H. $Ti_{61.48} – Fe_{29.56} – Al_{8.96}$, coarsening of (B2)TiFe with dendritic stringers, I. $Ti_{58.05} – Fe_{32.94} – Al_{9.01}$, increased volume fraction of (B2)TiFe.

Similar to what is observed in the binary Ti – Fe system, the volume fraction of (B2)TiFe relative to the βTi matrix increases as solute content increases. Minor additions of Fe after 30wt.%(25.83at.%) results in the immediate coarsening of the (B2)TiFe phase with attached dendritic “stringers”.

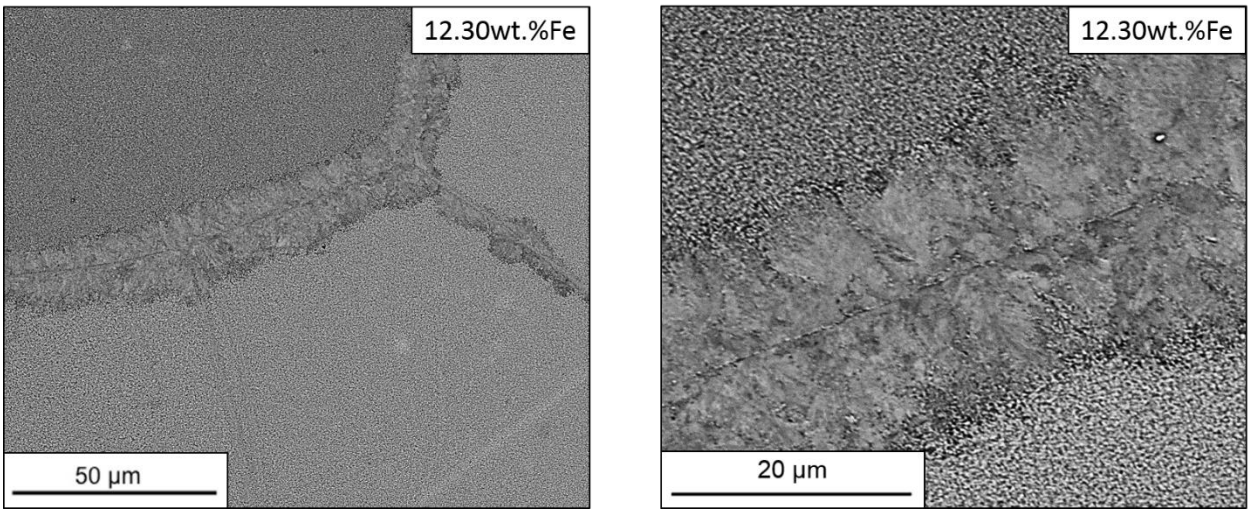

Figure 6.5. Scanning electron micrographs of a Ti – 12.30wt.%(10.33at.%)Fe – 5wt.%(8.69at.%)Al alloy taken at 1000X (left) and 2000X (right) that exhibit a fine scale microstructure with decorated grain boundaries.

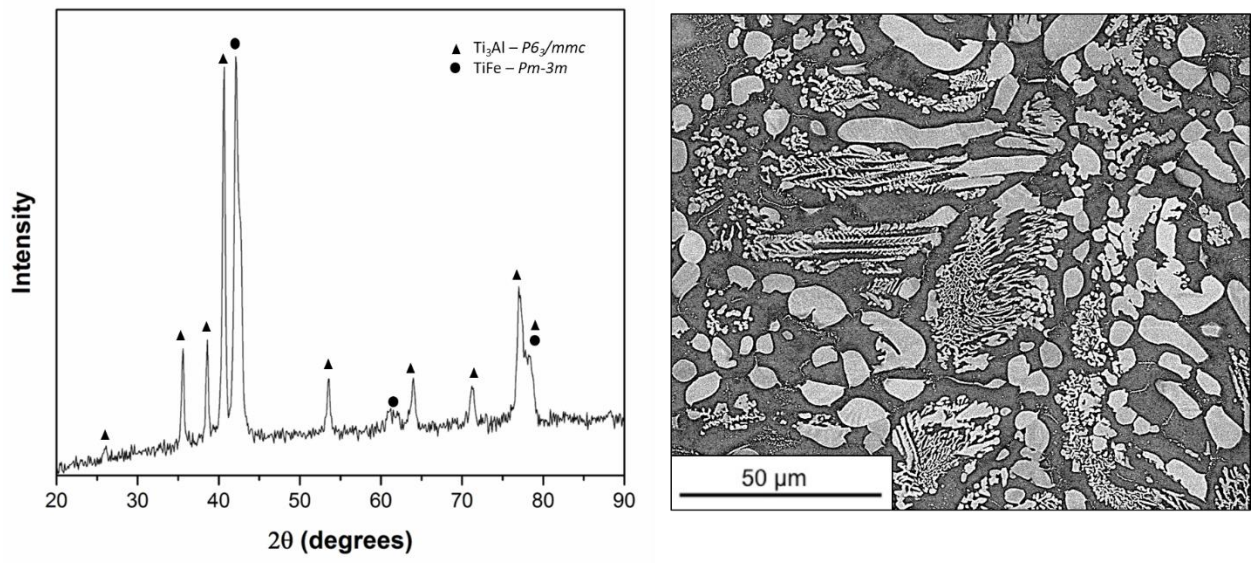

Figure 6.6. XRD spectra and the corresponding microstructure exhibiting the morphology of "primary" and dendritic (B2)TiFe. The peaks that correlate to the presence of Ti_3Al suggests that the α_2 phase has nucleated at a fine scale in the areas around (B2)TiFe.

6.3.1.2 Vickers Microhardness

The Ti – *x*Fe – 5Al specimen directly aged at 550°C for 4 hours exhibited a large range of microhardness values as the local composition of Fe increased. The lowest hardness values for the specimen was recorded at 2.24wt.%(1.85at.%)Fe (334HV). This is largely due to the low composition of Fe present in the β phase and the high volume fraction of α–Ti relative to the retained β–Ti phase displayed in Figure 6.7. (A.) and (B.). This composition (Ti – 5wt.%(8.57at.%)Al – 2.24wt.%(1.85at.%)Fe) is closer to the minimum Fe (composition, wt.%) requirement for the commercially available Ti – 5 – 2.5Al (Tikrutan LT 35) Ti alloy. The recorded hardness value at 2.24wt.%(1.85at.%)Fe for the LENS^{TM} deposited specimen is within the hardness value range of 320 – 340HV for the technical alloy Ti – 5Al – 2.5Fe that has been deformed at 850°C and aged between the recommended temperatures of 400 – 700°C. This relatively high hardness value compared to that of the technical alloy of higher Fe content is attributed to the fine scale microstructure produced as a result of the LENS^{TM} process. The linear increase in hardness values as a function of Fe content plateaus above average compositions containing ~19.35wt.%(16.41at.%)Fe. Recorded hardness values tend to average between 700 and 800HV after this composition of Fe. The observed plateau in hardness value for this specimen aged at 550°C for 4 hours is believed to be attributed to both the morphology and the volume fraction of the specific morphology of (B2)TiFe (e.g. dendritic or "primary"). Microstructures from the indentation tests taken between compositions of 26 – 31wt.%Fe consisted of a (B2)TiFe with intragranular dendritic (B2)TiFe or the B2 phase with dendritic stringers (*presented in Figure 6.8.B.*). The highest recorded hardness value for the 550°C step quenched sample surprisingly didn't occur for the highest Fe content. The micrograph shown in Figure 6.8A. recorded a hardness value of 784HV. This hardness value is attributed to a solid

Vickers Microhardness vs. wt.%Fe in 550°C Aged Ti - xFe - 5wt.%Al LENS™ Deposited Gradient

(wt.%)(at.%)	Hv	L1	L2	Mpa	STD
2.24/1.85	334	72.65	76.35	1048	3.23
3.92/3.25	443	63.78	65.64	1469	1.34
4/3.32	429	66.25	65.19	1412	6.43
7.6/6.34	515	59.96	59.99	1768	12.76
12.24/10.28	565	56.53	58.09	1969	3.21
13.7/11.52	536	58.42	59.25	1850	7.43
19.35/16.41	659	52.75	53.32		15.72
23.83/20.33	737	49.43	50.92		9.32
26.38/22.59	743	49.77	50.15		11.87
29.29/25.19	719	49.94	51.62		2.54
32.46/28.04	748	48.83	50.73		1.09
33.46/28.95	742	49.78	50.2		21.78
37.3/32.45	762	47.98	50.67		5.76

Table 6.2. Graph displaying the HV as a function of Fe content in a Ti – *x*Fe – 5Al specimen subject to a β solution at 1100°C for 4 hours, step quenched to 550°C for 4 hours, then air cooled.

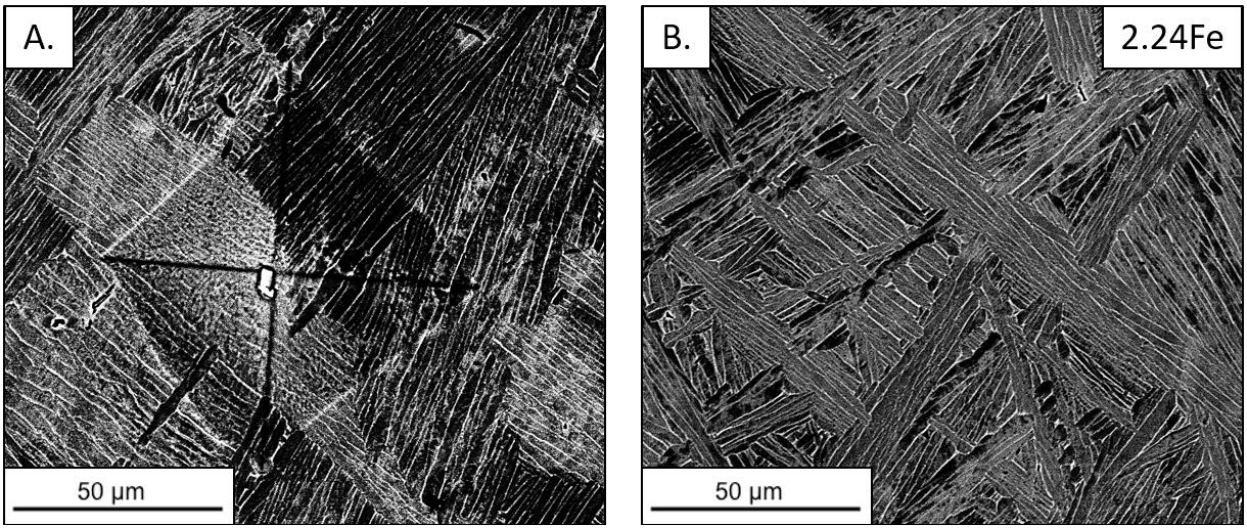

Figure 6.7. Backscatter electron micrographs displaying the Vickers microhardness indentation (A.) and local microstructure (B.)

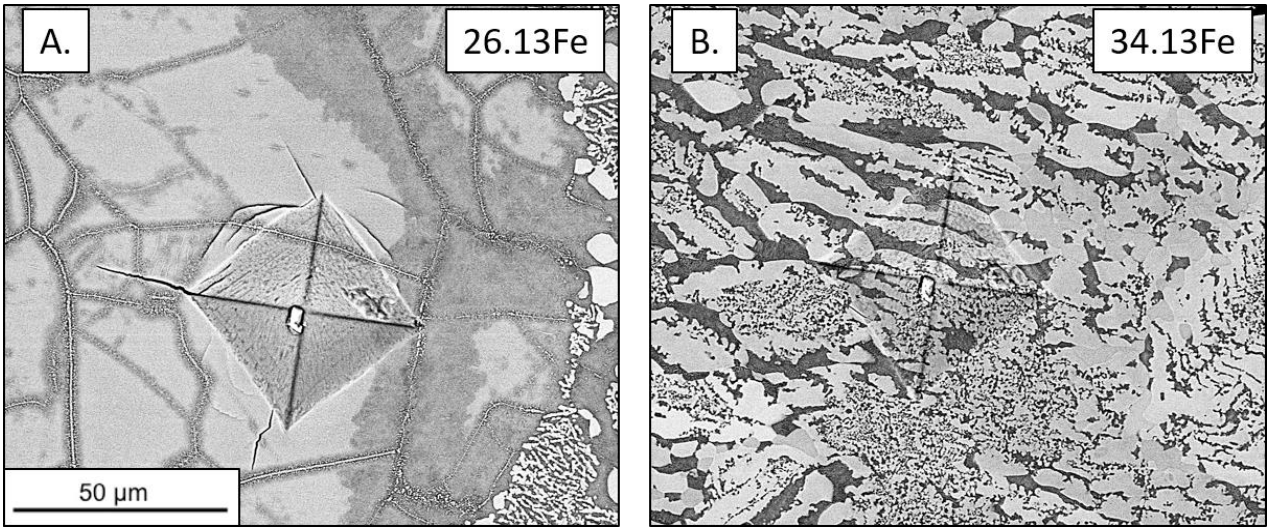

Figure 6.8. Backscatter electron micrographs displaying the Vickers microhardness indentation (A.) HV:784 at Ti – 26.13wt.%Fe – 5wt.%Al. Highest recorded value for Ti – *x*Fe – 5Al step quenched at 550°C. (B.) HV:726 at 60.87wt.%Ti – 34.13wt.%Fe – 5wt.%Al. Microstructure with highest Fe content of (B2)TiFe with dendritic stringers.

solution effect that relates to the maximum amount of Fe soluble in the β phase with the absence of (B2)TiFe in the local area of the indentation. The bimodal grain size within the vicinity of the indentation could also suggest a Hall Petch effect that is attributing to the recorded hardness.

6.3.1.3 Comparison of Ti – *x*Fe – *y*Al (y = 0) and Ti – *x*Fe – 5Al LEN™ Deposited Gradient Step Quenched at 550°C for 4 Hours

This section is dedicated to the comparison of the microstructure and Vickers microhardness values for a Ti – *x*Fe LENS™ deposited gradient and a Ti – *x*Fe – 5Al LENS™ deposited gradient that were both directly aged at 550°C for 4 hours after homogenization in the β phase field for 4 hours.

Recorded hardness values for the two compositionally graded specimens presented in Figure 6.9. shows that alloying 5wt.%Al to any composition of alloys belonging the binary Ti – Fe system results in an increase in recorded Vickers microhardness. From the microstructures

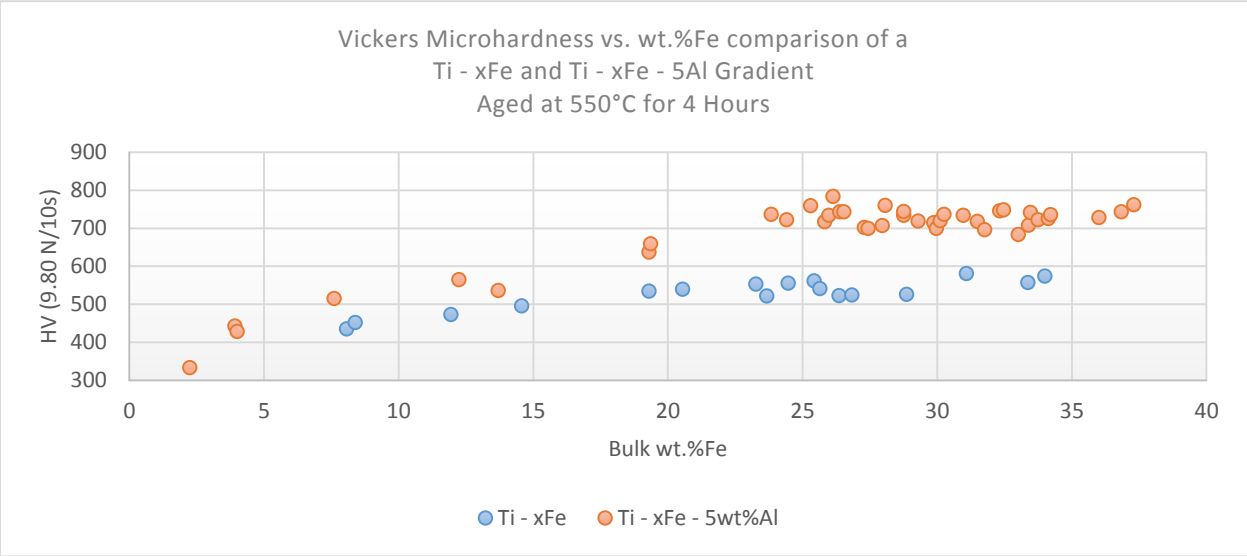

Figure 6.9. Comparison of Vickers microhardness in a Ti – xFe and Ti – xFe – 5Al LENS^{TM} deposited gradient specimen step quenched at 550°C for 4 hours.

presented in the previous section of this study of the Ti – xFe – 5Al gradient, this is believed to be attributed to the fine scale nucleation of Ti_3Al. It has been observed in the binary Ti – xFe study that there is a strong correlation between the recorded hardness value and the inter-particle spacing of the (B2)TiFe intermetallic. But this correlation is only observed in the Ti – *x*Fe LENS^{TM} deposited specimens directly aged to temperatures above the invariant point (595°C) for 4 hours. A comparison of the morphology and precipitation of the (B2)TiFe intermetallic compound in the Ti – *x*Fe and Ti – *x*Fe – 5Al LENS^{TM} deposited gradients is made in Figure 10. In the previous study of the binary Ti – Fe system, observed precipitation of (B2)TiFe occurred as a grain boundary product at ~20wt.%(16.97at.%)Fe by the reaction shown below:

$$\beta \rightarrow \alpha + (B2)TiFe$$

The very small volume fraction of β-Ti presented in Figure 6.10.A. is due to the hypereutectoid composition (eutectoid transformation occurs at 15wt.%(12.64at.%)Fe) of

20wt.%(16.97at.%)Fe. Confirmation from XRD experiments show peaks corresponding to the presence of the (B2)TiFe intermetallic for the Ti – *x*Fe – 5Al gradient. Essentially, alloying 5wt.% of Al to a binary Ti – 20wt.%Fe alloy suppress the scale at which the B2 phase nucleates. At ~25wt.%(21.37at.%)Fe, the microstructure for the binary Ti –*x*Fe gradient consists of "primary" (B2)TiFe (intergranular) and "secondary" (B2)TiFe (intragranular) with a spherical morphology. The corresponding microstructure for the same composition of Fe, but alloyed with 5wt.%Al exhibits (B2)TiFe at the grain boundaries. It is important to note that the thickness of (B2)TiFe precipitated at the grain boundaries in Figure 6.10B.(25wt.%(21.37at.%)Fe) is similar to that observed in Figure 6.10A.(20wt.%(16.97at.%)Fe). A comparison of 33wt.%(28.53at.%)Fe varies in morphology of the intermetallic also. The characteristic dendritic morphology of the B2 intermetallic compound is observed for both specimens. There is also considerable coarsen of the compound as a function of increasing Fe content. The first difference in microstructure for the two specimens occurs in the morphology of the dendritic variant of (B2)TiFe. Specifically, the morphology of TiFe for the composition of Ti – 33wt.%(28.53at.%)Fe – 5wt.%Al is "stringy" and fine relative to the coarse dendritic structure observed for Ti – 33wt.%(28.53at.%)Fe. Lastly, the composition of "primary" (B2)TiFe in the Ti – 33wt.%(28.53at.%)Fe – 5wt.%Al varies significantly in contrast to the intermetallic particles observed for the binary composition. The intermetallic particles in Figure 6.10.C. (33wt.%(28.53at.%)Fe – 5Al) exhibit compositions that are Fe rich given the contrast of the backscatter electron micrograph. clear to see that with increasing Fe content, the volume fraction of α-Ti decreases at a lower rate than observed in the Ti – *x*Fe – 5Al gradient directly aged at 550°C for 4 hours *(see Figure 6.8).* A fine scale lamellar structure is present in Figure 6.11.D. (and in higher magnification for Figure 6.12 (A.) and (B.))

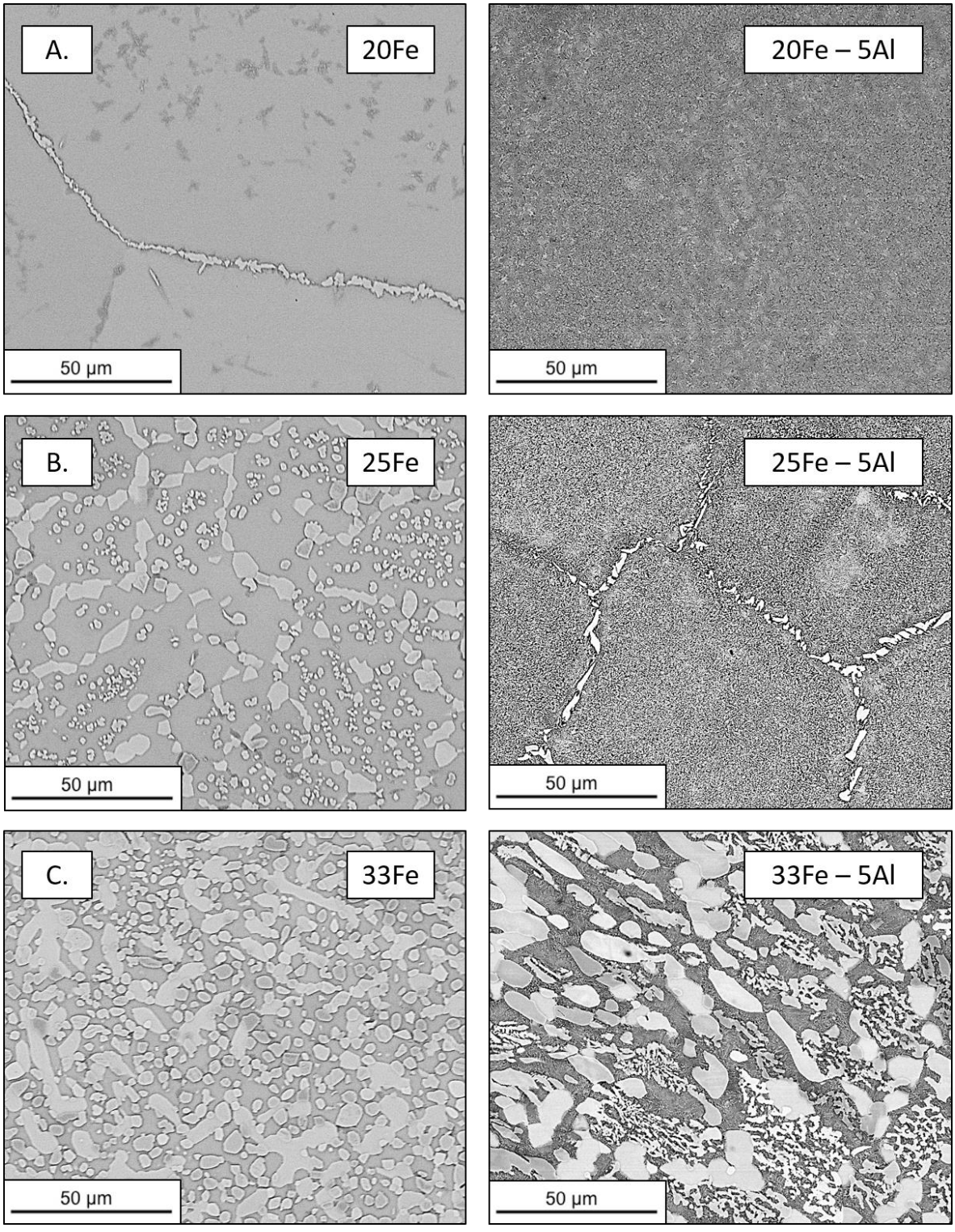

Figure 6.10. Comparison of in morphology and precipitation of the (B2)TiFe intermetallic compound in a Ti – *x*Fe and Ti – *x*Fe – 5Al LENS^{TM} deposited gradient step quenched to 550°C for 4 hours .

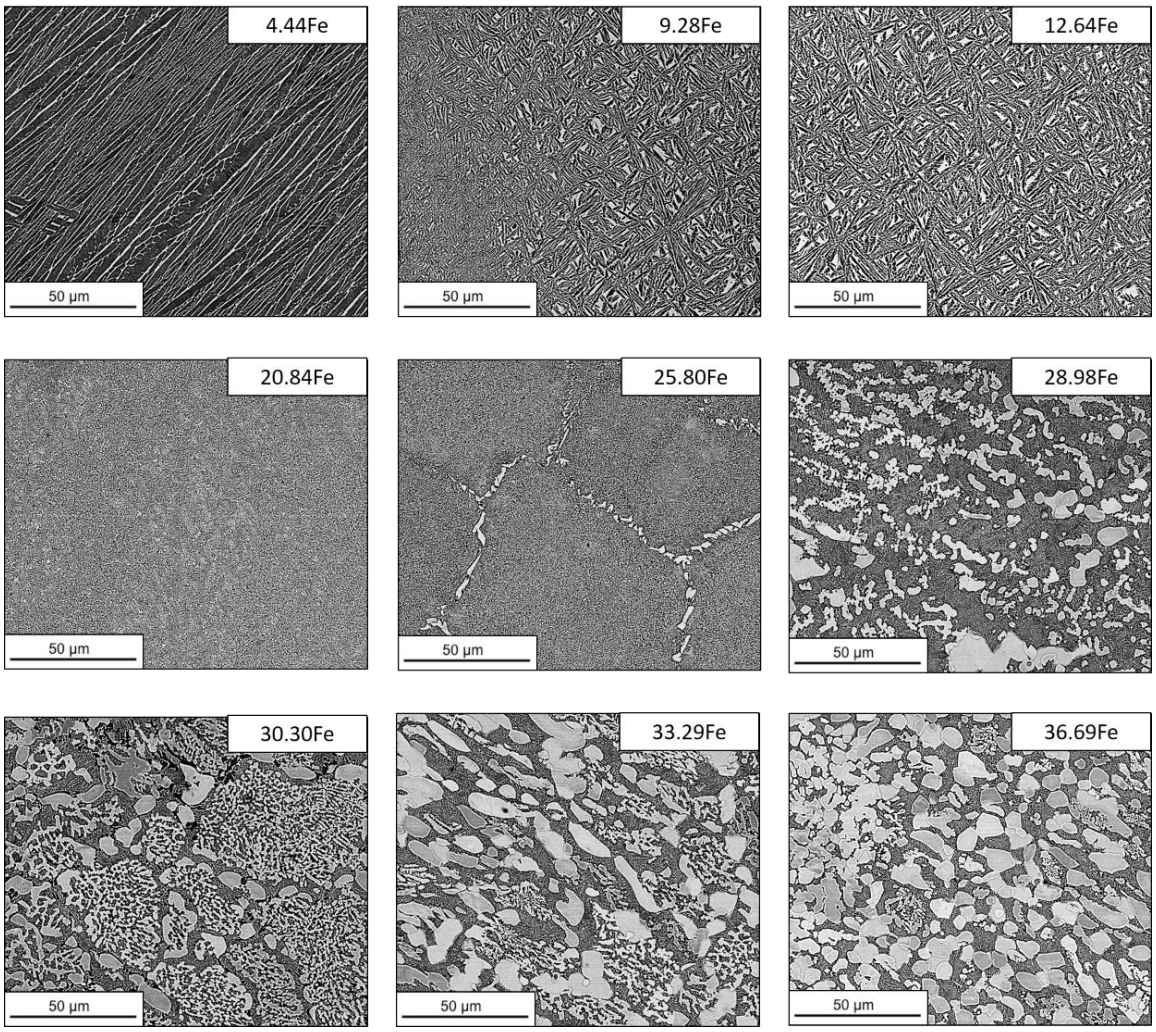

Figure 6.11. Comparison of microstructures observed in the Ti – xFe – 5Al LENS^{TM} deposited gradient step quenched to 650°C for 4 hours, then air cooled.

at ~ 20.84wt.%(17.71at.%)Fe. A scanning electron micrograph (SEM) taken at 2000X magnification provided in Figure 6.12.A. shows the lamellar structure has an inter-lamellar spacing that is sub-micron in scale. Further magnification reveals the presence of acicular a laths intermixed within the lamellar structure. The fine scale of the laths prevented elemental quantification of the microstructural feature. At ~ 25.80wt.%(22.08at.%)Fe, (B2)TiFe precipitates at the grain boundaries with no evidence of the dendritic morphology. For gradient compositions

>28wt.%(24.03at.%)Fe, the presentation of a complex microstructure of (B2)TiFe and the fine scale lamellar structure exists. This microstructure is consistent from comparisons of the 550°C aged Ti – *x*Fe – 5Al specimen and persists throughout the remainder of the compositionally graded alloy. XRD spectra from a region that contains the fine scale lamellar structure shows peaks that signify the presence of the ordered α_2 phase, Ti_3Al.

An unidentified phase was observed when collecting the local composition of an indentation test performed for the Ti – *x*Fe – 5Al 650°C specimen. Spot scans reveal a composition that doesn't correspond to the stoichiometry of (B2)TiFe or the C14 Laves Phase. Channeling contrast is observed displaying grains of varying orientation of the unidentified phase (*see Figure 6.13.*). This is an interesting find because this microstructural feature could be a (B2)β-Ti island of the soluble B2 phases (B2)β-Ti and (B2)TiFe that was retained from the 1100°C β solution. Spot scans performed on the connecting microstructural features are in fact (B2)TiFe with the lamellar structure surrounding both the island and intermetallic compound. Observable dendritic growth of the (B2)TiFe phase is also observed after compositions of > 28.98(24.91at.%)Fe. Vickers indentation tests taken for the Ti – xFe – 5Al deposited specimen shows a maximum hardness of HV705 for 30.85wt.%(26.59at.%)Fe. The micrograph in Figure 6.14. represents the local microstructure of the indentation taken at 30.85wt.%(26.59at.%)Fe. In this micrograph the microstructure consists of (B2)TiFe with an interconnecting dendritic morphology, as well as the spherical morphology of (B2)TiFe precipitated in the top right corner of the micrograph. A closer observation of the micrograph also shows the presence of Ti_3Al.

The initial microstructures observed for the Ti – *x*Fe – 5Al deposited gradient step quenched to 750°C for 4 hours exhibited coarse α phase Ti with β–Ti ribs appearing to originate

from the α layer nucleated at the grain boundaries. The recorded microhardness value for the average local composition of Ti – 2.38wt.%(1.97at.%)Fe – 5wt.%(8.57at.%)Al quenched at

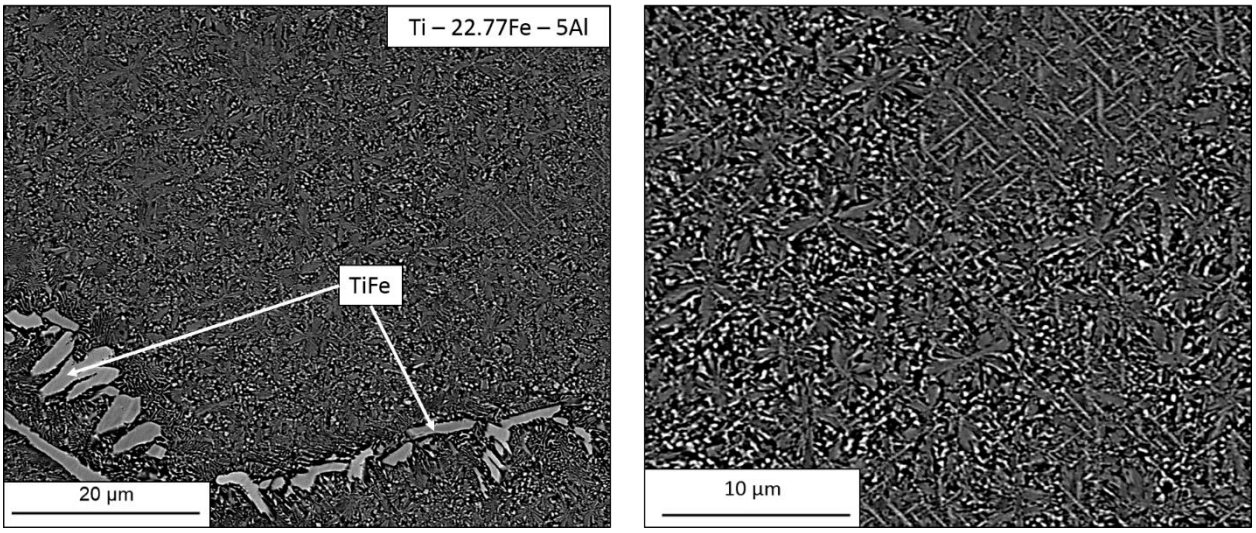

Figure 6.12. 2000X (left) and 4000X (right) magnification of the microstructure observed at the Ti – 22.77wt.%(19.40at.%)Fe – 5wt.%(8.82at.%)Al composition of a Ti – *x*Fe – 5Al LENS™ deposited gradient step quenched to 650°C for 4 hours.

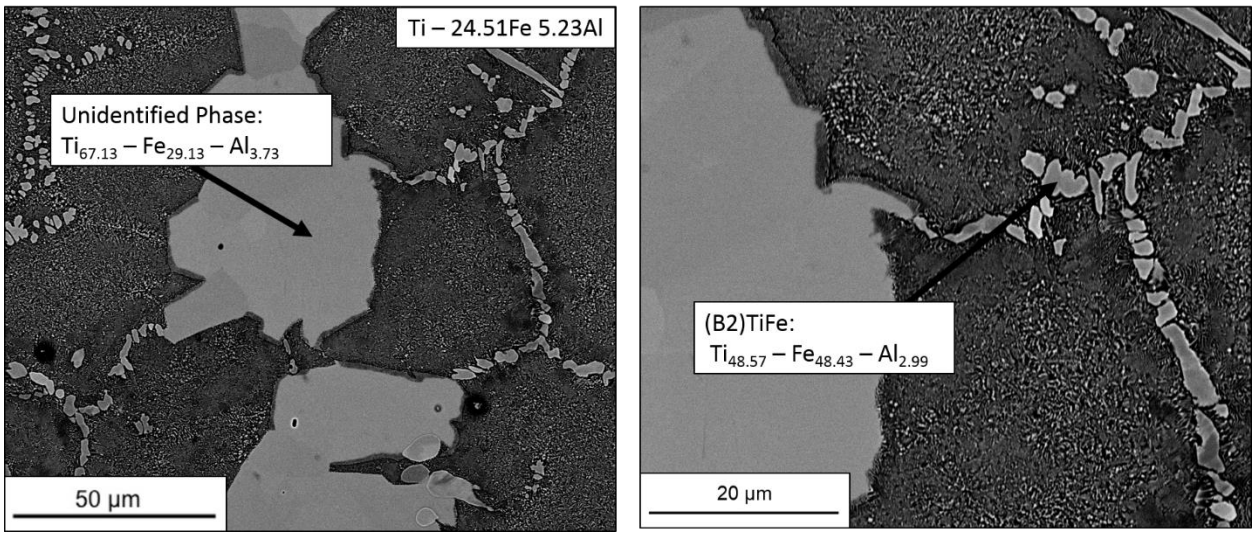

Figure 6.13. 1000X (left) and 2000X (right) magnification of the microstructure observed at the Ti – 24.77wt.%(21.16at.%)Fe – 5wt.%(8.84at.%)Al composition of a Ti – *x*Fe – 5Al LENS™ deposited gradient step quenched to 650°C for 4 hours.

Vickers Microhardness vs. wt.%Fe in 650°C Aged Ti - xFe - 5wt.%Al LENS™ Deposited Gradient

(Wt.%)(at.%)	Hv	L1	L2	Mpa	STD
2.5/2.07	327	75.61	75.01	1025	1.45
4.42/3.67	364	71.64	71.05	1162	0.5
9.28/7.76	452	64.1	64.05	1505	1.76
12.46/10.46	466	62.87	63.24	1561	3.56
16.83/14.22	510	60.02	60.62	1747	4.32
20.84/17.71	520	59.36	60.11	1788	16.87
24.25/20.70	539	58.35	58.91	1861	12.56
25.8/22.08	589	55.63	56.56	2055	5.87
26.73/22.90	579	55.64	57.54	2022	7.98
28.82/24.77	633	53.68	54.56	---	5.86
30.65/26.41	705	50.91	51.65	---	20.43
33.71/29.17	613	54.52	55.5	---	26.87

Table 6.3. Vickers microhardness vs. bulk wt.%Fe of a Ti – xFe – 5Al LENS™ deposited gradient step quenched to 650°C for 4 hours then air cooled.

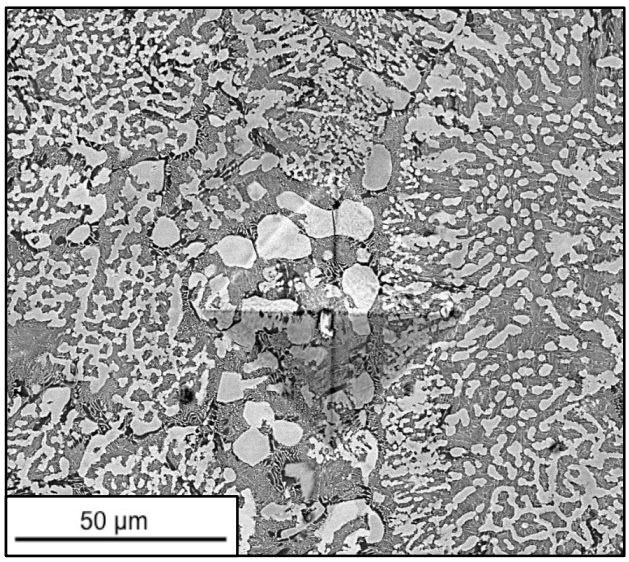

Figure 6.14. Vickers microhardness indentation test of located at Ti – 30.85wt.%(26.59at.%)Fe – 5wt.%(8.92at.%)Al for the 650°C aged specimen.

750°C is 417HV. This is higher than the recorded hardness values for the 550 and 650°C samples with the equivalent composition. The increase in hardness is attributed to the retained β phase with Fe in solid solution that is available. Although the volume fraction of the β phase that is present is small relative to α–Ti, the overall volume fraction β phase compared to the 550 and 650°C is higher. At ~13.33wt.%(11.21at.%)Fe, the microstructure has fully retained the β phase. This is an evolution in the microstructure as a function of increasing Fe content because literature provided by 1995Palm and Raghavan speak of a B2 field of continuous solubility between the two ordered B2 phases, (**B2**)β-Ti (ordered) and (**B2**)TiFe when sufficient Al content is achieved to cause the ordering transition:

(**A2**)β-Ti (disordered) → (**B2**)β-Ti (ordered)

When observing the region where the B2 field of continuous solution between (**B2**)β-Ti and (B2)TiFe is to occur, one can extrapolate from the 900 and 800°C isothermal section that this phase field should shrink with respect to Al content that is soluble as temperature decreases and as Fe content increases. Additionally, the maximum solubility of Fe in (A2)β-Ti decreases to roughly 24wt.%(20.48at.%) at 800°C. When considering the binary phase diagram, the maximum solubility at 750°C is ~20wt.%Fe, this is well within the range of the recorded composition of the micrograph presented in Figure 6.15. When observing the solubility of Al content in the provided isothermal sections, this recorded composition could suggest that the field is slightly higher than previously recorded for allowable Al content that is also soluble in the continuous B2 field at 750°C.

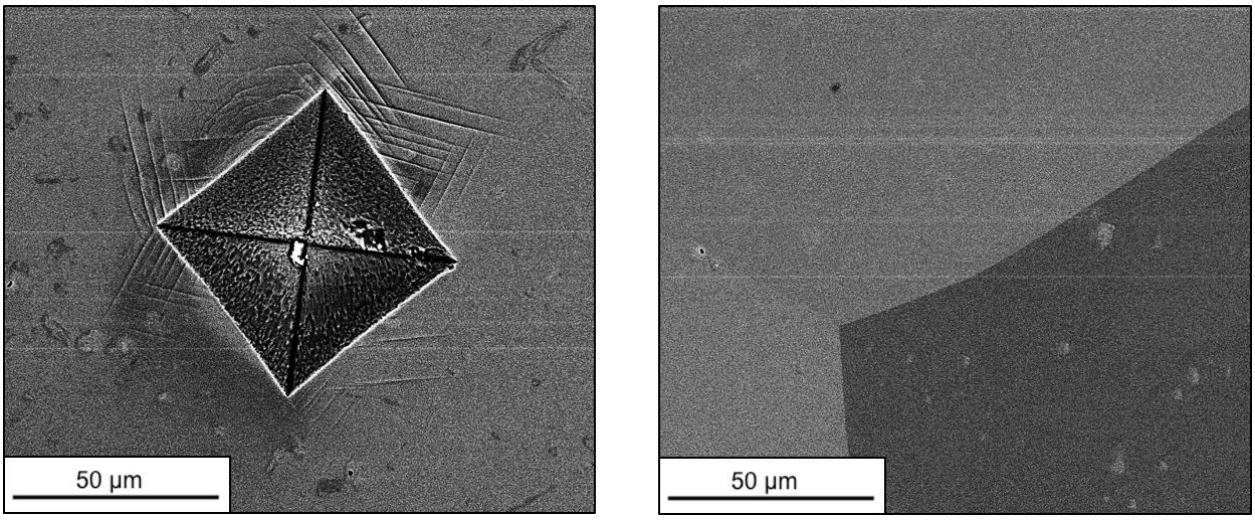

Figure 6.15. Vickers microhardness indentation test of located at Ti – 13wt.%(10.92at.%)Fe – 5wt.%(8.70at.%)Al for the 750°C aged specimen.

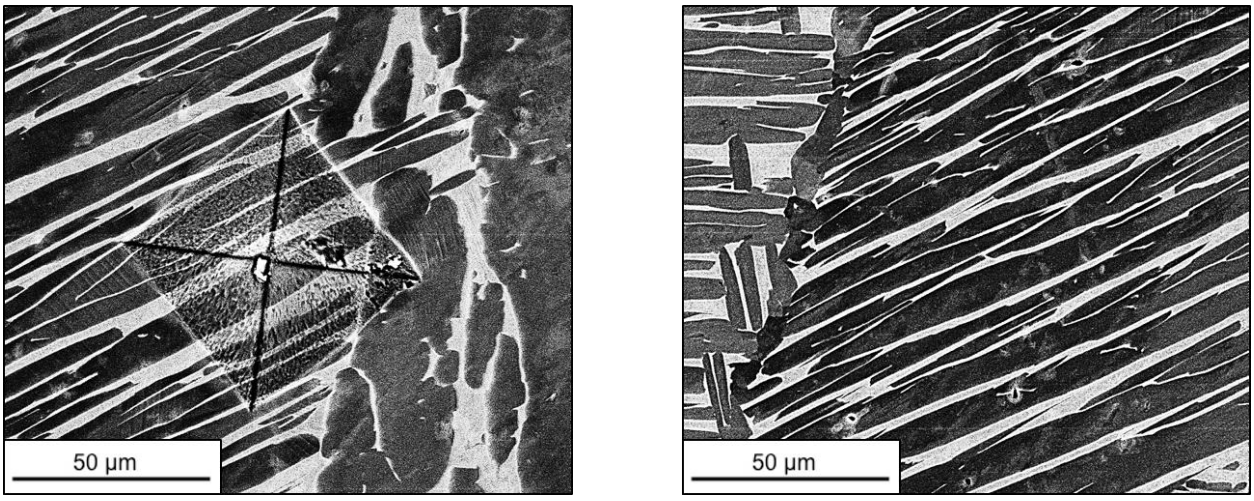

Figure 6.16. Vickers microhardness indentation test of located at Ti – 2.38wt.%(1.97at.%)Fe – 5wt.%(8.57at.%)Al for the 750°C aged specimen.

Vickers Microhardness vs. wt.%Fe in 750°C Aged Ti - xFe - 5wt.%Al LENS™ Deposited Gradient

(wt.%)/(at.%)	HV	L1	L2	Mpa	STD
3.08/2.55	379	68.68	71.23	1205	1.56
13.33/11.21	433	64.99	65.86	1430	2.54
15.26/12.86	455	63.48	64.14	1518	7.32
17.99/15.22	475	61.67	63.25	1597	12.87
21.57/18.35	491	60.77	62.12	1665	8.54
22.04/18.76	503	60.07	61.41	1717	20.54
26.03/22.28	531	58.83	59.4	1831	17.32
27.25/23.37	542	58.23	58.72	1873	4.98
30.52/26.29	571	56.49	57.51	1992	0.5
32.89/28.43	568	55.84	58.43	1981	2.98
35.64/30.93	588	55.66	56.67	2052	17.43
37.3/32.45	588	55.82	56.53	2052	43.21
38.56/33.61	627	53.56	55.16		8.21

Table 6.4. Vickers microhardness vs. bulk wt.%Fe of a Ti – xFe – 5Al LENS™ deposited gradient step quenched to 750°C for 4 hours then air cooled.

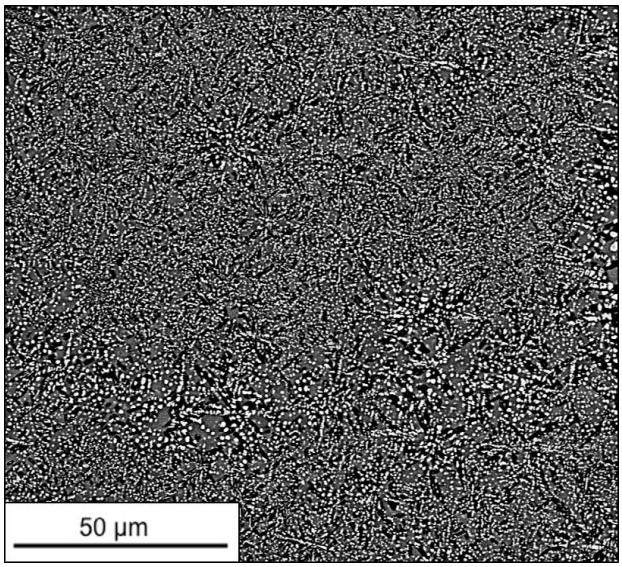

Figure 6.17. Vickers microhardness indentation test of located at Ti – 22.58wt.%(19.23at.%)Fe – 5wt.%(8.82at.%)Al for the 750°C aged

As shown in the backscatter electron micrograph *(Figure 6.17.)*, a fine scale homogenous distribution of a spherical phase rich in Fe, and of high volume fraction dominates the microstructure. The composition of the matrix is 81.32wt.%(79.79at.%)Ti – 13.68wt.%(11.51at.%)Fe – 5wt.%(8.71at.%)Al. XRD spectra obtained from experiments within the vicinity of the microhardness indentation test reveals that the phases present in this region of the LENS^{TM} deposited gradient are Ti_3Al and (B2)TiFe. This two phase field is expected for the 750°C isothermal section when observing the difference between the 550°C isothermal section and the 800°C isothermal section. As temperature decreases, the (B2)TiFe + Ti_3Al two phase field expands markedly with respect to. It is important to note when matching the peak intensities of the obtained XRD spectra that (B2)TiFe exhibited peaks that were slightly shifted. This is attributed to the affect Al content has on the lattice parameter of (B2)TiFe. The solubility of Al in (B2)TiFe increases with increasing temperature. As more Al atoms substitute for Fe atoms, the lattice parameter of (B2)TiFe increases. It can be assumed from the results of the XRD experiment that the dark phase in the micrograph is Ti_3Al. Additionally, it is observed in the binary Ti – Al system that α phase Ti orders to α_2 – Ti_3Al with increasing Al content. The recorded composition of Ti_3Al is 85.03wt.%(77.87at.%)Ti – 2.62wt.%(2.06at.%)Fe – 12.35wt.%(20.07at.%)Al. The low solubility of Fe in Ti_3Al is expected as this result is consistent with literature published on α_2 – Ti_3Al based alloys with additions of the β stabilizer Fe. The microhardness values recorded for the 750°C holding time increase linearly as the average composition of Fe content increases (*Provided in Table 6.4*). An interesting microstructural phenomena was observed at composition > 30wt.%Fe. Displayed in Figure 6.18. is a backscatter electron micrograph taken at 4000X magnification of a transformation front with two alternating phases. Specific area spot scans using EDAX software of a backscatter electron micrograph taken at 4000X magnification reveals the

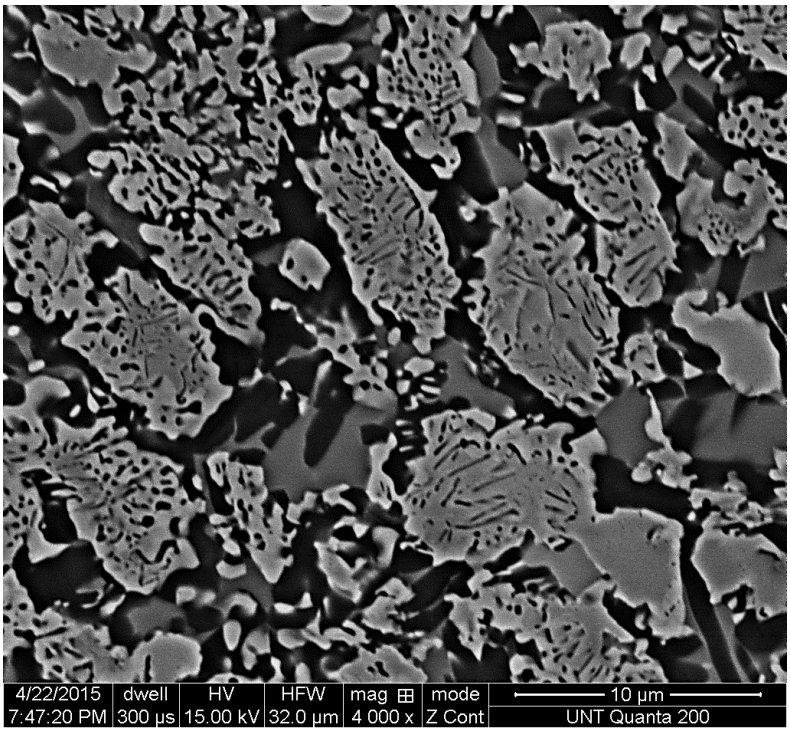

Figure 6.18. Backscatter electron micrograph of transformation front on (B2)TiFe intermetallic compound.

composition of the microstructural features within the transformation front on the (B2)TiFe intermetallic compound. The compositions taken for Figure 19. (A.) and (B.) were notable. (B2)TiFe is a stoichiometric intermetallic compound.. It appears from the recorded elemental quantification using energy dispersive spectroscopy (EDS) that there are composition fluctuations within the intermetallic that vary with respect to Al composition. The spot scan taken in Figure 6.19.A. recorded compositions of Ti and Fe that are within the stoichiometric range to determine that this is in fact the intermetallic compound (B2)TiFe with an addition of 5.71wt.%(10.36at.%)Al. The same can be said in regard to the elemental quantification recorded in Figure 6.19.C. The compositions for Ti and Fe are in the stoichiometric range to determine that this is also (B2)TiFe, but the Al content present within the scanned microstructural feature is 2.39wt.%(4.49at.%)Al. When considering similar features in the micrograph, the transformation

front appears to initiate from the contours of the intermetallic where the composition is assumed to have ~2.39wt.%(4.49at.%)Al present. It is in these light gray regions that the transformation of Ti_3Al and (B2)TiFe that has less than 5.71wt.%(10.36at.%)Al is observed. Regions of the intermetallic that are 5.71wt.%(10.36at.%)Al and greater are void of this transformation (these are the regions that are dark gray). The spot scan in Figure 6.19.B. is of an unidentified phase with the composition of 81.30wt.%(80.08at.%)Ti – 14.13wt.%(11.94at.%)Fe – 4.57wt.%(7.99at.%)Al

6.3.1.4 Summary of Ti – *x*Fe – 5wt.%Al

An initial investigation of the Ti – Fe – Al ternary system by assessing the microstructural changes in (B2)TiFe as well as Vickers microhardness across three isothermal sections when the binary Ti – Fe system is alloyed with 5wt.%Al. The morphology of (B2)TiFe varies significantly in volume fraction and composition where observable precipitation of the intermetallic at the grain boundaries occurs when 5wt.%Al is alloyed to the binary Ti – *x*Fe gradients for the 550°C aged gradient specimens. A comparison of microhardness values across the direct aging times shows that the highest hardness values where recorded in the 550°C Ti – *x*Fe – 5wt.%Al gradient. This is largely associated with the precipitation of (B2)TiFe in the regions of the grain that where decorated in a fine scale lamellar structure of what can be concluded to at least contain the ordered α_2 phase Ti_3Al from XRD spectra obtained from multiple regions beyond the bottom third of the gradient. But more importantly, the lower recorded hardness values across the 650 and 750C direct aging times is attributed to the brittleness of the α_2 phase Ti_3Al. Literature reports that the ductile-brittle transition of Ti_3Al occurs above 600°C and these recorded results are in agreement. The lowest microhardness values were recorded for the 750°C aged specimen. The microstructure consisted of coarse α lathes for low solute concentration and exhibited a transformation front on

the (B2)TiFe intermetallic compound for concentrations of Fe that exceeded 30wt.%. These microstructural features appear to have deleterious properties.

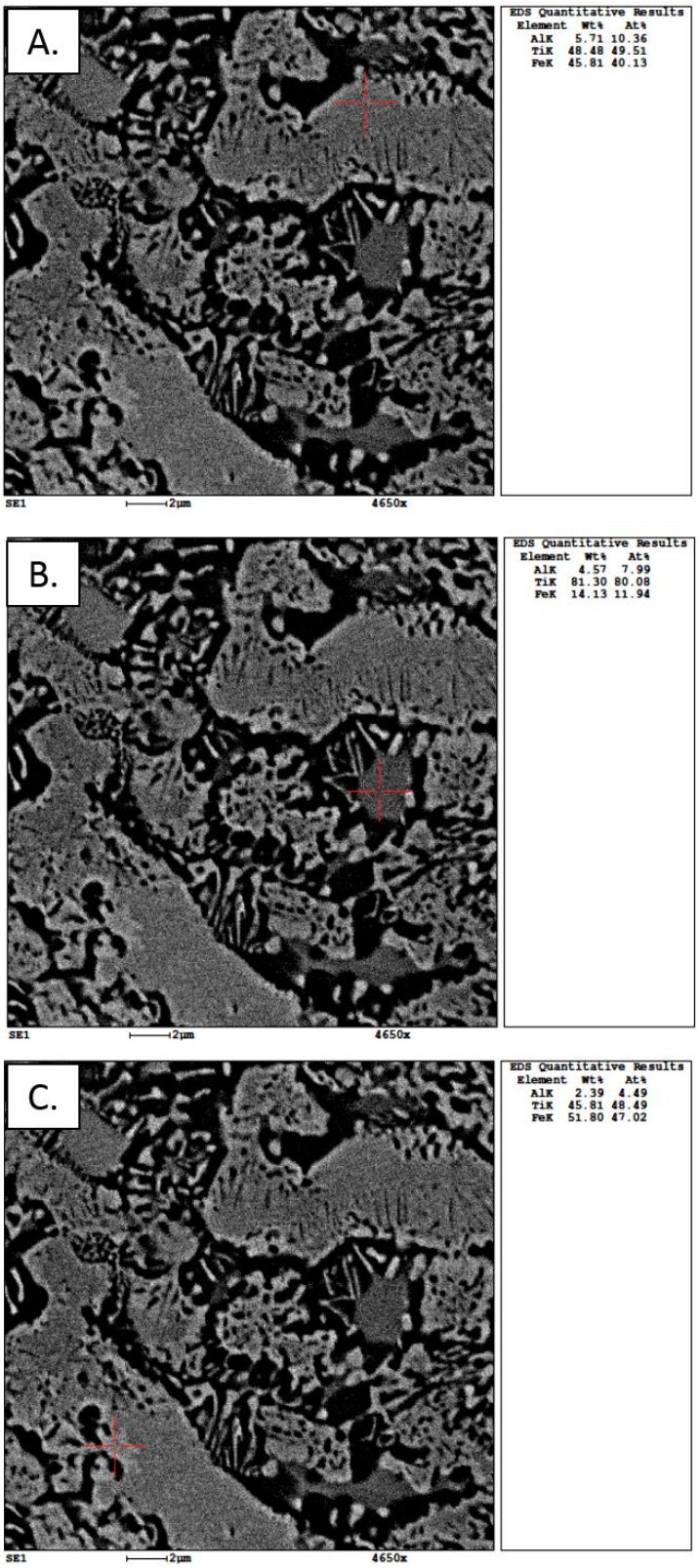

Figure 6.26. Series of Backscatter electron micrograph of transformation front on (B2)TiFe intermetallic compound with specific site EDS scan.

CHAPTER 7

CONCLUSIONS AND SUMMARY

Compositionally graded specimens were created using the LENS^{TM} process to rapidly asses the composition – microstructure – property relationships across the Ti – *x*W (0<x<40wt.%), Ti – *x*Fe (0<x<35wt.%), and Ti – *x*Fe – *y*Al (0<x<35wt.%; y=5,10,15) systems. This combinatorial approach resulted in the exploration of fields that are currently theoretically postulated with respect to the Ti – rich corner of the Ti – W and the Ti – Fe binary phase diagrams. Solute segregation, a historical challenge associated with the Ti – W binary system was avoided in the deposition of a compositionally graded specimen consisting of an energy density of 10×10^{-4}. Similarly, using the same energy density in the deposition of a Ti – xMo (0<x<40wt.%) compositionally graded specimen resulted in the reduction of partially reacted Mo particles. In contrast to the LENS^{TM} deposition of the Ti – xW gradient, the Ti – xMo specimen deposited using an energy density of 10×10^{-4} didn't achieve the targeted composition range due to the extended time the elemental blend of powder sat in the powder feedstock. This allowed for the Mo powder particles to settle limiting the maximum composition to 23wt.%Mo. Another result of the extended deposition time associated with the selected energy density was the microstructural response to the thermal gradient produced during the deposition process. For low concentrations of Mo, the microstructure consists of α lamellae, then transitions to a basketweave structure upon which the volume fraction of the α phase reduces with increasing Mo content.

Directly aging the Ti – *x*W gradient specimens to 800°C, above the proposed invariant point resulted in microstructures that consist of coarse α-lathes with no quantifiable reduction in

the volume fraction of α-Ti until 25wt.%W. At this composition, the equilibrium phase diagram shows for this composition, the corresponding microstructure should be fully retained β. This would correspond to the β phase field where Ti and W are mutually soluble. Experimental results that consist of an α + β microstructure for this composition suggests that upon cooling to room temperature after directly aging at 800°C for 50 hours the metastable β alloy transformed to an equilibrium microstructure as a result of the slow cooling of the quartz glass encapsulated Ti – *x*W specimen. Directly aging far below the proposed invariant point resulted in microstructures that were modestly influenced by the change in composition and appears to consist of a microtsture that is the product of martensite decomposition to an α + β microstructure throughout the entirety of the specimen.

The compositionally graded Ti – *x*Fe (0<x<35wt.%) LENS^{TM} deposited specimen displayed notable microstructures in the as deposited condition. Specifically, For compositions below 19wt%Fe the as-deposited microstructure of the Ti – *x*Fe gradient exhibited β-grains with no evidence of inter or intragranular precipitation of the hcp α-Ti or the (B2)TiFe intermetallic phase. Beyond ~19.08w% Fe, the microstructure could be described as exhibiting a bimodal distribution of grain sizes. This is interesting, as this bimodal distribution is seen in a β-alloy that has not been subjected to deformation and recrystallization, which is the common route to obtaining this variation in grain size for β-Ti alloys. A more dendritic like "primary" (B2)TiFe particle appears strongly suggesting that the invariant reaction:

$$L \rightarrow \beta + TiFe$$

occurs at a composition below what was previously hypothesized (~33wt%), although it is clear there is significant uncertainty in this portion of the binary phase diagram.

Comparing the results of the Ti – *x*Fe binary systems to that of the ternary Ti – *x*Fe – 5wt.%Al system showed that the introduction of 5wt.%Al to the any composition of alloys from the binary Ti – *x*Fe resulted in an increase in the microhardness values for the 550C directly aged specimens. This increase in microhardness values to be attributed to the introduction of Ti3Al as a fine scale precipitate for such low concentrations of Al. Specifically, just low enough to still allow for the ordering transition of α–Ti to α_2 – Ti_3Al to occur. In this microstructures, XRD spectra obtained displayed peaks that correlate to the presence of both α-Ti and Ti_3Al which is consistent with the proposed 550°C partial isothermal section provided by Volkova. Similar to what was observed in the study of the binary Ti – xFe system, the volume fraction and coarsening of the (B2) intermetallic compound TiFe increases as a function of increases Fe content. Conversely, the morphology of the B2 intermetallic compound in the Ti – Fe – Al ternary system readily exhibits a dendritic morphology when compared to similar compositions in the binary Ti – Fe system. An absence of the "secondary" spherical-like structure of TiFe is observed in the for the intermetallic compound in the ternary system, but the "primary" precipitation of TiFe strongly exhibits a tendency for the connection of dendritic stringers as Fe content increases. Lastly, the matrix microstructure in the ternary system for 5wt.%Al consist of a fine scale lamellar structure that consists of Ti_3Al, (B2)TiFe, and fine acicular α lathes at 4000X magnification.

CHAPTER 8

FUTURE WORK

It can be concluded from this work, specifically with attention to the LENS^{TM} deposited specimens of the Ti – *x*Fe – *y*Al ternary system that a better assessment of the Al powdered utilized is needed. Attempts in achieving the targeted Al content for the Ti – *x*Fe – 10Al and Ti – *x*Fe – 15Al specimens were unsuccessful. This is a result of the deflection of Al powder particles during the deposition process and more importantly the shape of the Al powder used. Moving forward, a suggestion of using a Ti – Al master alloy powder could mitigate the lack of control in achieving the targeted fixed composition of Al concentration.

With parameters achieved to successfully produce compositionally graded Ti – *x*W specimens with a high maximum range of W content (36.48wt.%(13.01at.%)), the future works regarding the Ti – *x*W system will focus on the inclusion of fixed compositions of 5,10, and 15wt.%Al to explore the Ti – *x*W – *y*Al ternary system.

Lastly, with a better understanding of the influence of composition on microstructure and properties for the individual Ti – *x*Fe, Ti – *x*Mo, and Ti – *x*Fe – *y*Al systems, these results can be applied to exploring the multicomponent Ti – *x*Fe – *y*Mo – *z*Al (*x*: $0<x<10$; *y*=0,5,10; *z*=0,5,10,15,30) system with a specific interest on the phases Fe_2Mo and Fe_3Mo_2

BIBLIOGRAPHY

1. A. Schlieter*, U. K. (2011). Anisotropic mechanical behavior of ultrafine eutectic TiFe cast under non - equilibrium conditions. *Intermetallics 19*, 327 - 335.
2. Boyer, R. (2005). The Use of B Titanium Alloys in the Aerospace Industry. *Journal of Materials and Engineering and Performance Vol. 14*, 681 - 685.
3. C.M. Craighead, O. S. (1950). Titanium Binary Alloys. *Transactions AIME, Journal of Metals Vol. 188*, 489 - 513.
4. Chun - Wei Su, C. -G.-F. (2007). Formatio of (B2 + D03) Two - Phase Microstructure in a Fe - 23 Al - 7 Ti Alloy. *Materials Transactions, Vol 48. No. 11*, 2993 - 2996.
5. Collings, E. (1994). *Materials Properties Handbook Titanium Alloys.* Materials Park, OH: ASM International.
6. D. Batalu, G. C. (2006). Critical Analysis of The Ti - Al Phase Diagram. *U.P.B. Sci. Bull., Series B, Vol. 68, No. 4*, 77 - 90.
7. D.B., C. (1982). Titanium - Tungsten Binary Alloy Phase Diagram . *Titanium and Titanium Alloys: Scientific and technology aspects*, 1307 - 1317.
8. D.J., M. (1953). Titanium - Tungsten Binary Alloy Phase Diagram. *Transactions of the American Institue of Mining and Metallurgical Engineers Inc.*, 231 - 237.
9. E., R. (1969). Titanium - Tungsten Binary Alloy Phase Diagram . *Compendium of Phase Diagram Data*, 69 - 71.
10. Elliott, R. P. (1962). *Diffusion in Titanium and Titanium Alloys.* Wright - Patterson Air Force Base, Ohio : Wright - Patterson Air Force .
11. G. W. Franti, J. C. (1978). A survey of eutectoid decomposition in ten Ti - X systems . *Metallurgical Transactions. A, Physical Metallurgy and Materials Science* , 1641 - 1649.
12. Gerd Lutjering, J. C. (2007). *Titanium.* Springer Berlin Heidelbergy New York: Springer.
13. Ghosh, G. (2008). Aluminium - Iron - Titanium. In M. Materials Science International Team, *Ternary Alloy Systems V. 11 SV. D Iron Systems Part 1. Selected Systems from Al - B - Fe to C - Co - Fe* (pp. 292 - 330). Springer Berlin Heidelberg New York: Landolt - Bornstein.
14. J. Das*, K. K. (2007). Bulk Ultra-fine eutectic structure in Ti - Fe base alloys . *Journal of Alloys and Compounds 434 - 435*, 28 - 31.
15. J.Q. Guo*, N. K. (1997). Mechanical properties of rapidly solidified Al - Ti - Fe, Al - Cu - Fe and Al - Fe - Cu - Ti based alloys extruded from their atomized powders. *Materials Science and Engineering A232* , 177 - 182.

16. Jonsson, S. (April 1998). Assessment of the Fe - Ti System. *Metallurgical and Materials Transactions V29B*, 361 - 369.

17. Katarina D. Ciric, V. J. (2012). A Study on Crystal structure, bonding and hydring properties of Ti - Fe - Ni intermetallics - Behind substitution of iron by nickel. *International Journal of Hydrogen Engergy*, 8408 - 8417.

18. Katrin I. Schwender, R. B. (2001). Direct laser deposition of alloys from elemental powder blends. *Scripta Materialia*, 1123 - 1129.

19. Kaufman, L. (1975). Calculation of Superalloy Phase Diagram. *Metallurgical Transaction A*, 1975 - 2123.

20. Khorev, A. I. (2011). Thermal and Thermomechanical Treatment of Titanium Alloys. *Russian Engineering Research*, 1227 - 1232.

21. Knyazeva, V. L. (2008). Metastable Phases in Titanium Alloys and Conditions of Their Formatio. *Metal Science and Heat Treatment Vol. 50*, 373 - 377.

22. M. Palm, G. I. (1995). The Fe - Al - Ti System . *Basic and Applied Research: Section 1*, 209 - 222.

23. M. Palm, J. L. (2006). Assessment of the Al - Fe - Ti system. *Intermetallics 14*, 1291 - 1303.

24. M. Terakubo, J. O. (2007). Freeform fabrication of Ti - Ni and Ti - Fe intermetallic alloys by 3D Micro Welding . *Intermetallics 15*, 133 - 138.

25. Mathew J. Donachie, J. (2000). *Titanium, A Technical Guide.* Materials Park, Ohio: ASM International.

26. Murray, J. (1981). The Ti - W (Titanium - Tungsten) System. *Bulletin of Alloy Phase Diagram* , 192 - 196.

27. O. Heinen*, D. H.-M. (2005). Phase selection during solidification of undercooled Ti - Fe, Ti - Fe - O and Ti - Fe - Si - O melts - Influence of oxygen and silicon. *Materials Science and Engineering A 449 - 451*, 662 - 665.

28. P.C. Collins, R. B. (2003). Laser Deposition of compositionally graded titanium - vanadium and titanium - molybdenum alloys. *Materials Science and Engineering A352*, 118 - 128.

29. P.C. Collins, R. B. (2003). The influence of the enthalpy of mixing during the laser depostion of complex titanium alloys using elemental blends . *Scripta Materialia 48*, 1445 - 1450.

30. Peterson, N. (1960). *Diffusion in Refractory Metals.* Wright - Patterson Air Force Base, Ohio: United States Air Force.

31. R. Banerjee, P. C. (2003). Microstructural evolution in laser depsoited compositionally graded a/b titanium - vanadium alloys. *Acta Materialia*, 3277 - 3292.

32. R. Kainuma, I. O. (2000). Stability of B@ ordered phase in the Ti - rich portion of Ti - Al - Cr and Ti - Al - Fe ternary systems. *Intermetallics 8*, 869 - 875.

33. R.J. Contieri, E. L. (2011). Microstructure of directionally solidified Ti - Fe eutectic alloy with low interstitial and high mechanical strength. *Journal of Crystal Growth 333*, 40 - 47.

34. Raghavan, V. (2002). Al - Fe - Ti (Aluminum - Iron - Titanium). *Journal of Phase Equilibria Vol. 23 No. 4* , 367 - 374.

35. S. Djanarthany, J. -C. (2001). An overview of monolithic titanium aluminides based on Ti3Al and TiAl. *Materials Chemistry and Physics 72*, 301 - 319.

36. S., J. (1996). Titanium - Tungsten Binary Alloy Phase Diagram. *Zeitschrift fu r Metalkunde*, 784 - 787.

37. S.K., L. (1986). Titanium - Tungsten Binary Alloy Phase Diagram . *CALPHAD; Computer Coupling of Phase Diagram and Thermochemistry*, 61 - 76.

38. Tae Wook Heo, D. S.-Q. (2014). Kinetic Pathways of Phase Transformations in Two Phase Ti Alloys. *Metallurgical and Materials Transactions Vol. 45A*, 3438 - 3444.

39. U. Prakash, G. S. (2001). Structure and Properties of Fe - Al - Ti intermetallic alloys. *Intermetallics 9*, 107 - 112.

40. V., O. S. (1971). Titanium - Tungsten Binary Alloy Phase Diagram . *Russian Metallurgy*, 130 - 133.

41. Ye. Zhumagaliev, S. B. (n.d.). Phase Diagram of Ti - Fe - Al System. *Chemical - Metallurgical Institute*.